arXiv:2103.01133v3 [cs.LG] 21 Oct 2021

Posterior Meta-Replay for Continual Learning

Christian Henning*, Maria R. Cervera*,
Francesco D'Angelo, Johannes von Oswald, Regina Traber,
Benjamin Ehret, Seijin Kobayashi, Benjamin F. Grewe, João Sacramento

*Equal contribution

Institute of Neuroinformatics
University of Zürich and ETH Zürich
Zürich, Switzerland
{henningc,mariacer}@ethz.ch

Abstract

Learning a sequence of tasks without access to i.i.d. observations is a widely studied form of continual learning (CL) that remains challenging. In principle, Bayesian learning directly applies to this setting, since recursive and one-off Bayesian updates yield the same result. In practice, however, recursive updating often leads to poor trade-off solutions across tasks because approximate inference is necessary for most models of interest. Here, we describe an alternative Bayesian approach where task-conditioned parameter distributions are continually inferred from data. We offer a practical deep learning implementation of our framework based on probabilistic task-conditioned hypernetworks, an approach we term *posterior meta-replay*. Experiments on standard benchmarks show that our probabilistic hypernetworks compress sequences of posterior parameter distributions with virtually no forgetting. We obtain considerable performance gains compared to existing Bayesian CL methods, and identify task inference as our major limiting factor. This limitation has several causes that are independent of the considered sequential setting, opening up new avenues for progress in CL.

1 Introduction

In recent years, a variety of continual learning (CL) algorithms have been developed to overcome the need to train neural networks with an independent and identically distributed (i.i.d.) sample. Most CL literature focuses on the particular scenario of continually learning a sequence of T tasks with datasets $\mathcal{D}^{(1)}, \ldots, \mathcal{D}^{(T)}$. Because only access to the current task is granted, successful training of a discriminative model that captures $p(\mathbf{Y} \mid \mathbf{X})$ has to occur without an i.i.d. training sample from the overall joint $\mathcal{D}^{(1:T)} \overset{i.i.d.}{\sim} p(\mathbf{X})p(\mathbf{Y} \mid \mathbf{X})$.

The advantages of a Bayesian approach for solving this problem are numerous and include the ability to drop all i.i.d. assumptions across and within tasks in a mathematically sound way, the ability to revisit tasks whenever new data becomes available, and access to principled uncertainty estimates capturing both data and parameter uncertainty. Up until now, Bayesian approaches to CL essentially focused on finding a combined posterior distribution via a recursive Bayesian update $p(\mathbf{W} \mid \mathcal{D}^{(1:T)}) \propto p(\mathbf{W} \mid \mathcal{D}^{(1:T-1)})p(\mathcal{D}^{(T)} \mid \mathbf{W})$. Because the posterior of the previous task is used as prior for the next task, these approaches are also known as **prior-focused** [17]. In theory, the

35th Conference on Neural Information Processing Systems (NeurIPS 2021).

above recursive update can always recover the posterior $p(\mathbf{W} \mid \mathcal{D}^{(1:T)})$, independently of how the data is presented. However, because proper Bayesian inference is intractable, approximations are needed in practice, which lead to errors that are recursively amplified. As a result, whether solutions that are easily found in the i.i.d. setting can be obtained via the approximate recursive update strongly depends on factors such as task ordering, task similarity and the considered family of distributions. These factors limit the effectiveness of the recursive update and have a detrimental effect on the performance of prior-focused methods, especially in task-agnostic CL settings.

To overcome these limitations, we propose an alternative Bayesian approach to CL that does not rely on the recursive update to learn distinct tasks and instead aims to learn task-specific posteriors (Fig. 1, refer to SM F.1 for a detailed discussion of the graphical model). In this view, finding trade-off solutions across tasks is not required, and knowledge transfer can be explicitly controlled for each task via the prior, which is no longer prescribed by the recursive update and can thus be set freely. By introducing probabilistic extensions of task-conditioned hypernetworks [91], we show how task-specific posteriors can be learned with a single shared meta-model, an approach we term **posterior meta-replay**.

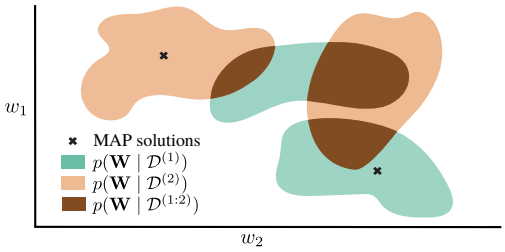

Figure 1: The proposed *posterior meta-replay* framework learns task-specific posteriors $p(\mathbf{W} \mid \mathcal{D}^{(t)})$ via a single shared meta-model, with task-specific point estimates (e.g., MAP) being a limit case. In this view, the modelled solution space is not limited to admissible solutions that lie in the overlap of all task-specific posteriors. By contrast, *prior-focused* methods learn a single posterior $p(\mathbf{W} \mid \mathcal{D}^{(1:T)})$ recursively and thus require the existence of trade-off solutions between learned and future tasks in the currently modelled solution space. Shaded areas indicate high density regions.

This approach introduces two challenges: forgetting at the level of the hypernetwork, and the need to know task identity to correctly condition the hypernetwork. We empirically show that forgetting at the meta-level can be prevented by using a simple regularizer that replays parameters of previous posteriors. In task-agnostic inference settings, often referred to as *class-incremental learning* in the context of classification benchmarks [88], the main hurdle therefore becomes task inference at test time. Here we focus on this task-agnostic setting, arguably the most challenging but also the most natural CL scenario, since the obtained models can be deployed just like those obtained via i.i.d. training (e.g., irrespective of the sequential training, the final model will be a classifier across all classes). In order to explicitly infer task identity from unseen inputs without resorting to generative models, we thoroughly study the use of principled uncertainty that naturally arises in Bayesian models. We show that results obtained in this task-agnostic setting with our approach constitute a leap in performance compared to prior-focused methods. Furthermore we show that limitations in task inference via predictive uncertainty are not related to our CL solution, but depend instead on the combination of approximate inference method, architecture, uncertainty measure and prior. Finally, we investigate how task inference can be further improved through several extensions.

We summarize our main contributions below:

- We describe a Bayesian CL framework where task-conditioned posterior parameter distributions are continually learned and compressed in a hypernetwork.
- In a series of synthetic and real-world CL benchmarks we show that our task-conditioned hypernetworks exhibit essentially no forgetting, both for explicitly parameterized and implicit posterior distributions, despite using the parameter budget of a single model.
- Compared to prior-focused methods, our approach leads to a leap in performance in task-agnostic inference while maintaining the theoretical benefits of a Bayesian approach.
- Our approach scales to modern architectures such as ResNets, and remaining performance limitations are linked to uncertainty-based out-of-distribution detection but not to our CL solution.
- Finally, we show how prominent existing Bayesian CL methods such as elastic weight consolidation can be dramatically improved in task-agnostic settings by introducing a small set of task-specific parameters and explicitly inferring the task.

2 Related Work

Continual learning. CL algorithms attempt to mitigate catastrophic interference while facilitating transfer of skills whenever possible. They can be coarsely categorized as (1) *regularization-methods* that put constraints on weight updates, (2) *replay-methods* that mimic pseudo-i.i.d. training by rehearsing stored or generated data and (3) *dynamic architectures* which can grow to allocate capacity for new knowledge [71]. Most related to our work is the study from von Oswald et al. [91] that introduces task-conditioned hypernetworks for CL, and already considers task inference via predictive uncertainty in the deterministic case. Our framework can be seen as a probabilistic extension of their work, which provides task-specific point estimates via a shared meta-model (cf. Sec. 3). Follow-up work also achieves task inference via predictive uncertainty, e.g., Wortsman et al. [94] use it to select a learned binary mask per task that modulates a random base network. Here we complement these studies by thoroughly exploring task inference via several uncertainty measures, disclosing the factors that limit task inference and highlighting the importance of parameter uncertainty.

A variety of methods tackling CL have been derived from a Bayesian perspective. A prominent example are *prior-focused* methods [17], which incorporate knowledge from past data via the prior and, in contrast to our work, aim to find a shared posterior for all data. Examples include (Online) EWC [38, 78] and VCL [65, 54]. Other methods like CN-DPM [46] use Bayes' rule for task inference on the joint $p(\mathbf{X}, C)$, where C is a discrete condition such as task identity. An evident downside of CN-DPM is the need for a separate generative and discriminative model per condition. More generally, such an approach requires meaningful density estimation in the input space, a requirement that is challenging for modern ML problems [64].

Other Bayesian CL approaches consider instead task-specific posterior parameter distributions. Lee et al. [47] learn separate task-specific Gaussian posterior approximations which are merged into a single posterior after all tasks have been seen. CBLN [49] also learns a separate Gaussian posterior approximation per task but later tries to merge similar posteriors in the induced Gaussian mixture model. Task inference is thus required and achieved via predictive uncertainty, although for a more reliable estimation all experiments consider batches of 200 samples that are assumed to belong to the same task. Tuor et al. [85] also learn a separate approximate posterior per task and use predictive uncertainty for task-boundary detection and task inference. In contrast to these approaches, we learn all task-specific posteriors via a single shared meta-model and remain agnostic to the approximate inference method being used. A conceptually related approach is MERLIN [33], which learns task-specific weight distributions by training an ensemble of models per task that is used as training set for a task-conditioned variational autoencoder. Importantly, MERLIN requires a fine-tuning stage at inference, such that every drawn model is fine-tuned on stored coresets, i.e., a small set of samples withheld throughout training. By contrast, our approach learns the parameters of an approximate Bayesian posterior $p(\mathbf{W} \mid \mathcal{D}^{(t)})$ per task t, and no fine-tuning of drawn models is required.

Bayesian neural networks. Because neural networks are expressive enough to fit almost any data [98] and are often deployed in an overparametrized regime, it is implausible to expect that any single solution obtained from limited data generalizes to the ground truth $p(\mathbf{Y} \mid \mathbf{w}, \mathbf{X}) \approx p(\mathbf{Y} \mid \mathbf{X})$ almost everywhere on $p(x)$. By contrast, Bayesian statistics considers a distribution over models, explicitly handling uncertainty to acknowledge data insufficiencies. This distribution is called the *posterior parameter distribution* $p(\mathbf{W} \mid \mathcal{D}) \propto p(\mathcal{D} \mid \mathbf{W})\, p(\mathbf{W})$, which weights models based on their ability to fit the data (via the likelihood $p(\mathcal{D} \mid \mathbf{W})$), while considering only plausible models according to the prior $p(\mathbf{W})$. Predictions are made by marginalizing over models (for an introduction see MacKay [57]). Bayesian neural networks (BNN) apply this formalism to network parameters $\mathbf{w}$, whereas for practical reasons hyperparameters like architecture are chosen deterministically [56].

While a deterministic discriminative model can only capture *aleatoric uncertainty* (i.e., uncertainty intrinsic to the data $p(\mathbf{Y} \mid \mathbf{X})$), a Bayesian treatment allows to also capture *epistemic uncertainty* by being uncertain about the model's parameters (*parameter uncertainty*). This proper treatment of uncertainty is of utmost importance for safety-critical applications, where intelligent systems are expected to *know what they don't know*. However, due to the complexity of modelling high-dimensional distributions at the scale of modern deep learning, BNNs still face severe scalability issues [82]. Here, we employ several approximations to the posterior based on variational inference [5] from prior work, ranging from simple and scalable methods with a mean-field variational family like Bayes-by-Backprop (BbB, [6]) to methods with complex but rich variational families like the spectral Stein gradient estimator [79]. For more details see Sec. 3 and SM C.

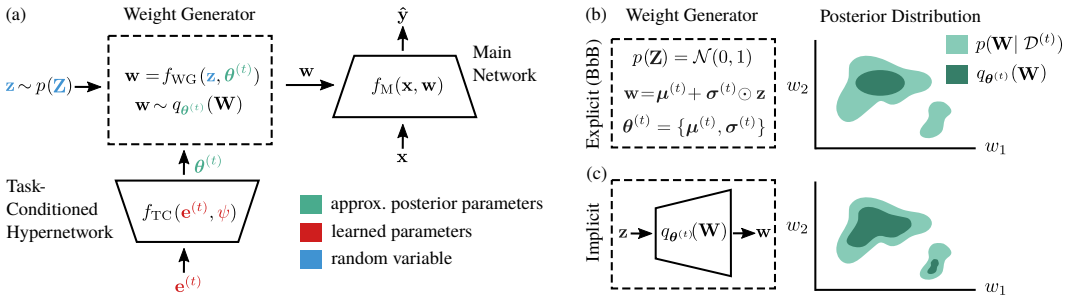

Figure 2: *Posterior meta-replay* for CL. **(a)** The architecture consists of a main network M that processes inputs $\mathbf{x}$ and generates predictions $\hat{\mathbf{y}}$ according to a set of weights $\mathbf{w}$ generated by a weight generator (WG). The WG is a deterministic function $f_{\text{WG}}(\mathbf{z}, \boldsymbol{\theta}^{(t)})$ that transforms a base distribution $p(\mathbf{Z})$ into a distribution over main network weights, where $\boldsymbol{\theta}^{(t)}$ are the parameters of the approximate posterior $q_{\boldsymbol{\theta}^{(t)}}(\mathbf{W})$. Crucially, $\boldsymbol{\theta}^{(t)}$ are task-specific, and generated by a task-conditioned (TC) hypernetwork, which receives task embeddings $\mathbf{e}^{(t)}$ as input. The embeddings and the parameters $\boldsymbol{\psi}$ of the TC are learned continually via a simple *meta-replay* regularizer (Eq. 1). **(b)** We refer to the approximate posteriors as *explicit* if f_{WG} is predefined. In Bayes-by-Backprop (BbB), for example, the reparametrization trick transforms Gaussian noise into weight samples. **(c)** More complex, *implicit* posterior approximations are parametrized by an auxiliary hypernetwork, which receives its task-conditioned parameters from the TC, which now plays the role of a hyper-hypernetwork. The obtained posterior approximations are more flexible and can, for example, capture multi-modality.

3 Methods

In this section we describe our *posterior meta-replay* framework (Fig. 2). We start by introducing task-conditioned hypernetworks as a tool to continually learn parameters of task-specific posteriors, each of which is learned using variational inference (SM C.1). We then explain how the framework can be instantiated for both simple, explicit posterior approximations, and complex ones parametrized by an auxiliary network, and describe how forgetting can be mitigated through the use of a meta-regularizer. We next explain how predictive uncertainty, naturally arising from a probabilistic view of learning, can be used to infer task identity for both **PosteriorReplay** methods, and **PriorFocused** methods that use a multihead output. Finally, we outline ways to boost task inference.

Task-conditioned hypernetworks. Traditionally, hypernetworks are seen as neural networks that generate the weights $\mathbf{w}$ of a main network $\mathbf{M}$ processing inputs as $\hat{\mathbf{y}} = f_{\text{M}}(\mathbf{x}, \mathbf{w})$ [22, 77]. Here, we consider instead hypernetworks that learn to generate $\boldsymbol{\theta}$, the *parameters of a distribution* $q_{\boldsymbol{\theta}}(\mathbf{W})$ over main network weights. By taking low-dimensional task embeddings $\mathbf{e}^{(t)}$ as inputs and computing $\boldsymbol{\theta}^{(t)} = f_{\text{TC}}(\mathbf{e}^{(t)}, \boldsymbol{\psi})$, task-conditional (**TC**) computation is possible. Sampling is realized by transforming a base distribution $p(\mathbf{Z})$ via a weight generator (**WG**) $f_{\text{WG}}(\mathbf{z}, \boldsymbol{\theta}^{(t)})$, whose choice determines the family of distributions considered for the approximation (i.e., the *variational family*). In our framework, weights $\mathbf{w} \sim q_{\boldsymbol{\theta}^{(t)}}(\mathbf{W})$ are directly used for inference without requiring any fine-tuning.

Importantly, all learnable parameters are comprised in the TC system, which can be designed to have less parameters than the main network, i.e., $\dim(\boldsymbol{\psi}) + \sum_t \dim(\mathbf{e}^{(t)}) < \dim(\mathbf{w})$. Such constraint is vital to ensure fairness when comparing different CL methods, and is enforced in all our computer vision experiments. Additional details can be found in SM C.2.

Posterior-replay with explicit distributions. Different families of distributions can be realized within our framework. In the special case of a point estimate $q_{\boldsymbol{\theta}^{(t)}}(\mathbf{W}) = \delta(\mathbf{W} - \boldsymbol{\theta}^{(t)})$, the WG system can be omitted altogether as it corresponds to the identity $\boldsymbol{\theta}^{(t)} = f_{\text{WG}}(\mathbf{z}, \boldsymbol{\theta}^{(t)})$. This reduces our solution to the deterministic CL method introduced by von Oswald et al. [91], which we refer to as **PosteriorReplay-Dirac**. However, capturing parameter uncertainty is a key ingredient of Bayesian statistics that is necessary for more robust task inference (cf. Sec. 4.2). We thus turn as a first step to *explicit* distributions $q_{\boldsymbol{\theta}^{(t)}}(\mathbf{W})$, for which the WG system samples according to a predefined function. We refer as **PosteriorReplay-Exp** to finding a mean-field Gaussian approximation via the BbB algorithm (SM C.3.1, [6]). In this case, $\boldsymbol{\theta}^{(t)}$ corresponds to the set of means and variances that define a Gaussian for each weight, which is directly generated by the TC. In the SM, we also report results for another instance of explicit distribution (cf. SM C.3.2).

Posterior-replay with implicit distributions. Since the expressivity of *explicit* distributions is limited, we also explore the more diverse variational family of *implicit* distributions [19, 31]. These are parametrized by a WG that now takes the form of an auxiliary neural network, making the parameters $\boldsymbol{\theta}^{(t)}$ of the approximate posterior dependent on the chosen WG architecture. This setting, referred to as **PosteriorReplay-Imp**, results in a hierarchy of three networks: a TC network generates task-specific parameters $\boldsymbol{\theta}^{(t)}$ for the approximate posterior, which is defined through an arbitrary base distribution $p(\mathbf{Z})$ and the WG hypernetwork, which in turn generates weights $\mathbf{w}$ for a main network M that processes the actual inputs of the dataset $\mathcal{D}^{(t)}$. Interestingly, the TC now plays the role of a *hyper-hypernetwork* as it generates the weights of another hypernetwork (Fig. 2a and Fig. 2c).

Variational inference commonly resorts to optimizing an objective consisting of a data-dependent term and a *prior-matching term* $\mathrm{KL}(q_{\boldsymbol{\theta}}(\mathbf{W}) \mid\mid p(\mathbf{W}))$. Estimating the *prior-matching term* when using implicit distributions is not straightforward since we do not have analytic access to the density nor the entropy of $q_{\boldsymbol{\theta}^{(t)}}(\mathbf{W})$. To overcome this challenge, we resort to the spectral Stein gradient estimator (SSGE, SM C.4.2, [79]). This method is based on the insight that direct access to the log-density is not required, but only to its gradient with respect to $\mathbf{W}$. Noticing that this quantity appears in Stein's identity, the authors consider a spectral decomposition of the term and use the Nyström method to approximate the eigenfunctions. We test an alternative method for dealing with implicit distributions in the SM that is based on estimating the log-density ratio (SM C.4.1).

As an additional challenge introduced by the use of implicit distributions, the support of $q_{\boldsymbol{\theta}^{(t)}}(\mathbf{W})$ is limited to a low-dimensional manifold when using an inflating architecture for WG, causing the *prior-matching term* to be ill-defined. To overcome this, we investigate the use of small noise perturbations in WG outputs (SM C.4.3). Normalizing flows [70] can also be utilized as WG architectures to gain analytic access to $q_{\boldsymbol{\theta}^{(t)}}(\mathbf{W})$, albeit at the cost of architectural constraints such as invertibility.

Overcoming forgetting via meta-replay. Since all learnable parameters are part of the TC system, forgetting only needs to be addressed at this meta-level. With $\mathcal{L}_{\text{task}}$ the task-specific loss (SM Eq. 3) and $\mathrm{D}(\cdot||\cdot)$ a divergence measure between distributions, the loss for task t becomes:

$$\mathcal{L}^{(t)}(\boldsymbol{\psi}, \mathcal{E}, \mathcal{D}^{(t)}) = \mathcal{L}_{\text{task}}(\boldsymbol{\psi}, \mathbf{e}^{(t)}, \mathcal{D}^{(t)}) + \beta \sum_{t'<t} \mathrm{D}\big(q_{\boldsymbol{\theta}^{(t',*)}}(\mathbf{W}) || q_{\boldsymbol{\theta}^{(t')}}(\mathbf{W})\big) \tag{1}$$

where $\mathcal{E} = \{\mathbf{e}^{(t')}\}_{t'=1}^{t}$ is the set of task embeddings up to the current task, β is the strength of the regularizer and $\boldsymbol{\theta}^{(t',*)} \equiv f_{\text{TC}}(\mathbf{e}^{(t',*)}, \boldsymbol{\psi}^*)$ are the parameters of the posterior approximation obtained from a checkpoint of the TC parameters before learning task t: $\{\boldsymbol{\psi}^*\} \cup \{\mathbf{e}^{(t',*)}\}_{t'<t}$. The checkpointed meta-model allows replaying posterior distributions from the past and retaining them via divergence minimization as detailed below, hence the name *posterior meta-replay*. Importantly, the loss on task t only depends on the corresponding dataset $\mathcal{D}^{(t)}$, but knowledge transfer across tasks is possible because task-specific models are learned through a shared meta-model.[1] Since the computation required to compute this regularizer linearly scales with the number of tasks, we also explore stochastically regularizing on a subset of randomly selected tasks in each update (cf. SM D.3), and show that this does not impair performance. Notably, our *PosteriorReplay* method does not incur in a significant increase of runtime or memory usage (SM F.2).

The evaluation of Eq. 1 requires estimates of a divergence measure to prevent changes in learned posterior approximations of past tasks. Because these are required at every loss evaluation and need to be cheap to compute, we do not consider sample-based estimates but only estimates that directly utilize posterior parameters. This goal is easy to achieve for families of posterior approximations that possess an analytic expression for a divergence measure (e.g., Gaussian distributions). More specifically, for *PosteriorReplay-Exp*, we consider the forward KL, backward KL and the 2-Wasserstein distance but did not observe that the specific choice of divergence measure is crucial in practice (cf. SM C.3.1 and Table S14). In all other cases, approximations are required. Specifically, we resort in our experiments to the use of an L2 regularizer at the output of the TC network:

$$\beta \sum_{t'<t} \| f_{\text{TC}}(\mathbf{e}^{(t',*)}, \boldsymbol{\psi}^*) - f_{\text{TC}}(\mathbf{e}^{(t')}, \boldsymbol{\psi}) \|_2^2 \tag{2}$$

Perhaps surprisingly, we observe that this crude regularization, reminiscent to the one used in von Oswald et al. [91] for point estimates, does not harm performance and leads to models that exhibit

[1] While this type of transfer is rather implicit, explicit knowledge transfer can be realized via task-specific priors (cf. SM F.7).

virtually no forgetting. However, we discuss in SM F.3 how this isotropic regularization could be improved given that the KL is locally approximated by a norm $\|\cdot\|_F$ induced by the Fisher information matrix F on $q_{\boldsymbol{\theta}}(\mathbf{W})$.

Task inference. A system with task-specific solutions requires access to task identity when processing unseen samples. In our framework, this amounts to selecting the correct task embedding to condition the TC. Although auxiliary systems can be used to infer task identity [24, 91], here we exploit predictive uncertainty, assuming task identity can be inferred from the input alone. For a task inference approach based on predictive uncertainty to work, the properties of the input data distribution $p^{(t)}(\boldsymbol{x})$ need to be reflected in the uncertainty measure, i.e., uncertainty needs to be low for in-distribution data and high for out-of-distribution (OOD) data [11]. Uncertainty-based task inference with deterministic discriminative models only captures aleatoric uncertainty, making its overall validity debatable. Indeed, aleatoric uncertainty is only calibrated in-distribution and its OOD behavior is hard to foresee. Instead, we argue that epistemic uncertainty arising naturally in a Bayesian setting is crucial for robust uncertainty-based task inference. In our case, epistemic uncertainty stems from the fact that the posterior parameter distribution $p(\mathbf{W}|\mathcal{D}^{(t)})$ in conjunction with the network architecture induces a distribution over functions. If this distribution captures a rich set of functions, a diversity of predictions on OOD data can be expected even if those functions agree in-distribution (cf. Sec. 4.2). Note, however, that inducing such diverse distribution over functions is not straightforward with neural networks, and that more research is required to justify uncertainty-based OOD detection [11].

We explore two different ways to quantify uncertainty for task inference. In **Ent** the task t leading to the lowest entropy on the predictive posterior $p(\mathbf{y} \mid \mathcal{D}^{(t)}; \tilde{\mathbf{x}})$ is selected, where $p(\mathbf{y} \mid \mathcal{D}^{(t)}; \tilde{\mathbf{x}}) = \int_{\mathbf{W}} p(\mathbf{y} \mid \mathbf{W}; \tilde{\mathbf{x}}) p(\mathbf{W}|\mathcal{D}^{(t)})\, d\mathbf{W}$ is approximated via Monte-Carlo with samples from $q_{\boldsymbol{\theta}^{(t)}}(\mathbf{W})$. This approach captures both aleatoric and epistemic uncertainty when used in a probabilistic setting. In **Agree** the task leading to the highest agreement in predictions across models drawn from $q_{\boldsymbol{\theta}^{(t)}}(\mathbf{W})$ is selected. This approach exclusively measures epistemic uncertainty and can therefore only be estimated in a probabilistic setting. Although we generally consider task inference for individual samples, we also explore batch-wise (**BW**) task inference for batches of 100 samples that are assumed to belong to the same task. Such approach drastically boosts task inference simply due to a statistical accumulation effect when having above chance level task inference for single inputs. Intuitively, *BW* corresponds to accumulating evidence to decrease uncertainty (e.g., an agent looking at an object from multiple perspectives). Further details can be found in SM C.6, and using uncertainty for task-boundary detection when training without explicit access to task identity is explored in SM D.8.

Facilitating task inference through coresets. A key advantage of Bayesian statistics is the ability to update models as new evidence arrives. When continually learning a sequence of tasks, posteriors may for example undergo a post-hoc fine-tuning on stored coresets to mitigate catastrophic forgetting of earlier tasks. Specifically, given a dataset split $\mathcal{D}^{(t)} \setminus \mathcal{C}^{(t)} \cup \mathcal{C}^{(t)}$, one can perform a final update $p(\mathbf{W}|\mathcal{D}^{(t)}) \propto p(\mathbf{W} \mid \mathcal{D}^{(t)} \setminus \mathcal{C}^{(t)}) p(\mathcal{C}^{(t)} \mid \mathbf{W})$ using a stored coreset $\mathcal{C}^{(t)}$ in conjunction with an already learned posterior approximation for $p(\mathbf{W} \mid \mathcal{D}^{(t)} \setminus \mathcal{C}^{(t)})$ that now acts as a prior. Interestingly, access to coresets after training on all tasks can also be exploited to facilitate task inference via predictive uncertainty. Here, we explore this idea by encouraging task-specific models to produce uncertain predictions for OOD samples (i.e., coresets from other tasks), an approach that we denote **CS** (SM C.7), and in which we store 100 inputs per task. Intriguingly, training on OOD inputs makes these become in-distribution, and therefore renders model agreement (*Agree*) inapplicable for task inference, which we empirically observe.

Improving prior-focused CL. We investigate ways to improve *PriorFocused* methods within our framework. First, we endow them with *implicit* posterior approximations $q_{\boldsymbol{\theta}}(\mathbf{W})$ parametrized by a WG hypernetwork, an approach we refer to as **PriorFocused-Imp**. Because the posterior is shared across tasks, no TC system is required and the parameters $\boldsymbol{\theta}$ can be directly optimized via SSGE. Second, we enrich *PriorFocused* methods with a small set of task-specific parameters that enable uncertainty-based task inference for prior-focused methods too. Specifically, the learned parameters $\mathbf{w}$ consist of a set of shared weights $\boldsymbol{\phi}$ and a set of task-specific output heads with weights $\{\xi^{(t)}\}_{t=1}^{T}$. This approach is in contrast with how *PriorFocused* methods like *Online EWC* are commonly deployed in task-agnostic inference settings, where the softmax output grows as new tasks arrive (e.g., [88]). The use of a growing softmax causes the model class parametrized by $\mathbf{w}$ to change over time, and therefore violates the Bayesian assumption that the approximate posterior is obtained from a model class containing the ground-truth model. We show that this leads to limitations that

can be overcome by a multihead approach. For *Online EWC*, we refer to the growing softmax and multihead scenarios as **EWC-growing** and **EWC-multihead**, respectively (cf. SM C.5.2). We also explore the prior-focused instantiation of BbB, known as **VCL** (cf. SM C.5.1).

4 Experiments

In this section, we start by illustrating the conceptual advantage of the *PosteriorReplay* approach compared to *PriorFocused* methods, as well as the importance of parameter uncertainty for robust task inference. We then explore scalability to more challenging computer vision CL benchmarks.

To assess forgetting, we provide **During** scores, measured directly after training each task, and **Final** scores, evaluated after training on all tasks. We consider two different testing scenarios: (1) either task-identity is explicitly given (**TGiven**) or (2) task-identity has to be inferred (**TInfer**), e.g. via predictive uncertainty. Unless explicitly mentioned, task inference is performed for each sample in isolation and is obtained using the *Ent* criterion (*TInfer-Final*). Whenever the wrong task is inferred, the sample is directly considered as incorrectly classified. Supplementary results and controls are provided in SM D, and all experimental details can be found in SM E.[2]

4.1 Simple 1D regression illustrates the pitfalls of prior-focused learning

To illustrate conceptual differences between *PosteriorReplay* and *PriorFocused* methods we study 1D regression, for which the predictive posterior can be visualized. Each task-specific posterior obtained with *PosteriorReplay-Exp* fits the training data well (Fig. 3a) and exhibits increasing uncertainty when leaving the in-distribution domain, as desired for successful task inference. Interestingly, when studying low-dimensional problems, we generally found it easier to find viable hyperparameter configurations for *PosteriorReplay* with *implicit* methods than with *explicit* ones. As we do not consider a multihead for this problem, *PriorFocused* methods have to fit a single posterior to all polynomials in a sequential manner and struggle to find a good fit (Fig. 3b), independent of the type of posterior approximation used. Results for other methods and an analysis of the correlations and multi-modality that can be captured by implicit methods in weight space can be found in SM D.1.

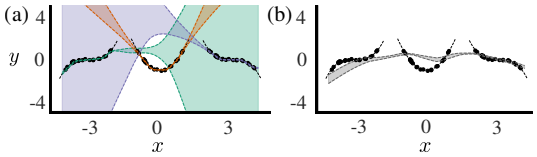

Figure 3: *PriorFocused* methods struggle to learn three 1D polynomial regression tasks. **(a)** Different colors represent the task-specific posterior approximations within the final *PosteriorReplay-Exp* model. For unseen inputs x the posterior with the lowest predictive uncertainty is chosen to make predictions. **(b)** Predictive posterior using the final approximation of $p(\boldsymbol{W} \mid \mathcal{D}^{(1:3)})$, obtained via *PriorFocused-Imp*. Shaded areas represent standard deviation, and black dots training samples.

Because we use a mean squared error (MSE) loss, the likelihood is a Gaussian with fixed variance (SM C.3.1) and all x-dependent uncertainty originates from parameter uncertainty. We next consider classification problems where both epistemic and aleatoric uncertainty can be explicitly modelled.

4.2 Maintaining parameter uncertainty is crucial for robust task inference

To investigate the importance of parameter uncertainty, we consider a 2D classification problem for which uncertainty can be visualized in- and out-of-distribution. Classification tasks are of special interest as it is possible to model arbitrary input-dependent discrete distributions, e.g. via a softmax at the outputs. This surprisingly often results in meaningful OOD performance in high-dimensional benchmarks without any treatment of parameter uncertainty [82].

Table 1: 2D mode classification accuracies (Mean $\pm$ standard error of the mean (SEM) in %, $n = 10$). Task identity is inferred via predictive uncertainty using an entropy (*Ent*) or model agreement (*Agree*) criterion. *PR* denotes *PosteriorReplay*.

Final Acc	TGiven	TInfer (Ent)	TInfer (Agree)
PR-Dirac	99.78 ± 0.21	44.90 ± 5.74	N/A
PR-Exp	100.0 ± 0.00	81.07 ± 6.78	90.02 ± 3.57
PR-Imp	100.0 ± 0.00	100.0 ± 0.00	100.0 ± 0.00

[2]Source code for all experiments (including all baselines) is available at: `https://github.com/chrhenning/posterior_replay_cl` .

Here, we consider a Gaussian mixture of two modes per task, each mode being a different class (Fig. 4a). *TInfer-Final (Agree)*, which is indicative of the importance of epistemic uncertainty for OOD detection, is the most robust measure for task inference in this experiment (Table 1). *PosteriorReplay-Dirac*, which does not incorporate epistemic uncertainty, performs poorly. Finally, *implicit* methods maintain an advantage over *explicit* ones, presumably due to the increased flexibility in modelling the posterior.

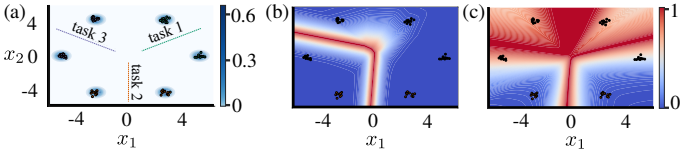

Figure 4: Parameter uncertainty is crucial for robust task inference. **(a)** Density of input distribution $p(\mathbf{x})$ across tasks. Dots represent training points, colors task-affiliation and lines decision boundaries for each of the three consecutively learned 2D binary classification tasks. **(b)** Entropy of predictive distribution induced by the approximate posterior of task 2 learned via *PosteriorReplay-Dirac*. **(c)** Same as (b) for *PosteriorReplay-Imp*.

To better understand why differences between methods arise we provide uncertainty maps over the input space (Fig. 4). Consistent with the observed low task inference accuracy, *PosteriorReplay-Dirac* displays arbitrary uncertainty away from the training data (Fig. 4b). By contrast, *PosteriorReplay-Imp* (Fig. 4c) approaches the desired behavior of displaying high uncertainty away from the training data of the corresponding task. We provide detailed analysis in SM D.2.

4.3 Multiple factors affect uncertainty-based task inference accuracy

To investigate the factors that affect uncertainty-based task inference, we next consider SplitMNIST [96], a popular variant of the MNIST dataset, adapted to CL by splitting the ten digit classes into five binary classification tasks. The results can be found in Table 2.

While all methods successfully prevent forgetting (i.e., *Final* scores are maxed-out and close to the *During* accuracies, SM D.3) and achieve acceptable *Final* accuracies when task identity is provided, large differences can be observed when the task needs to be inferred. Methods with task-specific solutions outperform by a large margin *PriorFocused* approaches such as *Online EWC*, whose performance substantially improves when using uncertainty-based task inference through a multihead. Despite superior performance of *PosteriorReplay* approaches, a gap in performance between task-inferred and task-given scenarios remains. However, training separate posteriors that are not embedded in a hypernetwork (**SeparatePosteriors**) leads to similar results, showing that task inference limitations are not linked to our solution. These limitations can be surmounted by inferring the task on batches rather than single samples (BW) or by using coresets to encourage high uncertainty for OOD data (CS), which leads to performances comparable to generative-replay methods which explicitly capture $p(\mathbf{X})$ (i.e., HNET+R and DGR).

Table 2: Accuracies of SplitMNIST experiments (Mean $\pm$ SEM in %, $n = 10$) after learning all tasks when task identity is provided (*TGiven-Final*) and when it needs to be inferred (*TInfer-Final*, based on the *Ent* criterion if explicit task-inference is required). Results are shown for an MLP with two hidden layers of 400 neurons (MLP-400,400), an MLP-100,100[1] or a Lenet[2]. *PR* denotes *PosteriorReplay* and *SP SeparatePosteriors*.

	TGiven-Final	TInfer-Final
EWC-growing [87]	N/A	19.96 ± 0.07
EWC-multihead	96.40 ± 0.62	47.67 ± 1.52
VCL-multihead	96.45 ± 0.13	58.84 ± 0.64
PR-Dirac	99.65 ± 0.01	70.88 ± 0.61
PR-Exp	99.72 ± 0.02	71.73 ± 0.87
PR-Imp	99.77 ± 0.01	71.91 ± 0.79
SP-Dirac	99.77 ± 0.01	70.39 ± 0.27
SP-Exp	99.81 ± 0.00	68.40 ± 0.23
PR-Exp-BW	99.72 ± 0.02	99.72 ± 0.02
PR-Exp-CS	98.50 ± 0.09	90.83 ± 0.24
DGR [87]	N/A	91.79 ± 0.32
HNET+R [91]	N/A	95.30 ± 0.13
PR-Dirac[1]	99.72 ± 0.01	63.41 ± 1.54
PR-Exp[1]	99.75 ± 0.01	70.07 ± 0.56
PR-Dirac[2]	99.87 ± 0.04	72.33 ± 2.75
PR-Exp[2]	99.20 ± 0.67	74.09 ± 1.38

To better understand the factors that influence task inference, we consider a variety of approximate inference methods and architectures. Since epistemic uncertainty seems to play a vital role for task inference, the approximate inference method will likely affect *TInfer* performance (e.g., *Exp* vs. *Imp*; in supplementary results). In addition, because diversity in function space enables uncertainty-based OOD detection and because different architectures induce different priors in function space [93], one can expect that prior and architecture play a key role as well, which we observe

by comparing the *TInfer* performance for different architectures. Additional SplitMNIST results can be found in SM D.3, and results showing scalability to sequences of up to 100 PermutedMNIST tasks can be found in SM D.4 and D.5.

4.4 PosteriorReplay scales to natural image datasets

While BNNs are advocated because of their theoretical promises, practitioners are often put off by scalability issues. Here we show that our approach scales to natural images by considering SplitCIFAR-10 [39], a dataset consisting of five tasks with two classes each. Results obtained with a Resnet-32 [23] (Table 3) show performance gains in the task-agnostic setting compared to recent methods like EBM [50], and to the *PriorFocused* method VCL.

Furthermore, our results reveal considerable improvements through the incorporation of epistemic uncertainty, as shown by differences between *PosteriorReplay-Exp* and *PosteriorReplay-Dirac*.

Notably, *PosteriorReplay-Exp-BW* solves CIFAR-10 with a performance comparable to a classifier trained on all data at once, with the caveat that successive unseen samples are assumed to belong to the same task. In contrast to low-dimensional problems, the *implicit* method *PosteriorReplay-Imp* does not exhibit a competitive advantage, as it appears to suffer from scalability issues. Other baselines and results for a WRN-28-10 can be found in SM D.6, and results showing that our framework scales to the SplitCIFAR-100 benchmark can be found in SM D.7.

Table 3: Accuracies of SplitCIFAR-10 experiments (Mean $\pm$ SEM in %, $n = 10$). *TInfer-Final* is based on the *Ent* criterion if explicit task-inference is required and *PR* denotes *Posterior-Replay*.

	TGiven-During	TGiven-Final	TInfer-Final
VCL-multihead	95.78 ± 0.09	61.09 ± 0.54	15.97 ± 1.91
PR-Dirac	94.59 ± 0.10	93.77 ± 0.31	54.83 ± 0.79
PR-Exp	95.59 ± 0.08	95.43 ± 0.11	61.90 ± 0.66
PR-Imp	94.25 ± 0.07	92.83 ± 0.16	51.95 ± 0.53
PR-Exp-BW	95.59 ± 0.08	95.43 ± 0.11	92.94 ± 1.04
PR-Exp-CS	95.15 ± 0.11	92.48 ± 0.13	64.76 ± 0.34
EBM [50]	N/A	N/A	38.84 ± 1.08

5 Discussion

In this study we propose *posterior meta-replay*, a framework for continually learning task-specific posterior approximations within a single shared meta-model. In contrast to *prior-focused* methods based on a recursive Bayesian update, our approach does not directly seek trade-off solutions across tasks. This results in more flexibility for learning new tasks but introduces the need to know task identity when processing unseen inputs.

Task Inference. Probabilistic inference on task identity can be achieved by additionally considering inputs and task embeddings as random variables, a strategy that would require task-conditioned generative models with tractable density [46]. However, learning generative models on high-dimensional data is a challenging problem and, even if tractable densities are accessible, these do not currently reflect the underlying data-generative process [64].[3] To sidestep these limitations, we study the use of predictive uncertainty for task inference [91] and show that an entropy-based criterion works best for both deterministic and Bayesian models. Nevertheless, we highlight that proper task inference requires epistemic uncertainty (e.g., measured in terms of model disagreement). Indeed, in-distribution samples with high aleatoric uncertainty can lead to high predictive entropy, causing them to be misclassified as OOD. This does not pose a problem in highly-curated ML datasets where samples with high aleatoric uncertainty are excluded [62], but drastically limits the applicability of entropy-based uncertainty estimation in more practical scenarios. For these reasons, we advocate for the use of Bayesian models whose epistemic uncertainty can induce diversity in function space for OOD inputs and enable more robust task inference.[4]

[3] Interestingly, a concurrent study by van de Ven et al. [89] successfully trains class-conditioned generative models, indicating that this approach could nevertheless be feasible to tackle task inference.

[4] Note, while also models with deterministic parameters may be well suited for OOD detection (e.g., Lakshminarayanan et al. [43], that utilizes a deterministic distance preserving input-to-hidden mapping), these solutions

Limitations. Compared to methods performing deterministic inference, the Bayesian model average incurs in significant computational overhead. This overhead is reinforced when performing uncertainty-based task inference, since each predictive posterior needs to be evaluated in parallel. Moreover, despite strong performance gains compared to *prior-focused* approaches, we observe general limitations of such task inference procedure. These could be overcome once a better understanding of how epistemic uncertainty influences OOD behavior in neural networks is available. In addition, our work builds on algorithms to perform variational inference, and is therefore only applicable to problems where these can be successfully deployed. Finally, all our experiments consist of a set of clearly defined tasks within which i.i.d. samples are available. Although this scenario is in line with most existing CL literature, it might be of limited relevance for practical CL problems, and a focus on established benchmarks adhering to these constraints could therefore misguide research on this area. Indeed, a more natural CL problem might arise from the need to online learn from a stream of autocorrelated samples. In this context, it is important to note that unlike non-Bayesian CL methods, our approach can utilize any type of online *prior-focused* method (such as FOO-VB [97]) to also learn *within* tasks in a non-i.i.d. manner. Therefore, as long as some coarse split into tasks is meaningful, such hierarchical approach holds great promise. However, it should be noted that any progress towards learning from non-i.i.d. data opens the door to training algorithms from raw, uncurated datasets, and could therefore counter some of the efforts that are currently done to mitigate algorithmic bias.

Conclusion. Taken together, our work shows that it is possible to continually learn an approximate posterior per task without an increased parameter budget, and that task-agnostic inference can be achieved via predictive uncertainty to obtain a Bayesian CL approach that is scalable to real-world data. Since forgetting is not a prevalent issue in our experiments and task inference limitations are not linked to our CL solution, progress in the field of uncertainty-based OOD detection will automatically translate into further improvements of our method.

Acknowledgements

This work was supported by the Swiss National Science Foundation (B.F.G. CRSII5-173721 and 315230_189251), ETH project funding (B.F.G. ETH-20 19-01) and funding from the Swiss Data Science Center (B.F.G, C17-18, J. v. O. P18-03). J.S. was supported by an Ambizione grant (PZ00P3_186027) from the Swiss National Science Foundation. We are grateful for discussions with Harald Dermutz, Simone Carlo Surace and Jean-Pascal Pfister. We also would like to thank Sebastian Farquhar for discussions on Radial posteriors and for proofreading our implementation of this method.

References

[1] T. Adel, H. Zhao, and R. E. Turner. Continual learning with adaptive weights (claw). In *International Conference on Learning Representations*, 2020.

[2] R. Aljundi, E. Belilovsky, T. Tuytelaars, L. Charlin, M. Caccia, M. Lin, and L. Page-Caccia. Online Continual Learning with Maximal Interfered Retrieval. *Advances in Neural Information Processing Systems*, 32, 2019.

[3] M. Arjovsky and L. Bottou. Towards principled methods for training generative adversarial networks. In *International Conference on Learning Representations*, 2017.

[4] O. Bachem, M. Lucic, and A. Krause. Coresets for nonparametric estimation - the case of dp-means. In F. Bach and D. Blei, editors, *Proceedings of the 32nd International Conference on Machine Learning*, volume 37 of *Proceedings of Machine Learning Research*, pages 209–217, Lille, France, 07–09 Jul 2015. PMLR.

[5] D. M. Blei, A. Kucukelbir, and J. D. McAuliffe. Variational inference: A review for statisticians. *Journal of the American Statistical Association*, 112(518):859–877, 2017. doi: 10.1080/01621459.2017.1285773.

[6] C. Blundell, J. Cornebise, K. Kavukcuoglu, and D. Wierstra. Weight uncertainty in neural networks. In F. Bach and D. Blei, editors, *Proceedings of the 32nd International Conference on*

are limited by the fact that the Bayesian recursive update is not applicable and therefore parameters cannot be updated in a sound way when learning continually.

Machine Learning, volume 37 of *Proceedings of Machine Learning Research*, pages 1613–1622, Lille, France, 07–09 Jul 2015. PMLR.

[7] Z. Borsos, M. Mutny, and A. Krause. Coresets via bilevel optimization for continual learning and streaming. In H. Larochelle, M. Ranzato, R. Hadsell, M. F. Balcan, and H. Lin, editors, *Advances in Neural Information Processing Systems*, volume 33, pages 14879–14890. Curran Associates, Inc., 2020.

[8] O. Chang, L. Flokas, and H. Lipson. Principled weight initialization for hypernetworks. In *International Conference on Learning Representations*, 2020.

[9] A. Chaudhry, M. Rohrbach, M. Elhoseiny, T. Ajanthan, P. K. Dokania, P. H. Torr, and M. Ranzato. Continual learning with tiny episodic memories. *arXiv*, 2019.

[10] Y. Chen, T. Diethe, and P. Flach. Discriminative representation loss (drl): Connecting deep metric learning to continual learning. *arXiv*, 2020.

[11] F. D'Angelo and C. Henning. Uncertainty-based out-of-distribution detection requires suitable function space priors. *arXiv*, 2021.

[12] M. De Lange and T. Tuytelaars. Continual prototype evolution: Learning online from non-stationary data streams. *arXiv*, 2020.

[13] S. Depeweg, J.-M. Hernandez-Lobato, F. Doshi-Velez, and S. Udluft. Decomposition of uncertainty in bayesian deep learning for efficient and risk-sensitive learning. In *International Conference on Machine Learning*, pages 1184–1193. PMLR, 2018.

[14] V. Dwaracherla, X. Lu, M. Ibrahimi, I. Osband, Z. Wen, and B. V. Roy. Hypermodels for exploration. In *International Conference on Learning Representations*, 2020.

[15] B. Ehret, C. Henning, M. R. Cervera, A. Meulemans, J. von Oswald, and B. F. Grewe. Continual learning in recurrent neural networks. In *International Conference on Learning Representations*, 2021.

[16] S. Farquhar and Y. Gal. Towards Robust Evaluations of Continual Learning. *Lifelong Learning: A Reinforcement Learning Approach Workshop at ICML*, 2018.

[17] S. Farquhar and Y. Gal. A unifying bayesian view of continual learning. *Bayesian Deep Learning Workshop at NeurIPS*, 2018.

[18] S. Farquhar, M. A. Osborne, and Y. Gal. Radial bayesian neural networks: Beyond discrete support in large-scale bayesian deep learning. In S. Chiappa and R. Calandra, editors, *Proceedings of the Twenty Third International Conference on Artificial Intelligence and Statistics*, volume 108 of *Proceedings of Machine Learning Research*, pages 1352–1362. PMLR, 26–28 Aug 2020.

[19] I. Goodfellow, J. Pouget-Abadie, M. Mirza, B. Xu, D. Warde-Farley, S. Ozair, A. Courville, and Y. Bengio. Generative adversarial nets. In Z. Ghahramani, M. Welling, C. Cortes, N. D. Lawrence, and K. Q. Weinberger, editors, *Advances in Neural Information Processing Systems 27*, pages 2672–2680. Curran Associates, Inc., 2014.

[20] I. J. Goodfellow, M. Mirza, D. Xiao, A. Courville, and Y. Bengio. An empirical investigation of catastrophic forgetting in gradient-based neural networks. *arXiv*, 2013.

[21] A. Gretton, K. M. Borgwardt, M. J. Rasch, B. Schölkopf, and A. Smola. A kernel two-sample test. *Journal of Machine Learning Research*, 13(25):723–773, 2012.

[22] D. Ha, A. Dai, and Q. Le. Hypernetworks. In *International Conference on Learning Representations*, 2017.

[23] K. He, X. Zhang, S. Ren, and J. Sun. Deep residual learning for image recognition. In *Proceedings of the IEEE conference on computer vision and pattern recognition*, pages 770–778, 2016.

[24] X. He, J. Sygnowski, A. Galashov, A. A. Rusu, Y. W. Teh, and R. Pascanu. Task agnostic continual learning via meta learning. *arXiv*, 2019.

[25] M. Hein, M. Andriushchenko, and J. Bitterwolf. Why relu networks yield high-confidence predictions far away from the training data and how to mitigate the problem. In *Proceedings of the IEEE/CVF Conference on Computer Vision and Pattern Recognition*, pages 41–50, 2019.

[26] D. Hendrycks and K. Gimpel. A Baseline for Detecting Misclassified and Out-of-Distribution Examples in Neural Networks. *arXiv*, 2016.

[27] C. Henning, J. von Oswald, J. Sacramento, S. C. Surace, J.-P. Pfister, and B. F. Grewe. Approximating the predictive distribution via adversarially-trained hypernetworks. In *NeurIPS Bayesian Deep Learning Workshop*, 2018.

[28] G. Hinton, O. Vinyals, and J. Dean. Distilling the knowledge in a neural network. *arXiv*, 2015.

[29] S. Hochreiter and J. Schmidhuber. Flat minima. *Neural Computation*, 9(1):1–42, Jan. 1997.

[30] T. Hu, Z. Chen, H. Sun, J. Bai, M. Ye, and G. Cheng. Stein neural sampler. *arXiv*, 2018.

[31] F. Huszár. Variational inference using implicit distributions. *arXiv*, 2017.

[32] F. Huszár. Note on the quadratic penalties in elastic weight consolidation. *Proceedings of the National Academy of Sciences*, 115(11):E2496–E2497, Mar. 2018.

[33] J. K J and V. N Balasubramanian. Meta-consolidation for continual learning. In H. Larochelle, M. Ranzato, R. Hadsell, M. F. Balcan, and H. Lin, editors, *Advances in Neural Information Processing Systems*, volume 33, pages 14374–14386. Curran Associates, Inc., 2020.

[34] T. Karaletsos and T. D. Bui. Hierarchical gaussian process priors for bayesian neural network weights. In H. Larochelle, M. Ranzato, R. Hadsell, M. F. Balcan, and H. Lin, editors, *Advances in Neural Information Processing Systems*, volume 33, pages 17141–17152. Curran Associates, Inc., 2020.

[35] T. Karaletsos, P. Dayan, and Z. Ghahramani. Probabilistic meta-representations of neural networks. *arXiv*, 2018.

[36] D. P. Kingma and M. Welling. Auto-encoding variational bayes. In *International Conference on Learning Representations*, 2014.

[37] D. P. Kingma, T. Salimans, and M. Welling. Variational dropout and the local reparameterization trick. In C. Cortes, N. Lawrence, D. Lee, M. Sugiyama, and R. Garnett, editors, *Advances in Neural Information Processing Systems*, volume 28, pages 2575–2583. Curran Associates, Inc., 2015.

[38] J. Kirkpatrick, R. Pascanu, N. Rabinowitz, J. Veness, G. Desjardins, A. A. Rusu, K. Milan, J. Quan, T. Ramalho, A. Grabska-Barwinska, D. Hassabis, C. Clopath, D. Kumaran, and R. Hadsell. Overcoming catastrophic forgetting in neural networks. *Proceedings of the National Academy of Sciences*, 114(13):3521–3526, Mar. 2017.

[39] A. Krizhevsky and G. Hinton. Learning multiple layers of features from tiny images. *Master's thesis, Department of Computer Science, University of Toronto*, 2009.

[40] D. Krueger, C.-W. Huang, R. Islam, R. Turner, A. Lacoste, and A. Courville. Bayesian Hypernetworks. *arXiv*, 2017.

[41] R. Kurle, B. Cseke, A. Klushyn, P. van der Smagt, and S. Günnemann. Continual learning with bayesian neural networks for non-stationary data. In *International Conference on Learning Representations*, 2020.

[42] B. Lakshminarayanan, A. Pritzel, and C. Blundell. Simple and scalable predictive uncertainty estimation using deep ensembles. In I. Guyon, U. V. Luxburg, S. Bengio, H. Wallach, R. Fergus, S. Vishwanathan, and R. Garnett, editors, *Advances in Neural Information Processing Systems*, volume 30, pages 6402–6413. Curran Associates, Inc., 2017.

[43] B. Lakshminarayanan, D. Tran, J. Liu, S. Padhy, T. Bedrax-Weiss, and Z. Lin. Simple and principled uncertainty estimation with deterministic deep learning via distance awareness. In *Advances in Neural Information Processing Systems 33*, 2020.

[44] Y. LeCun, L. Bottou, Y. Bengio, and P. Haffner. Gradient-based learning applied to document recognition. *Proceedings of the IEEE*, 86(11):2278–2324, 1998.

[45] K. Lee, H. Lee, K. Lee, and J. Shin. Training confidence-calibrated classifiers for detecting out-of-distribution samples. In *International Conference on Learning Representations*, 2018.

[46] S. Lee, J. Ha, D. Zhang, and G. Kim. A neural dirichlet process mixture model for task-free continual learning. In *International Conference on Learning Representations*, 2020.

[47] S.-W. Lee, J.-H. Kim, J. Jun, J.-W. Ha, and B.-T. Zhang. Overcoming catastrophic forgetting by incremental moment matching. In I. Guyon, U. V. Luxburg, S. Bengio, H. Wallach, R. Fergus, S. Vishwanathan, and R. Garnett, editors, *Advances in Neural Information Processing Systems*, volume 30, pages 4652–4662. Curran Associates, Inc., 2017.

[48] A. Li, A. J. Boyd, P. Smyth, and S. Mandt. Variational beam search for novelty detection. In *Third Symposium on Advances in Approximate Bayesian Inference*, 2021.

[49] H. Li, P. Barnaghi, S. Enshaeifar, and F. Ganz. Continual learning using bayesian neural networks. *IEEE Transactions on Neural Networks and Learning Systems*, 2020.

[50] S. Li, Y. Du, G. M. van de Ven, A. Torralba, and I. Mordatch. Energy-based models for continual learning. *arXiv*, 2020.

[51] Y. Li and R. E. Turner. Gradient estimators for implicit models. In *International Conference on Learning Representations*, 2018.

[52] L.-J. Lin. Self-improving reactive agents based on reinforcement learning, planning and teaching. *Machine learning*, 8(3-4):293–321, 1992.

[53] Q. Liu, J. Lee, and M. Jordan. A kernelized stein discrepancy for goodness-of-fit tests. In M. F. Balcan and K. Q. Weinberger, editors, *Proceedings of The 33rd International Conference on Machine Learning*, volume 48 of *Proceedings of Machine Learning Research*, pages 276–284, New York, New York, USA, 20–22 Jun 2016. PMLR.

[54] N. Loo, S. Swaroop, and R. E. Turner. Generalized variational continual learning. In *International Conference on Learning Representations*, 2021.

[55] C. Louizos and M. Welling. Multiplicative Normalizing Flows for Variational Bayesian Neural Networks. In *Proceedings of the 34th International Conference on Machine Learning - Volume 70*, ICML'17, pages 2218–2227. JMLR.org, 2017.

[56] D. J. MacKay. A practical bayesian framework for backpropagation networks. *Neural computation*, 4(3):448–472, 1992.

[57] D. J. MacKay. *Information theory, inference and learning algorithms*. Cambridge university press, 2003.

[58] A. Malinin, B. Mlodozeniec, and M. Gales. Ensemble distribution distillation. In *International Conference on Learning Representations*, 2020.

[59] J. Martens. New insights and perspectives on the natural gradient method. *Journal of Machine Learning Research*, 21(146):1–76, 2020.

[60] M. Masana, X. Liu, B. Twardowski, M. Menta, A. D. Bagdanov, and J. van de Weijer. Class-incremental learning: survey and performance evaluation on image classification. *arXiv*, 2020.

[61] L. Mescheder, S. Nowozin, and A. Geiger. Adversarial variational bayes: Unifying variational autoencoders and generative adversarial networks. In *Proceedings of the 34th International Conference on Machine Learning*, volume 70 of *Proceedings of Machine Learning Research*, pages 2391–2400, International Convention Centre, Sydney, Australia, 06–11 Aug 2017. PMLR.

[62] J. Mukhoti, A. Kirsch, J. van Amersfoort, P. H. Torr, and Y. Gal. Deterministic neural networks with appropriate inductive biases capture epistemic and aleatoric uncertainty. *arXiv*, 2021.

[63] M. Mundt, Y. W. Hong, I. Pliushch, and V. Ramesh. A wholistic view of continual learning with deep neural networks: Forgotten lessons and the bridge to active and open world learning. *arXiv*, 2020.

[64] E. Nalisnick, A. Matsukawa, Y. W. Teh, D. Gorur, and B. Lakshminarayanan. Do deep generative models know what they don't know? In *International Conference on Learning Representations*, 2019.

[65] C. V. Nguyen, Y. Li, T. D. Bui, and R. E. Turner. Variational continual learning. In *6th International Conference on Learning Representations, ICLR 2018, Vancouver, BC, Canada, April 30 - May 3, 2018, Conference Track Proceedings*, 2018.

[66] F. Nielsen. Cramér-rao lower bound and information geometry. In *Connected at Infinity II*, pages 18–37. Springer, 2013.

[67] S. Nowozin, B. Cseke, and R. Tomioka. f-gan: Training generative neural samplers using variational divergence minimization. In D. Lee, M. Sugiyama, U. Luxburg, I. Guyon, and R. Garnett, editors, *Advances in Neural Information Processing Systems*, volume 29, pages 271–279. Curran Associates, Inc., 2016.

[68] J. V. Oswald, S. Kobayashi, J. Sacramento, A. Meulemans, C. Henning, and B. F. Grewe. Neural networks with late-phase weights. In *International Conference on Learning Representations*, 2021.

[69] P. Pan, S. Swaroop, A. Immer, R. Eschenhagen, R. Turner, and M. E. E. Khan. Continual deep learning by functional regularisation of memorable past. In H. Larochelle, M. Ranzato, R. Hadsell, M. F. Balcan, and H. Lin, editors, *Advances in Neural Information Processing Systems*, volume 33, pages 4453–4464. Curran Associates, Inc., 2020.

[70] G. Papamakarios, E. Nalisnick, D. J. Rezende, S. Mohamed, and B. Lakshminarayanan. Normalizing flows for probabilistic modeling and inference. *arXiv*, 2019.

[71] G. I. Parisi, R. Kemker, J. L. Part, C. Kanan, and S. Wermter. Continual lifelong learning with neural networks: A review. *Neural Networks*, 113:54–71, May 2019. ISSN 0893-6080. doi: 10.1016/j.neunet.2019.01.012.

[72] R. Pascanu and Y. Bengio. Revisiting natural gradient for deep networks. *arXiv*, 2013.

[73] N. Pawlowski, A. Brock, M. C. Lee, M. Rajchl, and B. Glocker. Implicit weight uncertainty in neural networks. *arXiv*, 2017.

[74] A. Prabhu, P. H. Torr, and P. K. Dokania. Gdumb: A simple approach that questions our progress in continual learning. In *European Conference on Computer Vision*, pages 524–540. Springer, 2020.

[75] S.-A. Rebuffi, A. Kolesnikov, G. Sperl, and C. H. Lampert. icarl: Incremental classifier and representation learning. In *Proceedings of the IEEE conference on Computer Vision and Pattern Recognition*, pages 2001–2010, 2017.

[76] H. Ritter, A. Botev, and D. Barber. Online structured laplace approximations for overcoming catastrophic forgetting. In S. Bengio, H. Wallach, H. Larochelle, K. Grauman, N. Cesa-Bianchi, and R. Garnett, editors, *Advances in Neural Information Processing Systems*, volume 31, pages 3738–3748. Curran Associates, Inc., 2018.

[77] J. Schmidhuber. Learning to Control Fast-Weight Memories: An Alternative to Dynamic Recurrent Networks. *Neural Comput.*, 4(1):131–139, Jan 1992. ISSN 0899-7667. doi: 10.1162/neco.1992.4.1.131.

[78] J. Schwarz, W. Czarnecki, J. Luketina, A. Grabska-Barwinska, Y. W. Teh, R. Pascanu, and R. Hadsell. Progress & compress: A scalable framework for continual learning. In J. Dy and A. Krause, editors, *Proceedings of the 35th International Conference on Machine Learning*, volume 80 of *Proceedings of Machine Learning Research*, pages 4528–4537, Stockholmsmässan, Stockholm Sweden, 10–15 Jul 2018. PMLR.

[79] J. Shi, S. Sun, and J. Zhu. A spectral approach to gradient estimation for implicit distributions. In J. Dy and A. Krause, editors, *Proceedings of the 35th International Conference on Machine Learning*, volume 80 of *Proceedings of Machine Learning Research*, pages 4644–4653, Stockholmsmässan, Stockholm Sweden, 10–15 Jul 2018. PMLR.

[80] H. Shin, J. K. Lee, J. Kim, and J. Kim. Continual Learning with Deep Generative Replay. In I. Guyon, U. V. Luxburg, S. Bengio, H. Wallach, R. Fergus, S. Vishwanathan, and R. Garnett, editors, *Advances in Neural Information Processing Systems 30*, pages 2990–2999. Curran Associates, Inc., 2017.

[81] L. Smith and Y. Gal. Understanding Measures of Uncertainty for Adversarial Example Detection. *arXiv*, 2018.

[82] J. Snoek, Y. Ovadia, E. Fertig, B. Lakshminarayanan, S. Nowozin, D. Sculley, J. Dillon, J. Ren, and Z. Nado. Can you trust your model's uncertainty? evaluating predictive uncertainty under dataset shift. In *Advances in Neural Information Processing Systems*, pages 13969–13980, 2019.

[83] S. Swaroop, C. V. Nguyen, T. D. Bui, and R. E. Turner. Improving and understanding variational continual learning. *Continual Learning Workshop at NeurIPS*, 2018.

[84] M. K. Titsias, J. Schwarz, A. G. de G. Matthews, R. Pascanu, and Y. W. Teh. Functional regularisation for continual learning with gaussian processes. In *International Conference on Learning Representations*, 2020.

[85] T. Tuor, S. Wang, and K. Leung. Continual learning without knowing task identities: Do simple models work? *OpenReview*, 2021.

[86] G. M. van de Ven and A. S. Tolias. Generative replay with feedback connections as a general strategy for continual learning. *arXiv*, 2018.

[87] G. M. van de Ven and A. S. Tolias. Three scenarios for continual learning. *arXiv*, Apr 2019.

[88] G. M. van de Ven, H. T. Siegelmann, and A. S. Tolias. Brain-inspired replay for continual learning with artificial neural networks. *Nature communications*, 11(1):1–14, 2020.

[89] G. M. van de Ven, Z. Li, and A. S. Tolias. Class-incremental learning with generative classifiers. In *Proceedings of the IEEE/CVF Conference on Computer Vision and Pattern Recognition (CVPR) Workshops*, pages 3611–3620, June 2021.

[90] V. K. Verma, K. J. Liang, N. Mehta, P. Rai, and L. Carin. Efficient feature transformations for discriminative and generative continual learning. In *Proceedings of the IEEE/CVF Conference on Computer Vision and Pattern Recognition*, pages 13865–13875, 2021.

[91] J. von Oswald, C. Henning, J. Sacramento, and B. F. Grewe. Continual learning with hypernetworks. In *International Conference on Learning Representations*, 2020.

[92] F. Wenzel, K. Roth, B. Veeling, J. Swiatkowski, L. Tran, S. Mandt, J. Snoek, T. Salimans, R. Jenatton, and S. Nowozin. How good is the Bayes posterior in deep neural networks really? In H. D. III and A. Singh, editors, *Proceedings of the 37th International Conference on Machine Learning*, volume 119 of *Proceedings of Machine Learning Research*, pages 10248–10259. PMLR, 13–18 Jul 2020.

[93] A. G. Wilson and P. Izmailov. Bayesian deep learning and a probabilistic perspective of generalization. In *Advances in Neural Information Processing Systems*, 2020.

[94] M. Wortsman, V. Ramanujan, R. Liu, A. Kembhavi, M. Rastegari, J. Yosinski, and A. Farhadi. Supermasks in superposition. In *Advances in Neural Information Processing Systems*, 2020.

[95] S. Zagoruyko and N. Komodakis. Wide residual networks. In *Proceedings of the British Machine Vision Conference*, 2016.

[96] F. Zenke, B. Poole, and S. Ganguli. Continual Learning Through Synaptic Intelligence. In *Proceedings of the 34th International Conference on Machine Learning - Volume 70*, ICML'17, pages 3987–3995. JMLR.org, 2017.

[97] C. Zeno, I. Golan, E. Hoffer, and D. Soudry. Task-agnostic continual learning using online variational bayes with fixed-point updates. *Neural Computation*, 33(11):3139–3177, 2021.

[98] C. Zhang, S. Bengio, M. Hardt, B. Recht, and O. Vinyals. Understanding deep learning requires rethinking generalization. In *International Conference on Learning Representations*, 2017.

Supplementary Material:
Posterior Meta-Replay for Continual Learning

Christian Henning*, Maria R. Cervera*, Francesco D'Angelo, Johannes von Oswald, Regina Traber, Benjamin Ehret, Seijin Kobayashi, Benjamin F. Grewe, João Sacramento

Table of Contents

A Acronyms **2**

B Summary of Notation **2**

C Algorithms **3**
C.1 Variational inference . . . 3
C.2 Task-conditioned hypernetworks . . . 3
C.3 Posterior-Replay with explicit parametric distributions . . . 5
C.4 Posterior-Replay with implicit distributions . . . 7
C.5 Prior-Focused Continual Learning . . . 11
C.6 Task inference . . . 15
C.7 Posterior-Replay CL with Coreset Fine-Tuning . . . 16
C.8 Experience Replay . . . 17

D Supplementary Experiments and Results **17**
D.1 1D Polynomial Regression . . . 18
D.2 2D Mode Classification . . . 19
D.3 SplitMNIST . . . 23
D.4 PermutedMNIST-10 . . . 26
D.5 PermutedMNIST-100 . . . 28
D.6 SplitCIFAR-10 . . . 28
D.7 SplitCIFAR-100 . . . 30
D.8 Task boundary detection during training . . . 31

E Experimental Details **32**
E.1 1D Polynomial Regression Dataset . . . 32
E.2 2D Mode Classification Dataset . . . 32
E.3 Hyperparameter selection . . . 34

F Further Discussion and Remarks **34**
F.1 On Posterior Meta-Replay as a Bayesian method . . . 34
F.2 Runtime and storage complexity . . . 35
F.3 Continual learning regularization in distribution space . . . 37
F.4 Optimization considerations in Posterior-Replay . . . 38
F.5 Deep Ensembles . . . 38
F.6 Continual learning in function space . . . 39
F.7 Graceful forgetting . . . 39

A Acronyms

For clarity, we provide a list of acronyms used throughout the paper in Table S1.

Table S1: List of acronyms.

ML	Machine learning
CL	Continual learning
MLP	Multilayer perceptron
SEM	Standard error of the mean
SD	Standard deviation
MSE	Mean-squared error
NLL	Negative log-likelihood
BNN	Bayesian neural network
VI	Variational inference
ELBO	Evidence lower-bound
RKL/FKL	Reverse/Forward Kullback-Leibler divergence
W2	2-Wasserstein distance
MC	Monte Carlo
AVB	Adversarial variational Bayes
BBB	Bayes-by-Backprop
EWC	Elastic weight consolidation
SSGE	Spectral Stein gradient estimator
VCL	Variational continual learning
PF	Prior-focused
PR	Posterior meta-replay
M	Main network
WG	Weight generator
TC	Task-conditioning network
BW	Task inference using batches
CS	Final fine-tuning using coresets
SP	Separate posteriors per task
OOD	Out of distribution
TGIVEN	Task identity is given
TINFER	Task identity is inferred
ENT	Task inference via minimum entropy
CONF	Task inference via maximum confidence
AGREE	Task inference via maximum model agreement

B Summary of Notation

We summarize here the mathematical notation used throughout the paper and reintroduce the role of important variables. Whenever applicable, we denote random variables by capital letters, random variates by lowercase letters and sample spaces using calligraphic font, e.g., the prior density of $w \in \mathcal{W}$ is $p(W = w)$. In general, sets use calligraphic font. Vectors are assumed to be column vectors and highlighted as bold symbols. Indexing is performed using subscripts, e.g., x_i is the i-th component of $\mathbf{x} \in \mathcal{X}$. Superscripts are used to disambiguate external factors such as task identity. Matrices also use capital letters, and it is clearly stated whenever a variable has to be interpreted as matrix, e.g., the *Fisher information matrix* F.

In this study, we distinguish between three different networks with clearly defined roles (plus a *discriminator* network when using AVB). The *main network* (M), $\hat{\mathbf{y}} = f_{\text{M}}(\mathbf{x}, \mathbf{w})$, processes inputs $\mathbf{x}$ to generate predictions $\hat{\mathbf{y}}$ using trainable parameters $\mathbf{w}$. This notation is chosen for mathematical convenience, but it should be noted that in most cases $f_{\text{M}}(\cdot)$ represents a likelihood function. For instance, in the case of a C-way classification with labels $y \in \mathcal{Y} = \{1, \dots, C\}$, the output of the main network is an element of the probability simplex $\Delta(\mathcal{Y})$, and in regression $f_{\text{M}}(\cdot)$ represents the mean of a normal distribution $\mathcal{N}\big(f_{\text{M}}(\cdot), \sigma_{\text{ll}}^2\big)$ with variance σ_{ll}^2. The *task-conditioned hypernetwork* (TC), $\boldsymbol{\theta}^{(t)} = f_{\text{TC}}(\mathbf{e}^{(t)}, \boldsymbol{\psi})$, has parameters $\boldsymbol{\psi}$ and processes task embeddings $\mathbf{e}^{(t)}$ to generate the

parameters $\boldsymbol{\theta}^{(t)}$ of the *weight generator* (WG). In the deterministic case (e.g., *PosteriorReplay-Dirac*), the weight generator simply reduces to $\mathbf{w}^{(t)} \equiv \boldsymbol{\theta}^{(t)} = f_{\text{WG}}(\cdot, \boldsymbol{\theta}^{(t)})$. In all other cases, it transforms noise samples $\mathbf{z} \sim p(\mathbf{Z})$ into main network parameter configurations.

A dataset is a set of input-output tuples $\mathcal{D} = \{(\mathbf{x}^{(n)}, \mathbf{y}^{(n)})\}_{n=1}^{N}$. If not noted otherwise, a dataset is considered an i.i.d. sample from some unknown data-generating process $\mathcal{D} \overset{i.i.d.}{\sim} p(\mathbf{X})p(\mathbf{Y} \mid \mathbf{X})$.

We consider a Bayesian treatment of main network parameters $\mathbf{w}$ to incorporate parameter uncertainty [56]. The prior is denoted by $p(\mathbf{W})$, the likelihood by $p(\mathcal{D} \mid \mathbf{W}) \equiv \prod_{n=1}^{N} p(\mathbf{y}^{(n)} \mid \mathbf{W}; \mathbf{x}^{(n)})$, the posterior parameter distribution by $p(\mathbf{W} \mid \mathcal{D})$ and the posterior predictive distribution for an unseen input $\tilde{\mathbf{x}}$ by $p(\mathbf{Y} \mid \mathcal{D}; \tilde{\mathbf{x}})$. We consider families of distributions parametrized by $\boldsymbol{\theta}$ to approximate the posterior parameter distribution $q_{\boldsymbol{\theta}}(\mathbf{W}) \approx p(\mathbf{W} \mid \mathcal{D})$, e.g., for the deterministic case we have $q_{\boldsymbol{\theta}}(\mathbf{W}) = \delta(\boldsymbol{\theta} - \mathbf{W})$, where $\delta(\cdot)$ denotes the Dirac delta function.

C Algorithms

In this section we provide details about the different algorithms used throughout the paper. We start by quickly reviewing variational inference, and explain how it can be applied to task-conditioned hypernetworks in the context of CL in order to obtain task-specific approximate posterior distributions. Then, we present several variational algorithms that we employed to obtain the approximate posteriors, either based on a predefined function (*explicit* posterior) or based on a parametrization by an auxiliary network (*implicit* posterior). We also explain how *prior-focused* CL can be achieved within our framework, and how it can be rendered more flexible by allowing the parameter posteriors to be approximated by *implicit* distributions, and by incorporating a set of task-specific parameters alongside the shared ones. Because task-specific solutions require having access to the identity of the task, we explain how task identity can be inferred via predictive uncertainty for both *prior-focused* and *posterior meta-replay* approaches. Finally, we explain how coresets can be used in our framework to perform a fine-tuning stage after training which mitigates forgetting and facilitates task inference.

C.1 Variational inference

Whenever confronted with unseen inputs $\tilde{\mathbf{x}}$, we aspire to obtain predictions via the posterior predictive distribution: $p(\mathbf{y} \mid \mathcal{D}; \tilde{\mathbf{x}}) = \int_{\mathbf{W}} p(\mathbf{y} \mid \mathbf{W}; \tilde{\mathbf{x}}) p(\mathbf{W}|\mathcal{D})\, d\mathbf{W}$. Unfortunately, the posterior parameter distribution $p(\mathbf{W}|\mathcal{D})$ is in general intractable. Furthermore, since sampling cannot be efficiently performed and would require high storage demands, we need to approximate this distribution in order to evaluate the posterior predictive distribution. For this purpose, we apply variational inference (VI), a standard approximate probabilistic inference technique (see e.g., Blei et al. [5]) where we look for approximations $q_{\boldsymbol{\theta}}(\mathbf{W})$ within a certain family of distributions $\mathcal{Q}$, referred to as the *variational family*, with members parametrized by $\boldsymbol{\theta} \in \Theta$. In VI, this problem is solved by optimizing for nearest approximations within $\mathcal{Q}$ according to some divergence, most often the Kullback-Leibler (KL) divergence: $\text{KL}(q_{\boldsymbol{\theta}}(\mathbf{W}) \mid\mid p(\mathbf{W} \mid \mathcal{D}))$. The choice of the reverse KL allows rewriting the above expression such that it does not contain the intractable posterior. The resulting expression (known as the evidence lower bound; ELBO) is therefore a suitable optimization objective that needs to be maximized:

$$\mathbb{E}_{q_{\boldsymbol{\theta}}(\mathbf{W})}\big[\log p(\mathcal{D} \mid \mathbf{W})\big] - \text{KL}(q_{\boldsymbol{\theta}}(\mathbf{W}) \mid\mid p(\mathbf{W})) \equiv -\mathcal{L}_{\text{task}}(\mathcal{D}) \tag{3}$$

where the first term corresponds to minimizing the negative log-likelihood (NLL) of the data $\mathcal{D}$ (cf. SM C.3.1), and the second term can be seen as a regularization that aims to match the approximation $q_{\boldsymbol{\theta}}(\mathbf{W})$ to the prior $p(\mathbf{W})$, and is referred to as *prior-matching term*. Finding an optimal approximation within the variational family amounts to optimizing the parameters $\boldsymbol{\theta}$. Since in our framework these are task-specific and their optimization depends only on the corresponding dataset $\mathcal{D}^{(t)}$ we write from here on $q_{\boldsymbol{\theta}^{(t)}}(\mathbf{W})$.

C.2 Task-conditioned hypernetworks

Task-conditioned hypernetworks, which generate task-specific weights for a main network, have recently been proposed as an effective method to continually learn several tasks [91]. The outputs of the hypernetwork are made task-specific by providing low-dimensional task embeddings $\mathbf{e}^{(t)}$ as input,

which are learned continually alongside the hypernetwork's parameters $\boldsymbol{\psi}$. Catastrophic forgetting at this meta level can be prevented using a simple L2 regularizer (cf. Eq. 2 in the main text) which makes sure that the outputs of the hypernetwork for previously learned tasks do not change. When learning task t the loss thus becomes:

$$\mathcal{L}^{(t)}(\boldsymbol{\psi}, \mathcal{E}, \mathcal{D}^{(t)}) = \mathcal{L}_{\text{task}}(\boldsymbol{\psi}, \mathbf{e}^{(t)}, \mathcal{D}^{(t)}) + \beta \sum_{t'<t} \| f_{\text{TC}}(\mathbf{e}^{(t',*)}, \boldsymbol{\psi}^*) - f_{\text{TC}}(\mathbf{e}^{(t')}, \boldsymbol{\psi}) \|^2 \tag{4}$$

Notably, shifting CL to the meta-level simplifies the problem considerably, because only a single input-output mapping per task needs to be fixed.

Chunking. Here we consider hypernetworks that parameterize target models in a compressed form using a simple but effective technique called *chunking*: the hypernetwork is iteratively invoked using an additional input $\mathbf{c}$ at each step, which addresses a distinct subset of parameters (e.g., a distinct layer of the target neural network). To be precise, chunk embeddings $\mathbf{c}^{(l)}$, $l = 1..L$, are unconditional parameters (i.e., not task-specific). Thus, the hypernetwork parameters $\boldsymbol{\psi}$ can be split into a set of chunk embeddings $\{\mathbf{c}^{(l)}\}_{l=1}^{L}$ and a set of weights $\tilde{\boldsymbol{\psi}}$, which are the actual weights of the network that produces individual chunks. This introduces soft weight sharing, as the entire set of target model parameters $\mathbf{w}$ depends on $\tilde{\boldsymbol{\psi}}$. Note, that modern graphics hardware allows the parallel generation of all chunks (batch-processing). For more details, please refer to von Oswald et al. [91] and Ehret et al. [15]. For all experiments other than the low-dimensional toy problems, we apply the chunking strategy to the TC and WG networks. Low-dimensional problems utilize MLP hypernetworks, where $\mathbf{w}$ is directly the output of the network. Both task and chunk embeddings are initialized according to a normal distribution with zero mean, whose variance is considered a hyperparameter.

Probabilistic extension of task-conditioned hypernetworks. In their original formulation, hypernetworks for CL provide a single main network weight configuration per task (*PosteriorReplay-Dirac*). Here, we extend this deterministic approach to a probabilistic setting and aim to model task-specific *distributions* over main network weights instead. Therefore, the outputs of the hypernetwork can no longer be interpreted as the weights $\mathbf{w}$ of the main network, but rather as parameters $\boldsymbol{\theta}^{(t)}$ defining the approximate distribution $q_{\boldsymbol{\theta}^{(t)}}(\mathbf{W})$, from which weights $\mathbf{w}$ for the main network can be sampled. In practice, $q_{\boldsymbol{\theta}^{(t)}}(\mathbf{W})$ is given by a function $f_{\text{WG}}(\mathbf{z}, \boldsymbol{\theta}^{(t)})$, which also depends on a base distribution $p(\mathbf{Z})$ from which inputs $\mathbf{z}$ for the hypernetwork are sampled.

Meta-regularizing in distribution space. Crucially, in this probabilistic setting, catastrophic forgetting is avoided via a regularizer that prevents the distributions $q_{\boldsymbol{\theta}^{(t)}}(\mathbf{W})$ of previously learned tasks to change, hence our naming *posterior meta-replay*. Whenever the utilized variational family for approximate posteriors has an analytic expression for a divergence measure, this can be achieved by turning the original hypernetwork regularizer into a divergence measure between the distributions (cf. Eq. 1) before and after any given task is being learned. However divergence measures cannot always be analytically evaluated, for example if the distributions are *implicit*, in which case other solutions are necessary. One option is to use a sample-based distance estimate between the distributions [21, 53], which would act upon the output of the WG network (i.e., the weight samples). However, due to the high dimensionality of $\mathbf{w}$, meaningful distance estimates in distribution space might be prohibitively expensive since the regularizer has to be evaluated in every training iteration. For this reason, whenever no analytic divergence measure is available, we resort to the use of a mean-squared error (MSE) regularizer at the output of the TC network (Eq. 2), as done in the deterministic case considered by von Oswald et al. [91]. Therefore, rather than ensuring that a distribution does not change, we ensure that the parameters of a distribution do not change. Note however, that this treatment forces an interpretation onto the TC network as encoding a Gaussian likelihood with isotropic variance.

While in our experiments forgetting is not a prevailing issue and we therefore were not urged to improve upon this simple regularization, we would still like to comment on potential improvements that can be considered by future work. One option would be to assign importance values to individual outputs of the TC network and thus transform the isotropic regularization of Eq. 2 into a weighted sum per previous task. Such importance values could incorporate the curvature of the loss landscape. As the task-specific loss is data-dependent, the importance values would need to be computed at the end of the training of each task, where data is still accessible. In our case, the task-specific loss is the ELBO (Eq. 3), which embodies the KL to the posterior $p(\mathcal{D} \mid \mathbf{W})$. Thus, if importance values reflect the Hessian of the ELBO with respect to the outputs of the TC network, the CL regularization

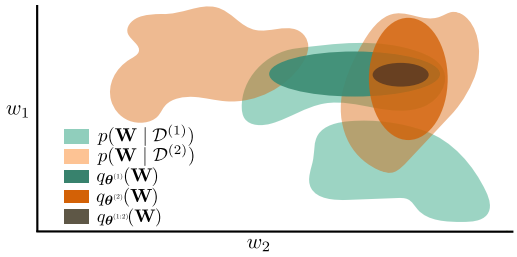

Figure S1: Differences between *prior-focused* and *posterior-replay* CL approaches when using Gaussian posterior approximations with diagonal covariance. In this case, the proposed *posterior meta-replay* framework can capture one mode of each task-specific posterior via $q_{\boldsymbol{\theta}^{(1)}}(\mathbf{W})$ and $q_{\boldsymbol{\theta}^{(2)}}(\mathbf{W})$. In contrast, a *prior-focused* method with this type of approximation (e.g., EWC [38] or VCL [65]) has to assume that the currently found mode $q_{\boldsymbol{\theta}^{(1:2)}}(\mathbf{W})$ also contains admissible solutions for upcoming tasks.

would target our posterior approximation criterion (i.e., the ELBO) directly, ensuring that parameter changes are only tolerated if the ELBO remains stable. In SM. F.3 we further elaborate on how importance values could be constructed such that this simple type of regularization can be interpreted as preserving distances in distribution space. Nonetheless, an imminent drawback of this procedure is the need to store the importance values of each previous task.[5] However, the memory implications of this shortcoming can be alleviated by using compression schemes for importance values or by distilling them into an auxiliary network [28].

C.3 Posterior-Replay with explicit parametric distributions

We now present the algorithms that can be used to obtain what we refer to as *explicit* approximate posterior distributions, i.e., simple posterior approximations $q_{\boldsymbol{\theta}^{(t)}}(\mathbf{W})$ that can be sampled from according to a predefined function (cf. Eq. 5 and Eq. 12). Although in the main text only results obtained for BbB are reported (noted *PosteriorReplay-Exp*), we consider here additional *explicit* methods and therefore denote each individual method as *PosteriorReplay-<method>*.

C.3.1 Bayes-by-Backprop

Blundell et al. [6] present Bayes-by-Backprop (BbB), a VI algorithm that uses a mean-field Gaussian approximation, i.e., $q_{\boldsymbol{\theta}}(\mathbf{W}) = \prod_i \mathcal{N}(W_i; \mu_i, \sigma_i^2)$, where $\boldsymbol{\theta}$ consists of vectors $\boldsymbol{\mu}$ and $\boldsymbol{\sigma}^2$ containing a mean and variance for each weight. To be able to optimize these two vectors, the authors make use of the *reparametrization trick* [36], which allows gradient computation with respect to $\boldsymbol{\mu}$ and $\boldsymbol{\sigma}$ through the stochastic sampling process of $q_{\boldsymbol{\theta}}(\mathbf{W})$. Specifically, samples $\mathbf{w}$ are obtained via:

$$\mathbf{w} = \boldsymbol{\mu} + \boldsymbol{\sigma} \odot \boldsymbol{\epsilon} \tag{5}$$

where $\boldsymbol{\epsilon} \sim \mathcal{N}(0, \mathbf{I})$.

Recall, that optimizing the ELBO (cf. Eq. 3) requires estimating the NLL $-\mathbb{E}_{q_{\boldsymbol{\theta}}(\mathbf{W})}[\log p(\mathcal{D} \mid \mathbf{W})]$, which in practice is achieved via a Monte-Carlo (MC) estimate of K samples $\mathbf{w}^{(k)} \sim q_{\boldsymbol{\theta}}(\mathbf{W})$:

$$\text{NLL} \approx -\frac{1}{K} \sum_{k=1}^{K} \log p(\mathcal{D} \mid \mathbf{W} = \mathbf{w}^{(k)}) \tag{6}$$

As a full summation $\log p(\mathcal{D} \mid \mathbf{W}) = \sum_{n=1}^{N} \log p(\mathbf{y}^{(n)} \mid \mathbf{W}; \mathbf{x}^{(n)})$ over the whole dataset at every training iteration is prohibitively expensive, this term is approximated via mini-batches $\mathcal{B}$ of size N_{mb}, which requires a corrective scaling:

$$\text{NLL} \approx -\frac{1}{K} \sum_{k=1}^{K} \frac{N}{N_{\text{mb}}} \sum_{(\mathbf{x},\mathbf{y}) \in \mathcal{B}} \log p(\mathbf{y} \mid \mathbf{w}^{(k)}; \mathbf{x}) \tag{7}$$

[5] Note, that also the original EWC formulation required the storage of one Fisher matrix per task [38].

How to compute the term $\log p(\mathbf{y} \mid \mathbf{w}; \mathbf{x})$ depends on the problem at hand. In regression tasks, it is common to model the likelihood as a Gaussian distribution. For simplicity, we only consider 1D regression and a model likelihood with fixed variance σ_{ll}^2 such that:

$$\log p(y \mid \mathbf{w}; x) = \text{const} - \frac{1}{2\sigma_{\text{ll}}^2} \big(f_{\text{M}}(x, \mathbf{w}) - y\big)^2 \tag{8}$$

Dropping all constant terms that do not affect the optimization, the NLL can be written as a properly scaled ($\frac{N}{2\sigma_{\text{ll}}^2}$) MSE loss inside an MC estimate:

$$\text{NLL} \approx \frac{N}{2KN_{\text{mb}}\sigma_{\text{ll}}^2} \sum_{k=1}^{K} \sum_{(x,y)\in\mathcal{B}} \big(f_{\text{M}}(x, \mathbf{w}^{(k)}) - y\big)^2 \tag{9}$$

In C-way classification problems, the likelihood of class c is computed as:

$$p(Y = c \mid \mathbf{w}; \mathbf{x}) = \text{sm}\big(f_{\text{M}}(\mathbf{x}, \mathbf{w})\big)_c \tag{10}$$

where $\text{sm}(\cdot)$ refers to the softmax, assuming the main network produces unnormalized logits for mathematical convenience. Under this notation, the NLL for classification problems can be estimated as follows:

$$\begin{aligned}
\text{NLL} &\approx -\frac{N}{KN_{\text{mb}}} \sum_{k=1}^{K} \sum_{(\mathbf{x},y)\in\mathcal{B}} \log\Big(\text{sm}\big(f_{\text{M}}(\mathbf{x}, \mathbf{w}^{(k)})\big)_y\Big) \\
&= \frac{N}{KN_{\text{mb}}} \sum_{k=1}^{K} \sum_{(\mathbf{x},y)\in\mathcal{B}} \Bigg(\\
&\quad \underbrace{-\sum_{c=1}^{C} [c = y] \log\Big(\text{sm}\big(f_{\text{M}}(\mathbf{x}, \mathbf{w}^{(k)})\big)_c\Big)}_{\text{cross-entropy loss with 1-hot targets}} \Bigg)
\end{aligned} \tag{11}$$

where $[\cdot]$ denotes the Iverson bracket. The second term in the ELBO, i.e., the *prior-matching term*, can be analytically evaluated if a Gaussian prior is used.

We adapt the BbB algorithm to our *posterior meta-replay* framework by having a task-conditioned (TC) network that generates task-specific $\boldsymbol{\mu}^{(t)}$ and $\boldsymbol{\sigma}^{(t)}$ (Fig. S1), an approach we denote **PosteriorReplay-BbB** (*PosteriorReplay-Exp* in the main text). Since outputs of the TC network are real-valued, variances $\boldsymbol{\sigma}^{(t)}$ are obtained through a softplus transformation of the network's outputs. The current task's loss $\mathcal{L}_{\text{task}}(\boldsymbol{\psi}, \mathbf{e}^{(t)}, \mathcal{D}^{(t)})$ corresponds to the negative ELBO and can be estimated as described above, where we use the analytic expression for the *prior-matching term*.

Since approximate posteriors in BbB correspond to Gaussian distributions, the CL regularizer can take the form of an explicit divergence measure in distribution space computed solely based on the TC network's output. We experiment with the forward (FKL) and reverse KL (RKL), and the 2-Wasserstein distance (W2). The loss when learning task t therefore becomes Eq. 1, where $\text{D}(\cdot||\cdot)$ corresponds to one of the above mentioned divergence measures. In practice, we do not observe a notable difference between any of these divergence measures and the L2 regularization in Eq. 2.

As a variance reduction trick to improve training stability, we also experiment with the *local reparametrization trick* [37] whenever the main network has an MLP architecture. Whether or not this trick is used is determined by a hyperparameter and therefore selected by the hyperparameter search of each experiment conducted with BbB or VCL (cf. SM C.5.1).

C.3.2 Radial Posteriors

As an alternative method to obtain *explicit* posterior approximations we also experimented with *radial* posteriors [18], which we briefly describe below.

Intuitively, one would expect that the probability mass of a Gaussian lies around the mean. This is however not the case in high dimensions, where the probability mass is clustered in a thin hyper-annulus far away from the mean. This happens because a sample point from an isotropic, high-dimensional Gaussian distribution can be interpreted as many sample points from the corresponding 1D Gaussian distribution, therewith representing with high probability an element of the typical set. Farquhar et al. [18] argues that training BNNs with a mean-field Gaussian approximation (as in BbB), can lead to gradient estimates with high variance and impaired training stability due to the effects that arise due to typicality in isotropic, high-dimensional Gaussian distributions. Based on this insight, Farquhar et al. [18] propose the following corrective normalization to Eq. 5, and argue it helps recover the intuitive behavior of Gaussian distributions in low dimensions:

$$\mathbf{w} = \boldsymbol{\mu} + \boldsymbol{\sigma} \odot \frac{\boldsymbol{\epsilon}}{\|\boldsymbol{\epsilon}\|} \cdot r \tag{12}$$

where $r \sim \mathcal{N}(0, 1)$ and $\boldsymbol{\epsilon} \sim \mathcal{N}(0, I)$. Here, we apply the corrective normalization layer-wise, but treating weights and biases separately, such that the dimensions of I correspond to the number of weights or biases in a given layer.

When computing the *prior-matching term* between a *radial* approximation and a Gaussian prior $p(\mathbf{W})$, we use the following expression for the negative entropy of a *radial* distribution (cf. Eq. 5 in Farquhar et al. [18]):

$$\int q_{\boldsymbol{\theta}}(\mathbf{W}) \log q_{\boldsymbol{\theta}}(\mathbf{W}) d\mathbf{W} = -\sum_i \log \sigma_i + \text{const} \tag{13}$$

The cross-entropy term is approximated via an MC estimate with samples from the *radial* posterior. Note, that the log-density of the Gaussian prior can be computed analytically.

We use *radial* posteriors within our framework (**PosteriorReplay-Radial**), where task-specific means $\boldsymbol{\mu}$ and "variances" $\boldsymbol{\sigma}^2$ are generated by a TC hypernetwork, whose outputs need to be regularized to prevent forgetting (cf. SM C.3.1). Because an analytic expression for a divergence between *radial* distributions is unknown, we resort to the L2 hypernetwork regularizer (Eq. 2) when working with *radial* distributions.

C.4 Posterior-Replay with implicit distributions

We also explore the use of *implicit* $q_{\boldsymbol{\theta}^{(t)}}(\mathbf{W})$ distributions as approximate posteriors. In our framework, these are parametrized by an auxiliary WG network, that has parameters $\boldsymbol{\theta}^{(t)}$ and receives samples from an arbitrary base distribution $p(\mathbf{Z})$ as inputs. In our experiments, we always consider a Gaussian base distribution with zero mean, and experiment with different variances.

The use of implicit posterior approximations introduces a challenge when optimizing the *prior-matching* term of the ELBO, since we do not have access to the analytic expression of the density, nor to its entropy. This problem can be avoided when the change-of-variables formula is applicable, i.e., when using an invertible architecture for the weight-generator network WG with tractable base distribution $p(\mathbf{Z})$ (cf. normalizing flows [70]). In this case, the ELBO objective can be approximated via an MC estimate and optimized via automatic differentiation.

Alternative approaches sidestep the need to have invertible networks, and aim to find other estimates that allow optimizing the ELBO objective. Multiple studies have already investigated the use of weight generators for BNNs [14, 27, 34, 35, 40], ranging from sample-based estimates of the *prior-matching term* [73] to the use of normalizing flows with shared influence on a set of weights for improved scalability [55]. Within the deep learning community, generative adversarial networks (GANs, Goodfellow et al. [19]) represent the most successful use case of implicit distributions. This approach is purely sample-based and requires an auxiliary network that engages in a minimax optimization. A wide range of loss functions can be used to approximately optimize different kinds of divergences or distances, including the KL required for the *prior-matching term*, [67] as done in AVB (cf. SM C.4.1). However, as training corresponds to playing a non-convex game and an inner-loop optimization is required, optimization difficulties arise when applying GAN-like approaches to high-dimensional problems. We experienced these difficulties and therefore also explore alternative ways to train implicit distributions, e.g., methods based on Stein's identity such as SSGE (cf. SM C.4.2). Although in the main text only results obtained using SSGE are reported (noted *PosteriorReplay-Imp*), we consider here additional *implicit* methods and therefore denote each individual method as *PosteriorReplay-<method>*.

In practice, approaches that do not require invertible networks are used with architectures that have a support of measure zero in weight space $\mathcal{W}$, which causes the KL to be ill-defined. We comment on this issue in SM C.4.3.

C.4.1 Adversarial Variational Bayes

Adversarial variational Bayes (AVB, Mescheder et al. [61]) was introduced as a method to estimate the log-density ratio of the *prior-matching term* by using the GAN framework. We denote using AVB to find approximate *implicit* posteriors within our *posterior meta-replay* framework as **PosteriorReplay-AVB**.

Given that the *prior-matching term* (Eq. 3) can be rewritten as $\mathbb{E}_{q_{\boldsymbol{\theta}}(\mathbf{W})}\big[\log q_{\boldsymbol{\theta}}(\mathbf{W}) - \log p(\mathbf{W})\big]$, AVB introduces an auxiliary *discriminator* network (**D**) that, within each training iteration, learns to approximate $\log q_{\boldsymbol{\theta}}(\mathbf{W}) - \log p(\mathbf{W})$. Mescheder et al. [61] show that this is achieved for a discriminator that maximizes the following expression:

$$\mathbb{E}_{q_{\boldsymbol{\theta}}(\mathbf{W})}[\log \sigma(f_{\mathrm{D}}(\mathbf{W}))] + \mathbb{E}_{p(\mathbf{W})}\left[\log(1 - \sigma(f_{\mathrm{D}}(\mathbf{W})))\right] \tag{14}$$

where $\sigma(\cdot)$ denotes the logistic sigmoid function and f_{D} the function performed by the discriminator. Having the optimal discriminator $f^*_{\mathrm{D}}(\mathbf{w})$, the *prior-matching term* can be approximated via an MC sample:

$$\begin{aligned}\mathbb{E}_{q_{\boldsymbol{\theta}}(\mathbf{W})}\big[\log \frac{q_{\boldsymbol{\theta}}(\mathbf{W})}{p(\mathbf{W})}\big] &= \mathbb{E}_{q_{\boldsymbol{\theta}}(\mathbf{W})}\big[f^*_{\mathrm{D}}(\mathbf{W})\big] \\ &\approx \frac{1}{K}\sum_{k=1}^{K} f^*_{\mathrm{D}}(\mathbf{w}^{(k)})\end{aligned} \tag{15}$$

This means that at every training iteration of $\boldsymbol{\theta}$ (or in our case $\boldsymbol{\psi}$) the parameters of the discriminator should be trained to optimality. In practice, however, discriminator weights are only fine-tuned for a few iterations in the inner loop.

Note that training requires access to $\nabla_{\boldsymbol{\theta}}\mathbb{E}_{q_{\boldsymbol{\theta}}(\mathbf{W})}\big[f^*_{\mathrm{D}}(\mathbf{W})\big]$, and that the optimal parameter configuration of the discriminator might also depend on $\boldsymbol{\theta}$ as it is an outcome of the optimization procedure described in Eq. 14. Fortunately, as shown in Mescheder et al. [61], the term $\mathbb{E}_{q_{\boldsymbol{\theta}}(\mathbf{W})}\big[\nabla_{\boldsymbol{\theta}} f^*_{\mathrm{D}}(\mathbf{W})\big]$ vanishes and no backpropagation through the discriminator is required.

We also employ a trick suggested in Mescheder et al. [61], termed *adaptive contrast*, which can be used whenever analytic access to the prior density is guaranteed (which is not the case when using AVB in a prior-focused setting, **PriorFocused-AVB**, except for the first task). The incentive for the trick is the fact that a density ratio, especially in high-dimensions, has high variance. Therefore, an auxiliary Gaussian distribution $r_{\boldsymbol{\alpha}}(\mathbf{W})$ is introduced, whose mean and variance parameters are set to the empirical mean and variance of $q_{\boldsymbol{\theta}}(\mathbf{W})$, assuming that the ratio when involving such $r_{\boldsymbol{\alpha}}(\mathbf{W})$ is "easier" to estimate. The ELBO is then rewritten in the following way to include $r_{\boldsymbol{\alpha}}(\mathbf{W})$:

$$\begin{aligned}&\mathbb{E}_{q_{\boldsymbol{\theta}}(\mathbf{W})}\big[\log p(\mathcal{D} \mid \mathbf{W})\big] - \mathrm{KL}(q_{\boldsymbol{\theta}}(\mathbf{W}) \mid\mid p(\mathbf{W})) \\ =& \mathbb{E}_{q_{\boldsymbol{\theta}}(\mathbf{W})}\big[\log p(\mathcal{D} \mid \mathbf{W}) - \log q_{\boldsymbol{\theta}}(\mathbf{W}) + \log r_{\boldsymbol{\alpha}}(\mathbf{W}) \\ &\qquad - \log r_{\boldsymbol{\alpha}}(\mathbf{W}) + \log p(\mathbf{W})\big] \\ =& \mathbb{E}_{q_{\boldsymbol{\theta}}(\mathbf{W})}\big[\log p(\mathcal{D} \mid \mathbf{W}) - \log r_{\boldsymbol{\alpha}}(\mathbf{W}) + \log p(\mathbf{W}) \\ &\qquad - \tilde{f}^*_{\mathrm{D}}(\mathbf{W})\big]\end{aligned} \tag{16}$$

where now $\tilde{f}^*_{\mathrm{D}}(\mathbf{w})$ is trained to approximate the log-density ratio $\log q_{\boldsymbol{\theta}}(\mathbf{W}) - \log r_{\boldsymbol{\alpha}}(\mathbf{W})$.

Because of this minimax optimization, AVB suffers in our experiments from scalability issues,[6] and we therefore only experimented with it for low-dimensional problems, where it turns out to be in general the best method, both in terms of performance of individual runs and in ease of finding suitable hyperparameters.

An interesting question regarding AVB is the choice of the discriminator's architecture, which processes complete weight samples $\mathbf{w}$ to determine whether they originate from the prior or from the

[6] Note, also Pawlowski et al. [73] reports difficulties when applying AVB to BNNs.

approximate posterior distribution. For low-dimensional problems, we use MLP architectures since the dimensionality of $\mathbf{w}$ is only in the order of 100 weights. For high-dimensional problems, where using a plain MLP is infeasible, we experimented with a chunking approach. Specifically, we used one MLP to reduce the dimensionality of individual weight chunks, which are then concatenated and fed as input to a second MLP that generates the actual output of the discriminator. However, we did not succeed with this approach, and leave the scaling of AVB to large main networks as an open problem for future work.

C.4.2 Spectral Stein Gradient Estimator

Stein's identity and the related Stein discrepancy have also been investigated to develop training methods for *implicit* distributions [30]. Li and Turner [51] and Shi et al. [79] observed that the training of *implicit* distributions (e.g., via VI) often only requires access to $\nabla_{\mathbf{w}} \log q_{\boldsymbol{\theta}}(\mathbf{w})$, a quantity that appears in Stein's identity. Notably, both approaches do no require an auxiliary network nor an inner-loop optimization.

Li and Turner [51] uses an MC estimate of Stein's identity in combination with ridge regression to obtain $\nabla_{\mathbf{w}} \log q_{\boldsymbol{\theta}}(\mathbf{w})$ estimates. Unfortunately, their method can only be used to estimate this quantity for sample points retrieved from $q_{\boldsymbol{\theta}}(\mathbf{w})$. When requiring an estimate for sample points obtained from a different distribution, as it is the case for the cross-entropy term appearing in a *prior-focused* setting, this method is not applicable.

Therefore, we consider an alternative, the spectral Stein gradient estimator (SSGE, Shi et al. [79]), referred to as **PosteriorReplay-SSGE** (*PosteriorReplay-Imp* in the main text) within our *posterior meta-replay* framework. For completeness, we sketch below the inner workings of SSGE.

Recall that our ultimate goal is to find the parameters $\boldsymbol{\theta}$ that maximize the ELBO, and we therefore need to evaluate the following expression:

$$\begin{aligned}\nabla_{\boldsymbol{\theta}} ELBO = \nabla_{\boldsymbol{\theta}} \mathbb{E}_{q_{\boldsymbol{\theta}}(\mathbf{W})}\Big[\log p(\mathcal{D} \mid \mathbf{W})\Big] \\ - \nabla_{\boldsymbol{\theta}} \mathbb{E}_{q_{\boldsymbol{\theta}}(\mathbf{W})}\Big[\log q_{\boldsymbol{\theta}}(\mathbf{W})\Big] + \nabla_{\boldsymbol{\theta}} \mathbb{E}_{q_{\boldsymbol{\theta}}(\mathbf{W})}\Big[\log p(\mathbf{W})\Big]\end{aligned} \tag{17}$$

Thus, the gradient acts on three distinct terms, the first term simply corresponds to the NLL when learning on the data $\mathcal{D}$, and we refer to the other two terms as the *entropy* and the *cross-entropy*. In this specific case, the NLL and cross-entropy term can be approximated using an MC estimate, and their gradient computation through individual samples becomes feasible by using the *reparametrization trick*. However, as explained previously, the entropy term is difficult to compute since we do not have access to the density of $q_{\boldsymbol{\theta}}(\mathbf{W})$. This term can be rewritten as follows:

$$\begin{aligned}&\nabla_{\boldsymbol{\theta}} \mathbb{E}_{q_{\boldsymbol{\theta}}(\mathbf{W})}\Big[\log q_{\boldsymbol{\theta}}(\mathbf{W})\Big] = \nabla_{\boldsymbol{\theta}} \int_{\mathbf{w}} q_{\boldsymbol{\theta}}(\mathbf{w}) \log q_{\boldsymbol{\theta}}(\mathbf{w}) d\mathbf{w} \\ &= \nabla_{\boldsymbol{\theta}} \int_{\mathbf{z}} p(\mathbf{z}) \log q\big(f_{\mathrm{WG}}(\mathbf{z}, \boldsymbol{\theta}), \boldsymbol{\theta}\big) d\mathbf{z} \\ &= \int_{\mathbf{z}} p(\mathbf{z}) \nabla_{\boldsymbol{\theta}} \log q\big(f_{\mathrm{WG}}(\mathbf{z}, \boldsymbol{\theta}), \boldsymbol{\theta}\big) d\mathbf{z} \\ &= \mathbb{E}_{p(\mathbf{Z})}\Big[\nabla_{\boldsymbol{\theta}} \log q\big(f_{\mathrm{WG}}(\mathbf{Z}, \boldsymbol{\theta}), \boldsymbol{\theta}\big)\Big] \\ &= \mathbb{E}_{p(\mathbf{Z})}\Big[\nabla_{\boldsymbol{\theta}} \log q\big(f_{\mathrm{WG}}(\mathbf{Z}, \boldsymbol{\theta}), \hat{\boldsymbol{\theta}}\big)\Big|_{\hat{\boldsymbol{\theta}}=\boldsymbol{\theta}}\Big] \\ &= \mathbb{E}_{p(\mathbf{Z})}\Big[\nabla_{\mathbf{w}} \log q(\mathbf{W}, \boldsymbol{\theta})\Big|_{W=f_{\mathrm{WG}}(\mathbf{Z}, \boldsymbol{\theta})} \nabla_{\boldsymbol{\theta}} f_{\mathrm{WG}}(\mathbf{Z}, \boldsymbol{\theta})\Big]\end{aligned} \tag{18}$$

where to get the second line we have used the following reparametrization $\mathbf{w} = f_{\mathrm{WG}}(\mathbf{z}, \boldsymbol{\theta})$ and $\mathbf{z} \sim p(\mathbf{Z})$, and rewritten $q_{\boldsymbol{\theta}}(\mathbf{W})$ as $q(\mathbf{W}, \boldsymbol{\theta})$ for clarity. Furthermore, to obtain the fifth line we computed the total derivative, and directly used the fact that $\mathbb{E}_{p(\mathbf{Z})}\big[\nabla_{\boldsymbol{\theta}} \log q(\mathbf{W}, \boldsymbol{\theta})\big|_{\mathbf{w}=f_{\mathrm{WG}}(\mathbf{z}, \boldsymbol{\theta})}\big]$

cancels out. Here is the derivation for completeness:

$$
\begin{aligned}
&\mathbb{E}_{p(\mathbf{Z})}\left[\nabla_{\boldsymbol{\theta}} \log q(\mathbf{W}, \boldsymbol{\theta})\big|_{\mathbf{W}=f_{\mathrm{WG}}(\mathbf{Z}, \boldsymbol{\theta})}\right] \\
&\quad = \mathbb{E}_{q_{\boldsymbol{\theta}}(\mathbf{W})}\left[\nabla_{\boldsymbol{\theta}} \log q(\mathbf{W}, \boldsymbol{\theta})\right] \\
&\quad = \int_{\mathbf{w}} q_{\boldsymbol{\theta}}(\mathbf{w}) \nabla_{\boldsymbol{\theta}} \log q(\mathbf{w}, \boldsymbol{\theta}) d\mathbf{w} \\
&\quad = \int_{\mathbf{w}} q_{\boldsymbol{\theta}}(\mathbf{w}) \frac{1}{q_{\boldsymbol{\theta}}(\mathbf{w})} \nabla_{\boldsymbol{\theta}} q(\mathbf{w}, \boldsymbol{\theta}) d\mathbf{w} \\
&\quad = \nabla_{\boldsymbol{\theta}} \int_{\mathbf{w}} q(\mathbf{w}, \boldsymbol{\theta}) d\mathbf{w} = \nabla_{\boldsymbol{\theta}} 1 = 0
\end{aligned} \tag{19}
$$

Coming back to Eq. 18, we see that two gradients need to be computed within the expectation. The second term $\nabla_{\boldsymbol{\theta}} f_{\mathrm{WG}}(\mathbf{z}, \boldsymbol{\theta})$ is simply the gradient of the output of the weight-generator hypernetwork with respect to its own parameters, and can therefore be easily obtained using automatic differentiation. The expression $\nabla_{\mathbf{w}} \log q_{\boldsymbol{\theta}}(\mathbf{w})$ is not accessible for implicit distributions, and needs to be estimated.

SSGE provides a way to estimate $\nabla_{\mathbf{w}} \log q_{\boldsymbol{\theta}}(\mathbf{w})$ by considering a spectral decomposition:

$$
\nabla_{w_i} \log q_{\boldsymbol{\theta}}(\mathbf{w}) = \sum_{j=1}^{\infty} \gamma_{ij} \varphi_j(\mathbf{w}) \tag{20}
$$

where $\boldsymbol{\varphi}$ are the eigenfunctions of a covariance kernel $k(\mathbf{w}^i, \mathbf{w}^j)$ with respect to $q_{\boldsymbol{\theta}}(\mathbf{w})$ and γ_{ij} are the coefficients of the spectral series. Both need to be estimated. The Nyström method is used to approximate the eigenfunctions. For this, SSGE considers the following eigenvalue problem $K\mathbf{u} \approx \lambda \mathbf{u}$, where $K \in \mathbb{R}^{S \times S}$ is the Gram matrix: $K_{ij} = k(\mathbf{w}^i, \mathbf{w}^j)$, S is the number of samples used for the gradient estimation. We only consider the radial basis function (RBF) kernel in this work. The J eigenvectors $\mathbf{u}^1 \ldots \mathbf{u}^J$ with the J largest eigenvalues $\lambda_1 \geq \ldots \geq \lambda_J$ are computed and later will be selected to approximate the spectral series. We discuss below how to set J. The j-th eigenfunction can now be estimated based on the Nyström method with:

$$
\varphi_j(\mathbf{w}) = \frac{\sqrt{S}}{\lambda_j} \sum_{s=1}^{S} u_s^j k(\mathbf{w}, \mathbf{w}^s) \tag{21}
$$

where u_s^j denotes the s-th element of the j-th eigenvector. Finally, Stein's identity allows finding the following expression for the coefficients γ:

$$
\gamma_{ij} = -\frac{1}{\sqrt{S}\lambda_j} \sum_{n=1}^{S} \sum_{s=1}^{S} \nabla_{w_i^n} k(\mathbf{w}^n, \mathbf{w}^s) u_s^j \tag{22}
$$

The estimated eigenfunctions and the corresponding coefficients can then be inserted back into a finite form of Eq. 20 to estimate $\nabla_{\mathbf{w}} \log q_{\boldsymbol{\theta}}(\mathbf{w})$, and multiplied by the gradient of f_{WG} with respect to $\boldsymbol{\theta}$ that we obtain via automatic differentation. Finally, taking the expectation over the base distribution $p(\mathbf{Z})$ allows obtaining an estimate for the gradient of the entropy term in the ELBO (Eq. 18). Note, that if $\boldsymbol{\theta}$ is the output of a TC network, then the gradient estimate $\nabla_{\boldsymbol{\theta}} \mathbb{E}_{q_{\boldsymbol{\theta}}(\mathbf{W})}\Big[q_{\boldsymbol{\theta}}(\mathbf{W})\Big]$ has to be further backpropagated to the parameters of the TC network, where it is accumulated with the gradient of the remaining loss terms, all of which have been automatically computed via automatic differentiation.

The use of SSGE introduces three extra hyperparameters that need to be tuned: the width of the RBF kernel, the number of samples S used for the eigenvalue decomposition, and the number J of eigenfunctions. For the kernel width, we explored setting it to some arbitrary small value or to the median of pairwise distances between all samples, as described in the original paper [79]. In our results, this choice did not considerably impact performance. For the number of eigenfunctions, we experimented with directly setting J to some fixed value or, as suggested in the original paper, with setting it based on a certain ratio τ of cumulative eigenvalues (i.e., select the minimum number of eigenfunctions J such that $\frac{\sum_{j=1}^{J} \lambda_j}{\sum_{j=1}^{S} \lambda_j} > \tau$).

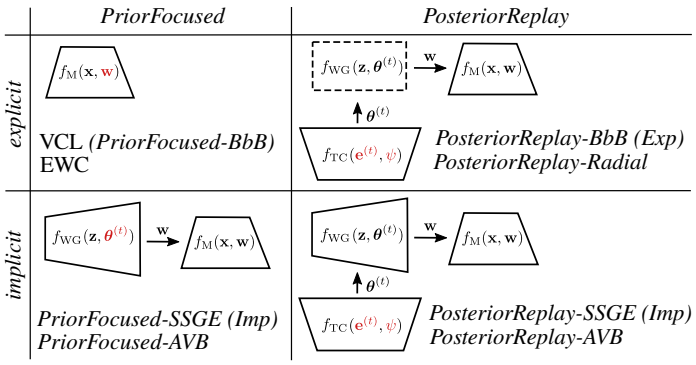

Figure S2: Summary of the different algorithms used to train BNNs, and how they fit into the described framework. We distinguish between approaches that learn a single shared posterior across tasks (*PriorFocused*) and approaches that learn task-specific posteriors (*PosteriorReplay*). We consider both *explicit* and *implicit* posterior approximations. Red indicates the parameters that are learned in each scenario.

C.4.3 Support of implicit approximate posterior distributions

Special attention needs to be payed to the support of the approximate posterior distribution when it is parametrized by an auxiliary network. Indeed, when using a WG architecture for which the output size is larger than the input size, or that contains some bottleneck layer, the support of $q_{\boldsymbol{\theta}}(\mathbf{W})$ will be limited to a set of measure zero (cf. Lemma 1 in Arjovsky and Bottou [3]). This causes the *prior-matching term* of the ELBO to be ill-defined as the KL definition requires $q_{\boldsymbol{\theta}}(\mathbf{W})$ to be absolutely continuous with respect to $p(\mathbf{W})$. To overcome this limitation, we injected small noise perturbations to the outputs of the WG, e.g.,

$$\mathbf{w} \sim q_{\boldsymbol{\theta}}(\mathbf{W}) \Leftrightarrow \mathbf{w} = f_{\text{WG}}(\mathbf{z}, \boldsymbol{\theta}) + \mathbf{u} \tag{23}$$

with $\mathbf{z} \sim p(\mathbf{Z})$ and $\mathbf{u} \sim p(\mathbf{U})$, where $p(\mathbf{U})$ is an additional noise distribution. Note, when using the *reparametrization trick* to rewrite expected values with respect to $q_{\boldsymbol{\theta}}(\mathbf{W})$, one now has to integrate over the joint of $\mathbf{Z}$ and $\mathbf{U}$.

Due to practical considerations, we use the following simplification in our implementation:

$$\mathbf{w} \sim q_{\boldsymbol{\theta}}(\mathbf{W}) \Leftrightarrow \mathbf{w} = f_{\text{WG}}(\mathbf{z}_{:n_z}, \boldsymbol{\theta}) + \sigma_{\text{noise}}\mathbf{z} \tag{24}$$

where $\mathbf{z}_{:n_z}$ refers to the first n_z elements of the vector $\mathbf{z}$, and both σ_{noise} and n_z are hyperparameters.

C.5 Prior-Focused Continual Learning

Prior-focused CL [17] is an alternative Bayesian approach to CL that is commonly used in the literature. As opposed to *posterior meta-replay*, a single set of shared parameters is recursively updated, and finding suitable solutions therefore relies on the existence of trade-off solutions across tasks. We first describe VCL and EWC, two existing algorithms that use a Gaussian approximation for the shared posterior, and then discuss how our framework can be used to render *prior-focused* methods more flexible through the use of *implicit* distributions. Note that *prior-focused* approaches can be implemented within our framework (denoted *PriorFocused*) by directly learning a single set of parameters $\boldsymbol{\theta}$ that define the shared posterior distribution, which is recursively instantiated as prior. Since $\boldsymbol{\theta}$ is not task-specific, no TC network is required. An overview of how *PriorFocused* and *PosteriorReplay* approaches fit in our proposed framework is given in Fig. S2.

C.5.1 Variational Continual Learning

Variational continual learning (VCL, Nguyen et al. [65], Swaroop et al. [83]) was introduced as a way to continually learn a single mean-field Gaussian posterior approximation across tasks by doing a recursive Bayesian update via VI. More specifically, VCL aims to learn a single approximate posterior $q_{\boldsymbol{\theta}^{(1:T)}}(\mathbf{W})$ by recursively considering the posterior of the previous task as the prior for the new task:

$$q_{\boldsymbol{\theta}^{(1:T)}}(\mathbf{W}) \propto p(\mathcal{D}^{(T)} \mid \mathbf{W}) q_{\boldsymbol{\theta}^{(1:T-1)}}(\mathbf{W}) \tag{25}$$

where $q_{\boldsymbol{\theta}^{(1:T-1)}}(\mathbf{W})$ is an approximation to the previous posterior $p(\mathbf{W} \mid \mathcal{D}^{(1:T-1)})$. Importantly, the CL requirements are not violated since only data from the current task $\mathcal{D}^{(T)}$ is required for the update. To learn the approximate posteriors, VCL uses BbB, and learns a mean-field Gaussian approximation parametrized by a mean and variance per weight, which are optimized by using the *reparametrization trick* (Eq. 5). An interesting contribution of this method is the mathematically sound posterior update based on coresets (i.e., a small set of samples stored from each task, [75, 4]) within their Bayesian framework. Importantly, the role of coresets in their approach is to help mitigate catastrophic forgetting. In contrast, in this work we mainly use coresets to facilitate task inference in a task-agnostic setting (see SM C.7 for details).

In our framework, VCL is realized via a main network and a simple WG function with parameters $\boldsymbol{\theta}$ as depicted in Fig. 2 for BbB. Conceptual differences between using BbB in a *prior-focused* setting (VCL), and using BbB using a *posterior meta-replay* approach (*PosteriorReplay-BbB*) are illustrated in Figure S1. We study this method in a multihead setting (*VCL-multihead*), where each head is task-specific and leads to a task-specific approximate posterior that induces epistemic uncertainty. Therefore, the predictive uncertainty of each head has a task-specific influence that we exploit for task inference. An interesting extension of this multihead setting (i.e., task-specific output parameters) could be CLAW [1] which builds on top of VCL and utilizes a set of task-specific neuronal parameters. Thus task-specific parameters are distributed throughout the whole network (not just the outputs), which might be beneficial for uncertainty-based task-inference. We also consider VCL with a growing head (**VCL-growing**), as described in SM C.5.2. Note, as we often apply likelihood-tempering in practice (SM D) for scalability reasons, our VCL version is often related to GVCL [54].

C.5.2 Elastic Weight Consolidation

Kirkpatrick et al. [38] propose elastic weight consolidation (EWC), a CL algorithm that limits the plasticity of weights that are considered important for solving previous tasks, and therefore mitigates forgetting. In contrast to VCL, the algorithm is based on a Laplace approximation of the posterior [56] where approximations are restricted to diagonal covariance matrices.[7] For completeness, we detail here the derivation of this algorithm, specifically of its more mathematically sound variant *Online EWC* [32, 78], which we simply refer to as EWC in the tables for brevity. Afterwards, we explain how this algorithm is commonly used in the literature in a task-agnostic setting, and propose an alternative solution based on a combination of shared and task-specific parameters that leads to improved performance.

Online EWC. The core idea of EWC (and of *prior-focused* methods in general) simply consists in performing a recursive Bayesian update of a single posterior distribution as new tasks arrive:

$$p(\mathbf{W} \mid \mathcal{D}^{(1:T)}) = \frac{p(\mathcal{D}^{(T)} \mid \mathbf{W}) p(\mathbf{W} \mid \mathcal{D}^{(1:T-1)})}{p(\mathcal{D}^{(T)} \mid \mathcal{D}^{(1:T-1)})} \tag{26}$$

where we have used the fact that $\mathcal{D}^{(1:T-1)}$ and $\mathcal{D}^{(T)}$ are conditionally independent given $\mathbf{W}$. For simplicity, we start by considering $T = 2$:

$$p(\mathbf{W} \mid \mathcal{D}^{(1:2)}) = \frac{p(\mathcal{D}^{(2)} \mid \mathbf{W}) p(\mathbf{W} \mid \mathcal{D}^{(1)})}{p(\mathcal{D}^{(2)} \mid \mathcal{D}^{(1)})} \tag{27}$$

This is almost identical to the original formulation (cf. Eq 2. in Kirkpatrick et al. [38]), except that the denominator contains $p(\mathcal{D}^{(2)} \mid \mathcal{D}^{(1)})$ and not simply $p(\mathcal{D}^{(2)})$, since the datasets are only conditionally independent, as noted by Huszár [32]. Optimizing the parameters $\mathbf{W}$ corresponds to finding their most probable value given the data:

$$\begin{aligned} &\arg\min_{\mathbf{W}} \big\{ -\log p(\mathbf{W} \mid \mathcal{D}^{(1:2)}) \big\} \Leftrightarrow \\ &\qquad \arg\min_{\mathbf{W}} \big\{ -\log p(\mathcal{D}^{(2)} \mid \mathbf{W}) - \log p(\mathbf{W} \mid \mathcal{D}^{(1)}) \big\} \end{aligned} \tag{28}$$

where we have dropped constant terms. Notice that $-\log p(\mathcal{D}^{(2)} \mid \mathbf{W})$ is simply the NLL and can easily be computed. The second term, $\log p(\mathbf{W} \mid \mathcal{D}^{(1)})$ is generally intractable, and for this reason

[7] An interesting extension with non-diagonal covariance matrices is described in Ritter et al. [76].

we consider a second order Taylor approximation around the minimum that was found after learning the first task $\mathbf{w}^{(1)}_{\text{MAP}}$, corresponding to the maximum a posteriori (MAP) estimate. First order terms vanish around the minimum and we obtain the following expression:

$$\log p(\mathbf{W} \mid \mathcal{D}^{(1)}) \approx const + \frac{1}{2}(\mathbf{W} - \mathbf{w}^{(1)}_{\text{MAP}})^T \mathcal{H}_{\log p(\mathbf{w}|\mathcal{D}^{(1)})}\Big|_{\mathbf{w}=\mathbf{w}^{(1)}_{\text{MAP}}} (\mathbf{W} - \mathbf{w}^{(1)}_{\text{MAP}}) \tag{29}$$

where $\mathcal{H}_{\log p(\mathbf{W}|\mathcal{D}^{(1)})}$ denotes the Hessian of $\log p(\mathbf{W} \mid \mathcal{D}^{(1)})$, which can be rewritten as:

$$\begin{aligned}\mathcal{H}_{\log p(\mathbf{W}|\mathcal{D}^{(1)})} &= \mathcal{H}_{\log p(\mathcal{D}^{(1)}|\mathbf{W})} + \mathcal{H}_{\log p(\mathbf{W})} \\ &= \nabla_{\mathbf{w}} \nabla^T_{\mathbf{w}} \big[\sum_{n=1}^{N} \log p(\mathbf{y}^{(1,n)} \mid \mathbf{W}, \mathbf{x}^{(1,n)}) \\ &\quad - \frac{1}{2\sigma^2_{prior}} \|\mathbf{W}\|^2_2 \big] \\ &= \sum_{n=1}^{N} \mathcal{H}_{\log p(\mathbf{y}^{(1,n)}|\mathbf{W},\mathbf{x}^{(1,n)})} - \frac{1}{\sigma^2_{prior}} I\end{aligned} \tag{30}$$

where $\mathbf{x}^{(1,n)}$ denotes the n-th sample of the first task and where we have used the fact that all N samples are independent given $\mathbf{w}$. Furthermore, we have assumed a Gaussian prior such that $p(\mathbf{W}) = \mathcal{N}(0, I\sigma^2_{prior})$, where I is the identity matrix. Recall the relationship between the Hessian and the Fisher information matrix F (e.g., cf. Eq. 3/4 in Martens [59]):

$$F = -\mathbb{E}_{p(\mathbf{y}|\mathbf{W},\mathbf{x})} \Big[\mathcal{H}_{\log(\mathbf{y}|\mathbf{W},\mathbf{x})} \Big] \tag{31}$$

Note that so far we have considered $\mathbf{x}$ fixed, but the model should perform well with respect to the input distribution $p(\mathbf{x})$:

$$\begin{aligned}\mathbb{E}_{p(\mathbf{x})} \Big[-F \Big] &= \mathbb{E}_{p(\mathbf{x})p(\mathbf{y}|\mathbf{W},\mathbf{x})} \Big[\mathcal{H}_{\log p(\mathbf{y}|\mathbf{W},\mathbf{x})} \Big] \\ &\approx \frac{1}{N} \sum_{n=1}^{N} \mathcal{H}_{\log p(\tilde{\mathbf{y}}^{(n)}|\mathbf{W},\mathbf{x}^{(n)})}\end{aligned} \tag{32}$$

where the approximation in the last line comes from an MC estimate using N samples drawn from the joint $p(\mathbf{y} \mid \mathbf{W}, \mathbf{x})p(\mathbf{x})$. Assuming $\mathbf{w}$ has been trained to optimality, i.e., $p(\mathbf{y} \mid \mathbf{W}, \mathbf{x}) \approx p(\mathbf{y} \mid \mathbf{x})$ for $\mathbf{x} \sim p(\mathbf{x})$, the samples used in Eq. 30 and Eq. 32 are essentially from the same joint distribution and we can write:

$$\frac{1}{N} \sum_{n=1}^{N} \mathcal{H}_{\log p(\mathbf{y}^{(n)}|\mathbf{W},\mathbf{x}^{(n)})} \approx \frac{1}{N} \sum_{n=1}^{N} \mathcal{H}_{\log p(\tilde{\mathbf{y}}^{(n)}|\mathbf{W},\mathbf{x}^{(n)})} \tag{33}$$

to obtain the following expression:

$$\mathcal{H}_{\log p(\mathbf{W}|\mathcal{D}^{(1)})} \approx -NF_{emp} - \frac{1}{\sigma^2_{prior}} I \tag{34}$$

where we have introduced the empirical Fisher, which is obtained using the sample points from the actual dataset $\mathcal{D}$, but given the optimality assumption above here it simply corresponds to $F_{emp} = \mathbb{E}_{p(\mathbf{x})}\big[F\big]$.[8] Plugging this result into Eq. 29, while using a diagonal approximation of the empirical Fisher matrix, and extending it to an arbitrary number of tasks by iteratively computing the posterior, we obtain the following expression (cf. Eq. 11 in Huszár [32]):

$$\log p(\mathbf{W} \mid \mathcal{D}^{(1:T)}) \approx const + \log p(\mathcal{D}^{(T)} \mid \mathbf{W}) - \frac{1}{2} \sum_i \Bigg(\sum_{t<T} N^{(t)} F_{emp^{(t)}_i} + \frac{1}{\sigma^2_{prior}} \Bigg) (w_i - w^{(T-1)}_{\text{MAP},i})^2 \tag{35}$$

[8]Note, that for mathematical convenience we include the expectation over $p(\mathbf{x})$ in the definition of the empirical Fisher.

where $N^{(t)}$ denotes the size of $\mathcal{D}^{(t)}$. Thus, per weight w_i there is a scalar importance value $\sum_{t<T} N^{(t)} F_{emp_i^{(t)}} + \frac{1}{\sigma^2_{prior}}$ which can be computed online such that there is no need to maintain the empirical Fisher matrices of individual tasks. This is in contrast to the original EWC formulation Kirkpatrick et al. [38], where each Fisher matrix had to be maintained in memory.

Crucially, in order to relate the sum over Hessians in Eq. 30 to the Fisher information matrix, we have to assume that $p(\mathbf{y} \mid \mathbf{W}, \mathbf{x})$ and $p(\mathbf{y} \mid \mathbf{x})$ are identical for $\mathbf{x} \sim p(\mathbf{x})$. In this case, the empirical Fisher and the (expected) Fisher are also identical and it mathematically does not matter which of the two is used for the algorithm.

Multihead EWC. When EWC is used in a task-agnostic inference setting, it is often trained with an output softmax that grows as new tasks are trained (e.g., van de Ven et al. [88]), which we refer to as *EWC-growing*. In this setting, where EWC performs poorly, the Bayesian assumption that the model class contains the ground-truth model is violated, since the model-class changes whenever the softmax changes in size. A simple way to overcome this issue when the number of tasks is known in advance, is to use a shared softmax that spans the outputs of all tasks from the beginning of training, which we refer to as **EWC-shared**. However, as we will show, this approach still performs poorly. We hypothesize this is due to the fact that the role played by output connections for their corresponding task is in conflict with that played for all other tasks (i.e., because the shared softmax pushes the weights of future heads to be highly negative). As a solution, we propose the use of a multihead when applying EWC to a task-agnostic inference setting (referred to as *EWC-multihead*). This results in a hybrid *prior-focused* approach, where the learned parameters $\mathbf{w}$ consist of a set of shared weights $\boldsymbol{\phi}$ and a set of task-specific output heads with weights $\{\xi^{(t)}\}_{t=1}^{T}$. Now, Eq. 27 becomes:

$$\begin{aligned} & p(\boldsymbol{\phi}, \boldsymbol{\xi}^{(1:2)} \mid \mathcal{D}^{(1:2)}) \\ & \quad = \frac{p(\mathcal{D}^{(2)} \mid \boldsymbol{\phi}, \boldsymbol{\xi}^{(2)}) p(\boldsymbol{\phi}, \boldsymbol{\xi}^{(1)} \mid \mathcal{D}^{(1)}) p(\boldsymbol{\xi}^{(2)})}{p(\mathcal{D}^{(2)} \mid \mathcal{D}^{(1)})} \end{aligned} \tag{36}$$

Repeating the procedure in the original derivation, i.e. considering a Taylor approximation around optimal parameters and recursively computing the posterior, we obtain the following expression:

$$\begin{aligned} & \log p(\boldsymbol{\phi}, \boldsymbol{\xi}^{(1:T)} \mid \mathcal{D}^{(1:T)}) \approx const \\ & \quad + \log p(\mathcal{D}^{(T)} \mid \boldsymbol{\phi}, \boldsymbol{\xi}^{(T)}) + \log p(\boldsymbol{\xi}^{(T)}) \\ & \quad - \frac{1}{2} \sum_i \left(\sum_{t<T} N^{(t)} F_{emp_i^{(t)}} + \frac{1}{\sigma^2_{prior}} \right) (w_i - w^{(T-1)}_{\text{MAP},i})^2 \end{aligned} \tag{37}$$

where we have assumed that all parameters $\mathbf{w} = [\boldsymbol{\phi}, \boldsymbol{\xi}^{(1)}, \ldots, \boldsymbol{\xi}^{(T)}]$ share the same prior. Importantly, for any t, $F_{emp^{(t)}}$ is a square diagonal matrix of dimension $\dim(\mathbf{w})$, where all entries related to weights $\boldsymbol{\xi}^{(s)}$ for $s \neq t$ are zero.

Recall, that the EWC importance values are reminiscent of the entries of a precision matrix of a multivariate Gaussian with diagonal covariance matrix. Together with the final MAP estimate $\mathbf{w}^{(T)}_{\text{MAP}}$ of $p(\mathbf{W} \mid \mathcal{D}^{(1:T)})$ we can explicitly construct the following approximate posterior in (Online) multihead EWC:

$$\begin{aligned} & \log p(\boldsymbol{\phi}, \boldsymbol{\xi}^{(1:T)} \mid \mathcal{D}^{(1:T)}) = \\ & \quad \mathcal{N}\left(\mathbf{w}^{(T)}_{\text{MAP}}, \left[\frac{1}{\sigma^2_{prior}} I + \sum_{t=1}^{T} N^{(t)} F_{emp^{(t)}} \right]^{-1} \right) \end{aligned} \tag{38}$$

This posterior induces predictive uncertainty at each output head, which can be used for task inference in task-agnostic inference settings.

C.5.3 Prior-focused CL with implicit distributions

Both VCL and EWC use a Gaussian approximation for the shared posterior. This means that, not only a trade-off solution across tasks needs to be found, but also that the expressivity of this posterior with respect to unknown future tasks is limited. To overcome this limitation, we explore *prior-focused*

methods with a more flexible variational family, a family of *implicit* distributions parametrized by a neural network. Although this approach does not overcome the need to find trade-off solutions across tasks, it can make better use of the existing overlaps by capturing, for example, multi-modality. Within our framework, *PriorFocused* methods with an *implicit* posterior distribution can be realised by directly learning the parameters $\boldsymbol{\theta}$ of a WG hypernetwork. This can be achieved using algorithms for learning with *implicit* distributions, such as AVB or SSGE, and we therefore refer to these methods as **PriorFocused-AVB** and **PriorFocused-SSGE**.

If not noted otherwise, we consider a hybrid approach with task-specific weights introduced by a multihead main network, such that task inference through task-specific predictive uncertainty is possible.

C.6 Task inference

When confronted with an unseen input $\tilde{\mathbf{x}}$, algorithms that maintain task-specific solutions, such as our *posterior meta-replay* framework, first have to explicitly assign the input to a certain task. In this work, we exclusively consider inferring task identity via predictive uncertainty, and explore four different ways of quantifying uncertainty as outlined below.

The *Ent* criterion, only considered in classification tasks, can be computed directly from the posterior predictive distribution $p(\mathbf{y} \mid \mathcal{D}^{(t)}; \tilde{\mathbf{x}}) = \int_{\mathbf{W}} p(\mathbf{y} \mid \mathbf{W}; \tilde{\mathbf{x}}) p(\mathbf{W}|\mathcal{D}^{(t)})\, d\mathbf{W}$. Due to intractability of this integral, we resort to an MC estimate using $K = 100$ models drawn from the approximate posterior parameter distribution $q_{\boldsymbol{\theta}^{(t)}}(\mathbf{W})$ of each task:

$$p(\mathbf{y} \mid \mathcal{D}^{(t)}; \tilde{\mathbf{x}}) \approx \frac{1}{K} \sum_{k=1}^{K} p(\mathbf{y} \mid \mathbf{w}^{(t,k)}; \tilde{\mathbf{x}}) \tag{39}$$

with $\mathbf{w}^{(t,k)} \sim q_{\boldsymbol{\theta}^{(t)}}(\mathbf{W})$. Note that for deterministic approaches such as *PosteriorReplay-Dirac*, only $K = 1$ is applicable. In the *Ent* criterion, the task leading to the lowest entropy is selected:

$$t_{\textit{Ent}} = \underset{t \in 1..T}{\arg\min}\, \mathcal{H}\big\{p(\mathbf{y} \mid \mathcal{D}^{(t)}; \tilde{\mathbf{x}})\big\} \tag{40}$$

where $\mathcal{H}\{\}$ denotes the entropy functional.

Similarly, in the **Conf** criterion [26], also only considered for classification problems, the task leading to the highest confidence is selected:

$$t_{\textit{Conf}} = \underset{t \in 1..T}{\arg\max}\, \max_{\mathbf{y} \in \mathcal{Y}} p(\mathbf{y} \mid \mathcal{D}^{(t)}; \tilde{\mathbf{x}}) \tag{41}$$

where $\mathcal{Y}$ denotes the set of class labels, which indeed could be task-specific.

These two criteria intuitively correspond to choosing the model with the most peaky predictive distribution, i.e. the highest certainty in the predicted class. However, uncertainty in the predictive distribution can also arise in-distribution due to noisy data, i.e., aleatoric uncertainty. In order to quantify epistemic uncertainty only, we additionally study model agreement as uncertainty measure. Note that, in regions where sufficient data has been observed, models drawn from the posterior parameter distribution should converge towards the data-generating distribution $p(\mathbf{Y} \mid \mathbf{X})$ and should therefore agree among each other. Conversely, regions where those models disagree have not observed enough data and can be considered OOD, assuming a rich enough prior in function space [11]. This intuition should be captured in *Agree*, where the task leading to the strongest agreement between models is selected. For C-way classification, we compute this quantity as the average standard deviation of predicted likelihood values for K models $\mathbf{w}^{(t,k)} \sim q_{\boldsymbol{\theta}^{(t)}}(\mathbf{W})$ [81]:

$$t_{\textit{Agree}} = \underset{t \in 1..T}{\arg\min}\, \frac{1}{C} \sum_{c=1}^{C} \mathrm{SD}\big\{p(Y = c \mid \mathbf{w}^{(t,k)}; \tilde{\mathbf{x}}) \quad \forall k\big\} \tag{42}$$

where $\mathrm{SD}(\cdot)$ refers to the standard deviation of the given set of values.

Alternatively, Depeweg et al. [13] propose a neat decomposition of the entropy into two terms:

$$\mathcal{H}\big\{p(\mathbf{y} \mid \mathcal{D}^{(t)}; \tilde{\mathbf{x}})\big\} = \mathbb{E}_{p(\mathbf{W}|\mathcal{D}^{(t)})} \mathcal{H}\big\{p(\mathbf{y} \mid \mathbf{W}; \tilde{\mathbf{x}})\big\} + \mathcal{I}(\mathbf{y}, \mathbf{W}) \tag{43}$$

where $\mathcal{I}(\mathbf{y}, \mathbf{W})$ denotes the mutual information between $\mathbf{y}$ and $\mathbf{W}$, given by:

$$\mathcal{I}(\mathbf{y}, \mathbf{W}) = \mathrm{KL}\big(p(\mathbf{y}, \mathbf{W} \mid \mathcal{D}; \tilde{\mathbf{x}}) || p(\mathbf{W}|\mathcal{D}^{(t)}) p(\mathbf{y} \mid \mathcal{D}^{(t)}; \tilde{\mathbf{x}})\big) \tag{44}$$

The two terms on the RHS of Eq. 43 are interpreted as aleatoric and epistemic uncertainty. Following the terminology from Malinin et al. [58], we refer to the mutual information term as *knowledge uncertainty* (noted **KU**). Note, that the remaining terms in Eq. 43 can be estimated via Monte-Carlo using the approximate posterior $q_{\boldsymbol{\theta}^{(t)}}(\mathbf{W})$ instead of $p(\mathbf{W}|\mathcal{D}^{(t)})$. Although we are unsure about whether these terms can be generally interpreted as epistemic and aleatoric uncertainty, we studied how this knowledge uncertainty estimate performs in practice in SplitMNIST-10 experiments.

Note, that choosing to use predictive uncertainty for task inference is a heuristic choice and, to the best of our knowledge, there is no guarantee that predictive uncertainty can lead to principled OOD detection in general [11]. However, except when exploring hybrid approaches, practitioners have to trade-off pros and cons when selecting a CL method that can be deployed in a task-agnostic setting. As discussed in the main text, if task identity can be inferred from inputs alone, in theory it seems reasonable to perform task inference directly on approximations of the unknown input distributions $p^{(t)}(\mathbf{x})$, e.g., via tractable density access [46]. While in practice this approach still seems to be out of reach for high-dimensional problems [64], generative models for data replay have been successfully applied to CL [80, 86, 91]. In this case, when a new task is trained, generated data from past tasks is replayed to train in a pseudo-i.i.d. setting. Because of the pseudo-parallel training on all tasks, task inference does not have to be handled explicitly anymore. Note, however, that a conceptual disadvantage exists when using replay approaches, i.e., the problem of training with non-i.i.d. data is not directly addressed and rather side-stepped completely for the target network by shifting CL to the generative model. Finally, we want to stress again that the task identity can also be externally provided to the TC, e.g., by an auxiliary system that processes context data (different than the main network's input) [24, 91].

C.7 Posterior-Replay CL with Coreset Fine-Tuning

As opposed to the deterministic setting, already acquired knowledge can be updated in a principled way when using a Bayesian perspective. When continually learning a sequence of tasks, this allows approximate posteriors to be revisited as new data comes in. This can be used in our *posterior meta-replay* framework to mitigate forgetting by storing task-specific coresets and using them to refresh all task-specific posteriors in a small fine-tuning stage at the end of training.

Specifically, we consider a dataset split per task $\mathcal{D}^{(t)} \setminus \mathcal{C}^{(t)} \cup \mathcal{C}^{(t)}$, where $\mathcal{D}^{(t)} \setminus \mathcal{C}^{(t)}$ is used for the initial CL training phase, and $\mathcal{C}^{(t)}$ is maintained in memory for the fine-tuning stage. More explicitly, when continually learning our meta-model we approximate the following posteriors:

$$q_{\tilde{\boldsymbol{\theta}}^{(t)}}(\mathbf{W}) \approx p(\mathbf{W} \mid \mathcal{D}^{(t)} \setminus \mathcal{C}^{(t)}) \tag{45}$$

after which $\mathcal{D}^{(t)} \setminus \mathcal{C}^{(t)}$ can be discarded, and only a small-sized coreset $\mathcal{C}^{(t)}$ needs to be maintained in memory until all tasks are learned.

The fine-tuning stage at the end of training is then performed in a multitask fashion on the stored coresets, which are all simultaneously available. To see how this final update can be performed we write our posterior distribution as follows:

$$\begin{aligned} p(\mathbf{W} \mid \mathcal{D}^{(t)}) &= \frac{p(\mathbf{W}) p(\mathcal{D}^{(t)} \mid \mathbf{W})}{p(\mathcal{D}^{(t)})} = \frac{p(\mathbf{W}) p(\mathcal{D}^{(t)} \setminus \mathcal{C}^{(t)} \mid \mathbf{W}) p(\mathcal{C}^{(t)} \mid \mathbf{W})}{p(\mathcal{D}^{(t)} \setminus \mathcal{C}^{(t)}, \mathcal{C}^{(t)})} \\ &\propto \frac{p(\mathbf{W}) p(\mathcal{D}^{(t)} \setminus \mathcal{C}^{(t)} \mid \mathbf{W}) p(\mathcal{C}^{(t)} \mid \mathbf{W})}{p(\mathcal{D}^{(t)} \setminus \mathcal{C}^{(t)})} = p(\mathbf{W} \mid \mathcal{D}^{(t)} \setminus \mathcal{C}^{(t)}) p(\mathcal{C}^{(t)} \mid \mathbf{W}) \end{aligned} \tag{46}$$

where we have used the fact that $\mathcal{D}^{(t)} \setminus \mathcal{C}^{(t)}$ and $\mathcal{C}^{(t)}$ are conditionally independent given $\mathbf{W}$. Eq. 47 shows that the desired posteriors $p(\mathbf{W} \mid \mathcal{D}^{(t)})$ can be obtained via a Bayesian update of the continually learned posteriors $p(\mathbf{W} \mid \mathcal{D}^{(t)} \setminus \mathcal{C}^{(t)})$ by using the task-specific coreset $\mathcal{C}^{(t)}$. Recall that in VI, we approximate this posterior with a distribution $q_{\boldsymbol{\theta}^{(t)}}(\mathbf{W})$ by minimizing $\mathrm{KL}(q_{\boldsymbol{\theta}^{(t)}}(\mathbf{W}) \mid\mid p(\mathbf{W} \mid \mathcal{D}^{(t)}))$. Based on our dataset split, the expression to be minimized can be rewritten as $\mathrm{KL}(q_{\boldsymbol{\theta}^{(t)}}(\mathbf{W}) \mid\mid \zeta p(\mathbf{W} \mid \mathcal{D}^{(t)} \setminus \mathcal{C}^{(t)}) p(\mathcal{C}^{(t)} \mid \mathbf{W}))$, where ζ is a normalization constant that accounts

for the fact that we dropped $\mathcal{C}^{(t)}$ from the denominator. Replacing $p(\mathbf{W} \mid \mathcal{D}^{(t)} \setminus \mathcal{C}^{(t)})$ by the approximations $q_{\tilde{\boldsymbol{\theta}}^{(t)}}(\mathbf{W})$ learned continually, we obtain the following VI objective:

$$\begin{aligned} &\arg\min_{\boldsymbol{\theta}^{(t)}} \mathrm{KL}\big(q_{\boldsymbol{\theta}^{(t)}}(\mathbf{W}) \,||\, \zeta q_{\tilde{\boldsymbol{\theta}}^{(t)}}(\mathbf{W}) p(\mathcal{C}^{(t)} \mid \mathbf{W})\big) \\ &\qquad = \arg\min_{\boldsymbol{\theta}^{(t)}} \Big[\mathrm{KL}\big(q_{\boldsymbol{\theta}^{(t)}}(\mathbf{W}) \,||\, q_{\tilde{\boldsymbol{\theta}}^{(t)}}(\mathbf{W})\big) - \mathbb{E}_{q_{\boldsymbol{\theta}^{(t)}}}\big[\log p(\mathcal{C}^{(t)} \mid \mathbf{W})\big]\Big] \end{aligned} \tag{47}$$

Note that the second term corresponds to integrating the evidence from the coreset into the new posterior, and therefore simply corresponds to minimizing the NLL on the coreset $\mathcal{C}^{(t)}$, while the first term ensures that the posterior does not change much, preventing forgetting. Notably, the KL term is now between two distributions from the same variational family, reminiscent of *prior-focused* learning as discussed in SM C.5. Therefore, it can be analytically evaluated for *PosteriorReplay-BbB* while other methods require estimation, e.g., using AVB or SSGE.

Crucially, having coresets available at the end of training can also be used to facilitate task inference based on predictive uncertainty (refer to SM C.6 for details). To do this, we perform the final update on a set of modified coresets, which encourage the prediction of a task-specific model on OOD data (i.e., on a coreset from another task) to be highly uncertain. More specifically, we use the modified coresets:

$$\tilde{\mathcal{C}}^{(t)} = \mathcal{C}^{(t)} \cup \bigcup_{s \in \{1,\ldots,T\} \setminus \{t\}} \hat{\mathcal{C}}^{(s)} \tag{48}$$

where $\hat{\mathcal{C}}^{(s)}$ is constructed from the same inputs contained in $\mathcal{C}^{(s)}$ but the labels are replaced by high uncertainty labels. We consider per-task coresets of size 100 and enforce high uncertainty in OOD inputs by either setting high-entropy softmax labels (i.e., uniform distribution; eg., [45]), or by using different random labels per mini-batch.

Intriguingly, when training with data from other tasks, this data becomes in-distribution and cannot be considered OOD anymore. Therefore, we expect our task inference criterion *Agree*, which is designed to capture only epistemic uncertainty, to become less reliable. In other terms, what was previously OOD data, that could have been detected via epistemic uncertainty, now became in-distribution data with high aleatoric uncertainty due to the way we design training targets. This intuition is reflected in our empirical observations (cf. SM D).

C.8 Experience Replay

Experience replay [52] refers to the idea of using a replay buffer (or coresets) to store current experiences that can later be replayed in order to mitigate forgetting. Implementations of this method might slightly differ in how coresets are assembled and how replayed data is incorporated into the loss [e.g., 2, 7, 9]. Our implementation of experience replay (**Exp-Replay**) is designed to be comparable to our proposed coreset fine-tuning (SM C.7). Therefore, we use task-specific coresets of size 100 (coresets are build using a random subset of a task's training set). A coreset only contains input samples, and a checkpointed model from the previous task is used to generate distillation targets [28]. Thus, a distillation loss is added to the overall loss. This distillation loss uses a mini-batch that is created by randomly sampling from all available coresets in a stratified manner.

D Supplementary Experiments and Results

In this section, we extend the results presented in the main text, and provide a more detailed discussion. Furthermore, we report additional baselines and supplementary experiments such as PermutedMNIST (cf. SM D.4).

Baselines. In addition to the methods and baselines that have already been introduced, we consider the following variations. To investigate the role played by the shared meta-model, we consider independently trained models per task (*SeparatePosteriors*); a baseline that by design is not affected by catastrophic interference, and therefore leads to identical *TGiven-During* and *TGiven-Final* scores. In this setting, task-specific solutions cannot benefit from knowledge transfer, but they are also less limited because the capacity of the meta-model is not shared with previous tasks.

We distinguish two cases for this baseline. In the first case, there is no TC network and $\boldsymbol{\theta}$ is trained directly (denoted *SeparatePosteriors-<method>*, e.g., **SeparatePosteriors-BbB**). However, one has

to keep in mind that the underlying architecture in combination with the chosen weight prior defines a prior in function space that will affect predictive uncertainty (cf. Sec. 3 and [93]), and it is therefore unclear how comparable task inference scores based on predictive uncertainty are in this case, e.g., between *SeparatePosteriors-BbB* and *PosteriorReplay-BbB*. For this reason, we include a second *SeparatePosteriors* baseline where the *TC* network remains but has no dedicated functional purpose (denoted *SeparatePosteriors-TC-<method>*, e.g., **SeparatePosteriors-TC-BbB**). Note that for this baseline, one TC network with a single task embedding is learned per task.

As a potential upper-bound we also consider **Fine-Tuning**, which simply refers to the continuous deterministic training of a main network without undertaking any measures against catastrophic forgetting. Thus, the achieved *TGiven-During* score can benefit from transfer while not being restricted to finding any trade-off that accommodates past tasks. In this case, the hyperparameter configuration is selected based on the best *TGiven-During* score. We only searched hyperparameters for this baseline in the PermutedMNIST and SplitCIFAR experiments, because the *TGiven-During* scores of other experiments are often maxed out. Importantly, whenever applicable and unless noted otherwise, all hyperparameter configurations have been selected based on the *TInfer-Final (Ent)* criterion. Hence, reported task-given (*TGiven*) scores do not necessarily reflect the ability of a method to combat forgetting. However, in most cases, forgetting does not seem to be a major challenge in the experiments we consider, and the reported *TGiven-During* and *TGiven-Final* scores are often very close. Please refer to SM E for details on the experimental setup and hyperparameter searches.

Tempering. All results involving Bayesian methods use a standard Gaussian prior $p(\mathbf{W}) = \mathcal{N}(\mathbf{0}, I)$. For high-dimensional problems and for methods trained with variational inference, we explore tempering the posterior to increase training stability (cf. SM E.3). Specifically, we downscale the *prior-matching term*, which effectively increases the emphasis on matching the data well (cf. SM E in Wenzel et al. [92]). Note, no such posterior tempering is used when studying the low-dimensional problems in SM D.1 and SM D.2.

D.1 1D Polynomial Regression

Table S2: Mean-squared-error (MSE) values for the 1D polynomial regression experiments. *TInfer* refers to the MSE when making predictions using the task embedding leading to lowest uncertainty for the given input. The column *ACC-inference* reports the accuracy for how often the correct task-embedding was chosen for (in-distribution) test inputs. All methods use a singlehead. Note, that singlehead *PriorFocused* methods do not require task inference, and thus the distinction between *TGiven* and *TInfer* does not apply (Mean $\pm$ SEM, *ACC-inference* in %, $n = 10$). PR refers to *PosteriorReplay* and PF to *PriorFocused* methods.

	TGiven-During	TGiven-Final	TInfer-Final	ACC-inference
PR-Dirac	0.01007 ± 0.00170	0.01037 ± 0.00162	N/A	N/A
PR-BbB	0.01036 ± 0.00112	0.01037 ± 0.00121	0.01175 ± 0.00103	98.07 ± 0.53
PR-Radial	0.01238 ± 0.00184	0.01108 ± 0.00090	0.03996 ± 0.02377	96.19 ± 1.77
PR-AVB	0.00504 ± 0.00061	0.00712 ± 0.00181	0.00712 ± 0.00181	100.00 ± 0.00
PR-SSGE	0.00236 ± 0.00016	0.00251 ± 0.00020	0.00476 ± 0.00208	99.80 ± 0.13
EWC	0.08004 ± 0.02444	2.55570 ± 1.07003	N/A	N/A
VCL	0.09787 ± 0.00982	0.23889 ± 0.06711	N/A	N/A
PF-AVB	0.24125 ± 0.00315	0.46187 ± 0.07851	N/A	N/A
PF-SSGE	0.01546 ± 0.00082	2.09433 ± 0.78611	N/A	N/A

In this section we expand on the discussion from Sec. 4.1 on continually learning a set of low-dimensional regression tasks. Details about the dataset can be found in SM E.1. Quantitative results for a ReLU MLP-10,10 main network can be found in Table S2.

PosteriorReplay methods are all able to fit the polynomials well and do not seem to be affected by catastrophic interference. Notably, due to the choice of Gaussian likelihood with fixed variance (cf. Eq. 9), the likelihood function is not able to represent x-dependent (aleatoric) uncertainty. Therefore, all x-dependent uncertainty corresponds to parameter uncertainty, which is not captured by *PosteriorReplay-Dirac*. Interestingly, the reported *PosteriorReplay-AVB* run is always able to pick the right task embedding in a random-seed robust way, such that *TGiven-Final* and *TInfer-Final* scores

are identical. All reported *PriorFocused* methods use a singlehead main network and therefore do not require task inference. Instead, they have to learn a single posterior continually that captures well all data across tasks. Here, we observe that these methods greatly suffer from the stability-plasticity dilemma [71]: having enough plasticity to accommodate new tasks causes catastrophic interference with existing knowledge, while excessive protection of the existing shared posterior does not give the flexibility required to fit new data.

Supplementary qualitative plots showing the final approximate posteriors found by the *PosteriorReplay* methods are depicted in Fig. S3. While these plots convey the intuition behind uncertainty-based task inference, it should be noted that the ground-truth posterior shape is unknown, and that hyperparameters have a strong influence on these plots.

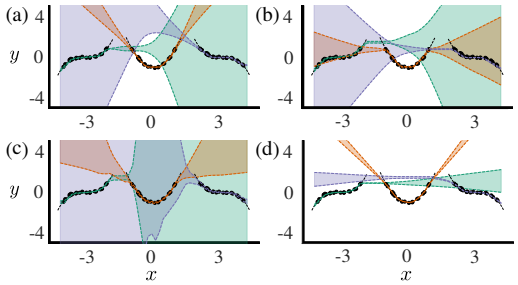

Figure S3: 1D polynomial regression task, where three polynomials need to be learned consecutively. Different colors represent the task-specific posterior approximations within the final model when training with different *PosteriorReplay* algorithms: **(a)** *PosteriorReplay-BbB*, **(b)***PosteriorReplay-Radial*, **(c)** *PosteriorReplay-AVB*, **(d)** *PosteriorReplay-SSGE*. The illustrations sketch the idea behind task inference via predictive uncertainty, i.e., for an input point x the posterior with the lowest predictive uncertainty can be chosen to make predictions. Note, if the input does not lie in the in-distribution space of any task, predictive uncertainty will be high for all posteriors.

Finally, to highlight a potential advantage of *implicit* methods, we qualitatively investigate the found posterior approximations by *PosteriorReplay-AVB* in Fig. S4. We provide joint density plots (using kernel density estimation) for random pairs of weights as well as Pearson correlation matrices for a random subset of weights. Note that these plots are not cherry-picked and are representative of the found posterior approximations. Weights in the posteriors of all tasks seem to be highly correlated, which is also to be expected for the unknown ground-truth posterior, since individual weight changes will affect the behavior of the neural network function and should therefore be coordinated to maintain stable in-distribution predictions. This is in contrast to mean-field approximations such as *PosteriorReplay-BbB* and *PosteriorReplay-Radial*, which by design are not able to capture weight correlations. In addition, the joint distribution plots for *PosteriorReplay-AVB* often exhibit multimodality. Presumably, this could be beneficial for OOD detection and thus task inference, since different modes in the posterior landscape may represent very different functions that exert vastly different behavior on OOD data and, indeed, when studying low-dimensional problems, we generally found it easier to find viable hyperparameter configurations with *implicit* methods than with *explicit* ones. However, such argument is purely speculative and should be considered with care given that single high-dimensional posterior modes might be flat in many directions and thus also be able to capture a diverse set of functions [29, 68].

D.2 2D Mode Classification

Next, we reconsider the 2D mode classification introduced in Sec. 4.2. All results are obtained with a ReLU MLP-10,10 main network. Details about this synthetic dataset can be found in SM E.2, and quantitative results are reported in Table S3.

As reflected in the *TGiven-Final* scores, forgetting is not a concern in this benchmark. Instead, we use this experiment to gain insights on how task inference based on predictive uncertainty works in classification tasks. Recall, that the softmax likelihood function can represent arbitrary $\mathbf{x}$-dependent discrete distributions, which (in contrast to Sec. 4.1) allows the model to exhibit $\mathbf{x}$-dependent aleatoric uncertainty. Deterministic approaches such as *PosteriorReplay-Dirac* only have access to aleatoric uncertainty, and therefore rely solely on it for task inference. However this has certain

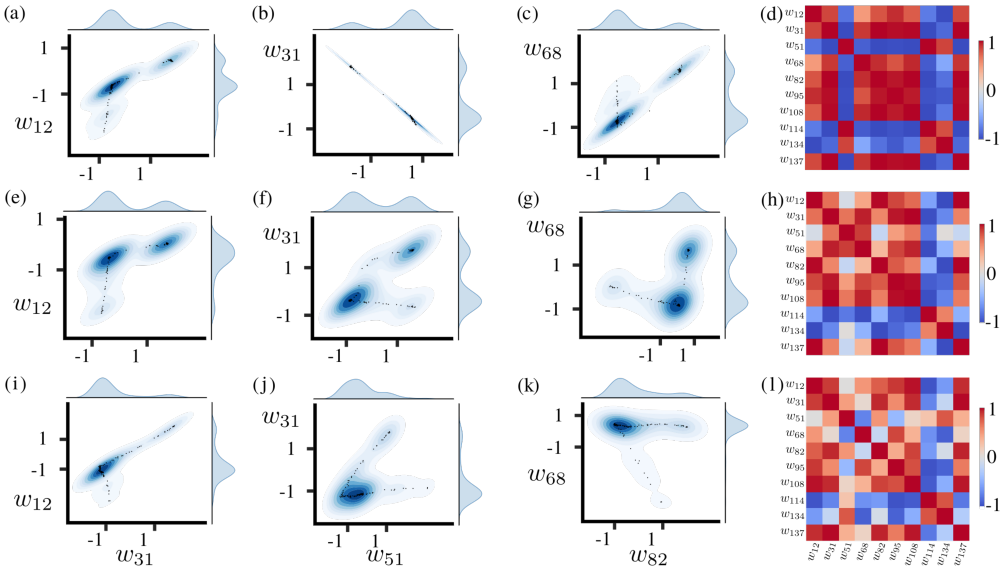

Figure S4: Example illustrations of weight distributions captured by the final approximate posteriors when learning the 1D polynomial regression task with *PosteriorReplay-AVB*. **(a)-(c)** Joint density plots of task 1 for three random pairs of weights. **(d)** Weight correlations in task 1 for a subset of randomly chosen weights. Same for the approximate posterior of task 2 **(e)-(h)** and task 3 **(i)-(l)**. Note, that unlike unimodal mean-field approximations (cf. *PosteriorReplay-BbB* and *PosteriorReplay-Radial*), *implicit* methods can capture correlations between weights and multi-modality.

Table S3: Accuracies for the 2D mode classification experiments (Mean $\pm$ SEM in %, $n = 10$). PR refers to *PosteriorReplay*, PF to *PriorFocused* methods and SP to *SeparatePosteriors*.

	TGiven-During	TGiven-Final	TInfer-Final (Ent)	TInfer-Final (Conf)	TInfer-Final (Agree)
PR-Dirac	100.0 ± 0.00	99.78 ± 0.21	44.90 ± 5.74	45.43 ± 5.84	N/A
PR-BbB	100.0 ± 0.00	100.0 ± 0.00	81.07 ± 6.78	81.07 ± 6.78	90.02 ± 3.57
PR-Radial	95.08 ± 2.38	95.08 ± 2.38	54.50 ± 5.01	54.50 ± 5.01	76.33 ± 4.18
PR-AVB	100.0 ± 0.00	100.0 ± 0.00	98.57 ± 1.33	98.57 ± 1.33	99.93 ± 0.06
PR-SSGE	100.0 ± 0.00	100.0 ± 0.00	100.0 ± 0.00	100.0 ± 0.00	100.0 ± 0.00
SP-Dirac	N/A	100.0 ± 0.00	70.92 ± 4.96	74.17 ± 3.78	N/A
SP-BbB	N/A	100.0 ± 0.00	85.13 ± 2.58	85.13 ± 2.58	87.92 ± 2.29
SP-AVB	N/A	100.0 ± 0.00	95.00 ± 2.09	95.00 ± 2.09	98.62 ± 1.23
VCL-multihead	100.0 ± 0.00	100.0 ± 0.00	45.17 ± 3.80	45.17 ± 3.80	47.13 ± 4.26
PF-AVB-multihead	100.0 ± 0.00	98.17 ± 1.57	64.53 ± 4.99	64.53 ± 4.99	65.40 ± 5.05
PF-SSGE-multihead	100.0 ± 0.00	95.92 ± 1.71	50.00 ± 3.33	49.40 ± 3.06	50.02 ± 3.33

limitations since aleatoric uncertainty is only calibrated in-distribution. For instance, the typical cross-entropy loss criterion used for classification tasks can be linked to the minimization of the quantity: $\mathbb{E}_{p(\mathbf{X})}\big[\mathrm{KL}\big(p(\mathbf{Y} \mid \mathbf{X}) || p(\mathbf{Y} \mid \mathbf{W}; \mathbf{X})\big)\big]$, where $p(\mathbf{X})p(\mathbf{Y} \mid \mathbf{X})$ denotes the unknown underlying data-generating process and $p(\mathbf{Y} \mid \mathbf{W}; \mathbf{X})$ is the model likelihood. Thus, the behaviour of aleatoric uncertainty as reflected in $p(\mathbf{Y} \mid \mathbf{W}; \mathbf{X})$ for OOD data (e.g., outside the support of $p(\mathbf{X})$) is not calibrated and can indeed be harmful for OOD detection (e.g., [25]). This intuition is validated by our *PosteriorReplay-Dirac* results, which exhibit rather arbitrary behavior on OOD data (Fig. S6). This might also explain the notable difference in the results reported for *PosteriorReplay-Dirac* and *SeparatePosteriors-Dirac* in Table S3, while probabilistic *PosteriorReplay* methods behave similarly. We provide uncertainty maps for all studied probabilistic *PosteriorReplay* methods in Fig. S5.

A desirable behavior for good OOD detection would entail having low uncertainty only where the training data of the corresponding task resides, while having high uncertainty elsewhere. As opposed to the deterministic case, Bayesian approaches reflect this intuition (cf. Fig. S6), despite not being

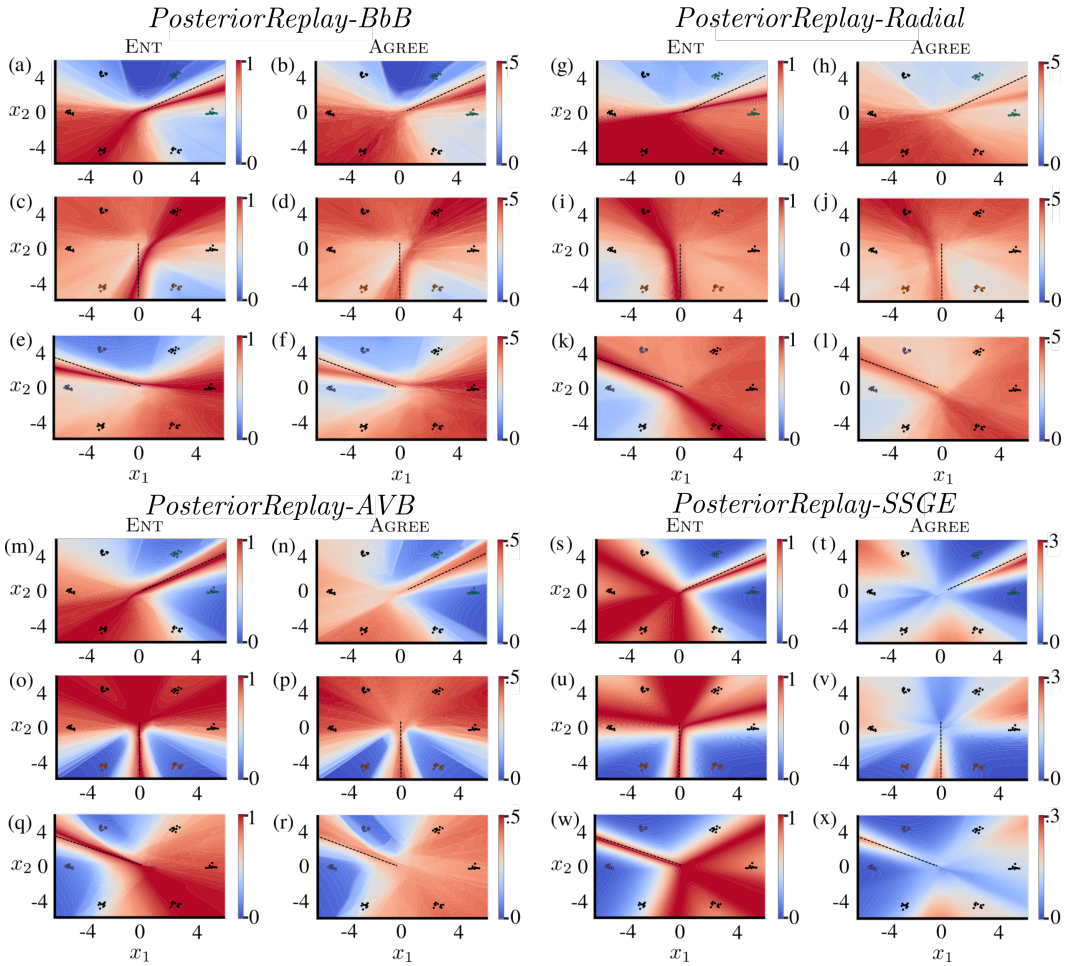

Figure S5: 2D mode classification uncertainty maps for probabilistic *PosteriorReplay* approaches. **(a)** Entropy of the predictive distribution (*Ent*) of task 1 across the input space covering in-distribution domains of all tasks, when training with *PosteriorReplay-BbB*. Dots represent training points and colors indicate task-affiliation. The dashed line represents the decision boundary for task 1. **(b)** Same as (a) but uncertainty here reflects model agreement (*Agree*). The same uncertainty maps are produced using the final approximate posteriors for task 2 **(c)**-**(d)** and 3 **(e)**-**(f)**. To show qualitative results for several probabilistic *PosteriorReplay* approaches, the uncertainty maps (a)-(f) are repeated for *PosteriorReplay-Radial* **(g)**-**(l)**, *PosteriorReplay-AVB* **(m)**-**(r)** and *PosteriorReplay-SSGE* **(s)**-**(x)**.

perfect OOD detectors. Note that, since the uncertainty map of the true Bayesian posterior is unknown, it remains unclear whether this imperfection originates from the approximate nature of the used posteriors, or whether it is innate to the real posterior. Importantly, the displayed uncertainty maps represent aggregated results over many models drawn from the approximate posteriors. Therefore, an interesting question arises, i.e., whether the depicted uncertainty maps result from models having high aleatoric uncertainty on OOD data, or from individual models behaving very differently on OOD data. To answer this question, we plot the softmax entropy maps for individual models drawn from the posterior of *PosteriorReplay-AVB* in Fig. S7.

Uncertainty maps from individual models look very different, suggesting that epistemic uncertainty is crucial for OOD detection in this experiment. This is supported by the fact that the *Ent* uncertainty map looks very similar to that obtained with *Agree*, even though *Ent* is supposed to capture both aleatoric and epistemic uncertainty. However, one needs to keep in mind that these are qualitative results which strongly depend the selected hyperparameter configuration, as can be seen for the chosen *PosteriorReplay-SSGE* results.

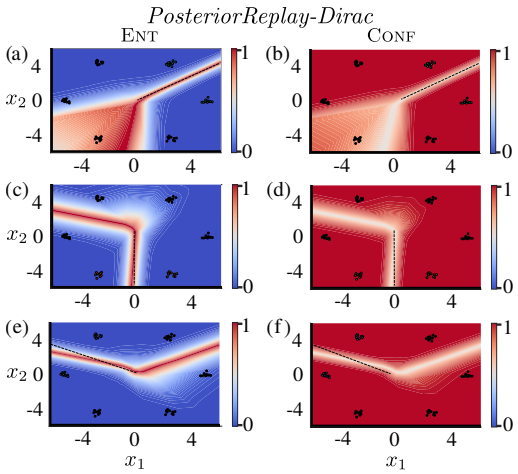

Figure S6: 2D mode classification uncertainty maps for *PosteriorReplay-Dirac*. **(a)** Entropy of the predictive distribution (*Ent*) of task 1 across the input space covering in-distribution domains of all tasks. Dots represent training points, colors task-affiliation and the dashed line the decision boundary for task 1. **(b)** Same as (a) but uncertainty here reflects the confidence of the predictive distribution (*Conf*). Same uncertainty maps with the final approximate posteriors for task 2 **(c)**-**(d)** and 3 **(e)**-**(f)**.

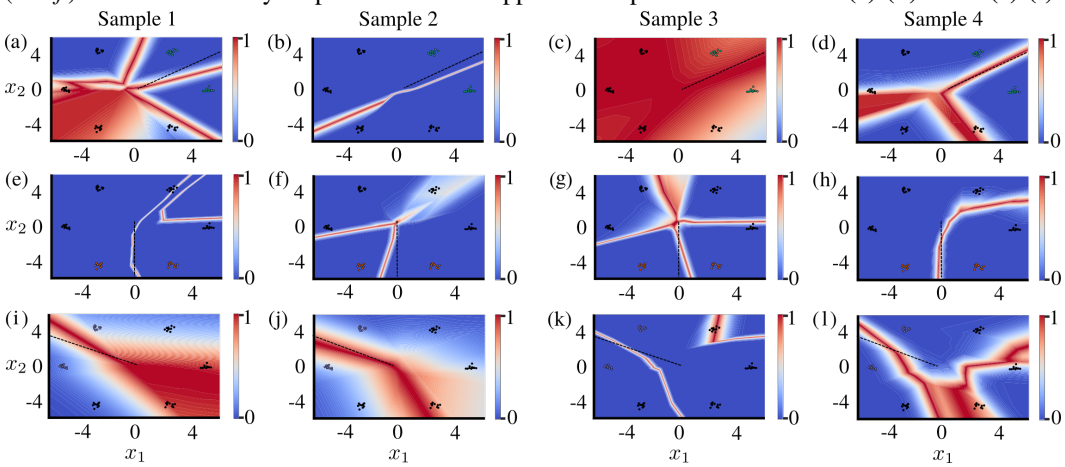

Figure S7: 2D mode classification uncertainty maps of single sample points drawn from the final approximate posteriors trained with *PosteriorReplay-AVB*. **(a)** Entropy of the softmax output for a sample point $\mathbf{w} \sim q_{\boldsymbol{\theta}^{(1)}}(\mathbf{W})$ of task 1 across the input space covering in-distribution domains of all tasks. **(b)**-**(d)** same as (a) for different sample points $\mathbf{w} \sim q_{\boldsymbol{\theta}^{(1)}}(\mathbf{W})$. Posterior draws for task 2 using $q_{\boldsymbol{\theta}^{(2)}}(\mathbf{W})$ are shown in **(e)**-**(h)** and for task 3 using $q_{\boldsymbol{\theta}^{(3)}}(\mathbf{W})$ are shown in **(i)**-**(l)**, respectively. Intriguingly, individual models tend to be overconfident (similar to Fig. S6), and different models exhibit very different uncertainty behavior. Thus, the overall uncertainty reflected in the predictive distribution (cf. Fig. S5) is likely induced through parameter uncertainty.

In this experiment, *PriorFocused* methods perform worse in uncertainty-based task inference than *PosteriorReplay* methods. A reason could be the impaired ability of *PriorFocused* methods to capture task-specific epistemic uncertainty. This may be due to the fact that data from all tasks is used to train a shared body, and thus the posterior models drawn from it should lead to similar hidden activations (i.e., low epistemic uncertainty) for data from all tasks. Thus, epistemic uncertainty, which we saw above is crucial for task inference, will mainly be introduced by the task-specific outputs heads which process those hidden activations. In contrast, the posterior of all weights in *PosteriorReplay* methods has only ever seen data from one task and can therefore exhibit high epistemic uncertainty when computing hidden activations for data from different tasks.

We also experiment with *EWC-multihead*, for which we obtain chance level predictions. To understand this effect, let's recall that EWC relies on the post-hoc construction of the posterior, for which the

computation of the empirical Fisher information matrix is required in order to approximate the loss curvature. In our results, we observe that some of the computed Fisher values are zero. Looking at Eq. 38 one can see that whenever Fisher values are very low for a certain weight, the variance of the posterior for that weight will be dominated by the variance of the prior, which was set to one in our experiments. We hypothesize that such high variance for certain weights in the constructed posterior is the reason for the low performance displayed by *EWC-multihead* in such a small network. Note, that the empirical Fisher values are computed as a sum of squared log-likelihood gradients computed across the whole training set. These gradients are zero for some weights, which might be due to overfitting; a conceivable problem given the low dataset size. We observed the same issue when testing *EWC-multihead* for the 1D regression experiment. Intriguingly, this observation also implies that the empirical Fisher approximation failed to appropriately approximate the Hessian and thus capture loss curvature.

D.3 SplitMNIST

Here we provide additional results obtained for the SplitMNIST experiment. In particular, we compare the different methods for three different main network architectures: Table S4 contains results obtained with a ReLU MLP with two hidden layers of 100 neurons (MLP-100,100), Table S5 for an MLP-400,400 and Table S6 for a Lenet [44] with a kernel size of 5, 20 resp. 50 feature maps in the two convolutional layers and 500 units in the penultimate fully-connected layer.

Table S4: Accuracies of SplitMNIST experiments when using an MLP-100,100 (Mean $\pm$ SEM in %, $n = 10$). Column *TInfer-Final* represents *TInfer-Final (Ent)* accuracies if applicable. Otherwise this column is used to report results of methods that learn a shared softmax across all tasks. PR refers to *PosteriorReplay* and PF to *PriorFocused* methods.

	TGiven-During	TGiven-Final	TInfer-Final	TInfer-Final (Conf)	TInfer-Final (Agree)
PR-Dirac	99.72 $\pm$ 0.01	99.72 $\pm$ 0.01	63.41 $\pm$ 1.54	48.41 $\pm$ 1.02	N/A
PR-BbB	99.75 $\pm$ 0.01	99.75 $\pm$ 0.01	70.07 $\pm$ 0.56	65.34 $\pm$ 0.66	70.11 $\pm$ 0.54
PR-Radial	99.55 $\pm$ 0.06	99.43 $\pm$ 0.10	63.00 $\pm$ 1.56	64.03 $\pm$ 1.19	63.06 $\pm$ 1.55
PR-SSGE	99.66 $\pm$ 0.02	99.65 $\pm$ 0.02	66.15 $\pm$ 0.92	47.89 $\pm$ 0.67	66.20 $\pm$ 0.92
EWC-growing	N/A	N/A	28.15 $\pm$ 0.51	N/A	N/A
EWC-shared	N/A	N/A	29.67 $\pm$ 0.86	N/A	N/A
EWC-multihead	99.01 $\pm$ 0.03	97.79 $\pm$ 0.30	46.61 $\pm$ 1.26	46.63 $\pm$ 1.27	19.97 $\pm$ 0.01
VCL-multihead	97.83 $\pm$ 0.03	96.05 $\pm$ 0.21	51.45 $\pm$ 1.11	51.45 $\pm$ 1.11	51.02 $\pm$ 1.22
PF-SSGE-multihead	99.74 $\pm$ 0.01	96.48 $\pm$ 0.54	51.26 $\pm$ 1.72	49.64 $\pm$ 1.72	51.59 $\pm$ 1.64
PR-BbB-BW	99.75 $\pm$ 0.01	99.75 $\pm$ 0.01	99.75 $\pm$ 0.01	99.75 $\pm$ 0.01	99.75 $\pm$ 0.01
PR-BbB-CS	99.41 $\pm$ 0.04	98.70 $\pm$ 0.05	90.42 $\pm$ 0.19	90.42 $\pm$ 0.19	59.09 $\pm$ 0.64
Exp-Replay	N/A	N/A	86.84 $\pm$ 0.51	N/A	N/A

Some general trends can be observed independent of the main network architecture used. Catastrophic forgetting is not a major issue in this experiment, as illustrated by similar *TGiven-During* and *TGiven-Final* scores across methods. Only *prior-focused* approaches seem slightly affected by forgetting and sometimes exhibit a slight drop in *TGiven-Final* accuracies, which however stay above 96% for all methods and architectures. Much wider variations can be observed in the task-agnostic setting where task identity needs to be inferred. Despite the fact that we could improve upon previously reported results for the *PosteriorReplay-Dirac* baseline in MLP-400,400 (termed HNET+ENT in von Oswald et al. [91]), this deterministic solution generally performs worse at inferring task identity than probabilistic approaches, notably *PosteriorReplay-BbB*. Interestingly, *PosteriorReplay-BbB* consistently outperforms *PosteriorReplay-Radial* in this experiment by a large extent, which is in disagreement with the performance gains reported by Farquhar et al. [18] on other datasets. A potential cause for the differences in performance can be that, as opposed to Farquhar et al. [18], we tempered the posteriors [92]. This was done because successful training for both *PosteriorReplay-Radial* and *PosteriorReplay-BbB* could only be accomplished when notably reducing the prior influence in the loss computation. When using *implicit* posterior distributions via *PosteriorReplay-SSGE*, performance gains can be observed over *PosteriorReplay-BbB* for MLP-400,400 and Lenet main networks. Using SSGE to learn a single *implicit* posterior distribution (*PriorFocused-SSGE-multihead*) leads however

Table S5: Accuracies of SplitMNIST experiments when using an MLP-400,400 (Mean $\pm$ SEM in %, $n = 10$). Column *TInfer-Final* represents final accuracies when task identity is inferred with the *Ent* criterion, if applicable. Otherwise this column is used to report results of methods that learn a shared softmax across all tasks. Results denoted with a * are taken from van de Ven and Tolias [87] and those denoted with a ** are taken from von Oswald et al. [91]. SI stands for *synaptic intelligence* [96], and DGR for *deep generative replay* Shin et al. [80]. HNET+TIR and HNET+R are CL methods based on hypernetwork-protected replay proposed in von Oswald et al. [91]. PR refers to *PosteriorReplay*, PF to *PriorFocused* methods and SP to *SeparatePosteriors*.

	TGiven-During	TGiven-Final	TInfer-Final	TInfer-Final (Conf)	TInfer-Final (Agree)
PR-Dirac	99.65 ± 0.02	99.65 ± 0.01	70.88 ± 0.61	56.56 ± 0.64	N/A
PR-BbB	99.73 ± 0.01	99.72 ± 0.02	71.73 ± 0.87	67.42 ± 0.68	71.73 ± 0.85
PR-Radial	99.64 ± 0.01	99.64 ± 0.01	66.01 ± 0.92	61.56 ± 0.38	66.22 ± 0.93
PR-SSGE	99.78 ± 0.01	99.77 ± 0.01	71.91 ± 0.79	55.15 ± 0.67	71.43 ± 0.77
EWC-growing	N/A	N/A	27.32 ± 0.60	N/A	N/A
EWC-shared	N/A	N/A	30.21 ± 0.52	N/A	N/A
EWC-multihead	99.70 ± 0.01	96.40 ± 0.62	47.67 ± 1.52	47.67 ± 1.52	47.52 ± 1.48
VCL-multihead	96.66 ± 0.19	96.45 ± 0.13	58.84 ± 0.64	58.84 ± 0.64	56.54 ± 0.94
PF-SSGE-multihead	99.79 ± 0.01	99.02 ± 0.16	62.70 ± 1.32	61.62 ± 1.31	62.76 ± 1.31
PR-Dirac-SR	99.65 ± 0.01	99.64 ± 0.01	71.34 ± 0.49	58.05 ± 0.35	N/A
PR-BbB-SR	99.73 ± 0.02	99.73 ± 0.02	72.38 ± 0.77	66.50 ± 0.76	72.39 ± 0.77
PR-BbB-BW	99.73 ± 0.01	99.72 ± 0.02	99.72 ± 0.02	99.72 ± 0.02	99.72 ± 0.02
PR-BbB-CS	99.34 ± 0.05	98.50 ± 0.09	90.83 ± 0.24	90.83 ± 0.24	59.74 ± 0.59
SP-Dirac	N/A	99.77 ± 0.01	70.39 ± 0.27	63.69 ± 0.10	N/A
SP-BbB	N/A	99.81 ± 0.00	68.40 ± 0.23	63.37 ± 0.85	68.37 ± 0.24
SP-SSGE	N/A	99.76 ± 0.04	71.53 ± 1.34	68.50 ± 0.99	71.36 ± 1.31
SP-TC-Dirac	N/A	99.79 ± 0.02	71.84 ± 0.49	50.69 ± 1.23	N/A
SP-TC-BbB	N/A	99.77 ± 0.01	72.74 ± 0.45	72.87 ± 0.57	72.79 ± 0.45
Exp-Replay	N/A	N/A	88.85 ± 0.39	N/A	N/A
EWC-growing*	N/A	N/A	19.96 ± 0.07	N/A	N/A
SI-growing*	N/A	N/A	19.99 ± 0.06	N/A	N/A
DGR*	N/A	N/A	91.79 ± 0.32	N/A	N/A
PR-Dirac**	N/A	N/A	69.48 ± 0.80	N/A	N/A
HNET+TIR**	N/A	N/A	89.59 ± 0.59	N/A	N/A
HNET+R**	N/A	N/A	95.30 ± 0.13	N/A	N/A

to a significant drop in performance across architectures, which highlights the potential of a system that learns task-specific posteriors. Yet, compared to *prior-focused* approaches that do not use *implicit* distributions, *PriorFocused-SSGE-multihead* generally performs better, illustrating that more flexible posterior approximations can lead to improved performance when trade-off solutions need to be found.

When applied with a growing (*EWC-growing*) or shared softmax (*EWC-shared*), EWC leads to very poor results in all architectures, even though we manage to considerably improve upon the existing *EWC-growing** baseline. The use of a multihead significantly improves performance, but even in this case the performance of EWC remains well below other *PriorFocused* methods such as *VCL-multihead*. A potential cause is the post-hoc construction of the posterior in EWC, as noted in SM D.2.

Note that, if task inference performance is above chance-level for individual inputs, it can be improved as a simple statistical effect by looking at multiple samples belonging to the same task. Indeed, in all three architectures, we observe that performance in a task-agnostic setting can be dramatically improved when task inference is performed on a set of 100 samples rather than individual ones. Task inference becomes perfect in all three architectures, leading to identical *TGiven-Final* and *TInfer-Final* accuracies. Even though we only report results for BbB (**PosteriorReplay-BbB-BW**), all methods equally benefit from such aggregated task inference. An additional way to considerably

Table S6: Accuracies of SplitMNIST experiments when using a Lenet (Mean $\pm$ SEM in %, $n = 10$). Column *TInfer-Final* represents final accuracies when task identity is inferred with the *Ent* criterion, if applicable. Otherwise this column is used to report results of methods that learn a shared softmax across all tasks. PR refers to *PosteriorReplay*, PF to *PriorFocused* methods and SP to *SeparatePosteriors*.

	TGiven-During	TGiven-Final	TInfer-Final	TInfer-Final (Conf)	TInfer-Final (Agree)
PR-Dirac	99.92 ± 0.01	99.87 ± 0.04	72.33 ± 2.75	57.22 ± 3.25	N/A
PR-BbB	98.96 ± 0.90	99.20 ± 0.67	74.09 ± 1.38	67.39 ± 1.39	74.13 ± 1.33
PR-Radial	99.85 ± 0.03	99.78 ± 0.05	68.99 ± 2.06	64.63 ± 2.79	69.41 ± 2.12
PR-SSGE	99.89 ± 0.01	99.89 ± 0.01	77.56 ± 1.01	57.29 ± 1.89	77.55 ± 1.02
EWC-growing	N/A	N/A	27.62 ± 0.55	N/A	N/A
EWC-shared	N/A	N/A	26.01 ± 1.02	N/A	N/A
EWC-multihead	98.09 ± 0.75	97.17 ± 0.54	49.78 ± 2.20	49.77 ± 2.20	49.85 ± 2.11
VCL-multihead	98.03 ± 0.07	97.43 ± 0.12	63.05 ± 0.63	63.05 ± 0.63	62.24 ± 0.73
PF-SSGE-multihead	99.94 ± 0.00	99.37 ± 0.10	74.18 ± 1.00	38.15 ± 0.90	74.12 ± 1.01
PR-BbB-BW	98.96 ± 0.90	99.20 ± 0.67	99.20 ± 0.67	99.20 ± 0.67	99.20 ± 0.67
PR-BbB-CS	99.76 ± 0.02	99.62 ± 0.02	95.73 ± 0.05	95.73 ± 0.05	60.69 ± 1.13
SP-Dirac	N/A	99.92 ± 0.00	85.50 ± 0.28	70.98 ± 0.34	N/A
SP-BbB	N/A	99.93 ± 0.00	85.52 ± 0.45	71.22 ± 1.41	85.47 ± 0.45
SP-TC-Dirac	N/A	99.91 ± 0.00	82.85 ± 0.60	55.38 ± 0.25	N/A
SP-TC-BbB	N/A	99.92 ± 0.00	84.16 ± 0.42	84.06 ± 0.41	84.04 ± 0.38

improve task inference performance is the use of coresets in a fine-tuning stage at the end of training (*CS*). This approach leads to results that are comparable to prior work based on generative replay (e.g., DGR*, HNET+TIR**). Although this approach leads to lower performance than the use of batches for inferring the task, the use of coresets does not rely on the assumption that a set of samples belongs to the same task, and when such an assumption is plausible both tricks can be simultaneously used to further boost performance.

The relative behavior of the three criteria for quantifying uncertainty is also stable across architectures. *Ent* and *Agree* generally lead to very similar results, while *Conf* often performs worse, except for *EWC-multihead* and *VCL-multihead*, where all three approaches behave similarly. Interestingly, when using coresets to facilitate task inference, OOD data becomes in-distribution, and hinders the ability of the *Agree* criterion to infer task identity, as shown by our *TInfer-Final (Agree)* results for *PosteriorReplay-BbB-CS*.

Training separate posteriors per task (*SeparatePosteriors*) controls for the influence of the shared system on performance and uncertainty-based task inference. Our results for MLP-400,400 indicate that the CL performance of *PosteriorReplay-Dirac* and *PosteriorReplay-SSGE* is very close to what is achieved when a different model can be allocated per task. To our surprise, however, BbB exhibits lower performance when used to learn independent posteriors (*SeparatePosteriors-BbB*), than when used in a CL setting (*PosteriorReplay-BbB*). Since *PosteriorReplay-SSGE* does not exhibit the same trend, the cause is likely not rooted in Bayesian inference for this model class, but rather in the particular approximation used. Interestingly, the *SeparatePosteriors* performance achieved in the deterministic case and with BbB (*SeparatePosteriors-Dirac*, *SeparatePosteriors-BbB*) improves marginally when the parameters of the approximate posteriors are not learned directly, but generated by a hypernetwork (*SeparatePosteriors-TC-Dirac*, *SeparatePosteriors-TC-BbB*). The results are somewhat different for a Lenet, where learning separate posteriors leads to a much larger performance improvement in *SeparatePosteriors-Dirac* and *SeparatePosteriors-BbB* compared to the *PosteriorReplay* setting. In this case, however, the use of a hypernetwork to generate main network weights does not lead to increased *SeparatePosteriors* performance, highlighting the complicated influence of the architectural setup on uncertainty, and therefore task inference.

For the MLP-400,400 we provide *PosteriorReplay* results for the case where, in each update, the CL regularization is only applied to a subset of tasks chosen randomly, denoted as stochastic

Table S7: Accuracies of SplitMNIST experiments when using an MLP-400,400 (Mean $\pm$ SEM in %, $n = 10$) using the *KU* task-inference criterion.

	TInfer-Final (KU)
PR-BbB	46.53 ± 1.04
PR-SSGE	53.68 ± 0.43
PR-BbB-CS	42.86 ± 1.31

regularization (**SR**).[9] Thus, the regularization cost does not increase with the number of tasks. For both *PosteriorReplay-Dirac-SR* and *PosteriorReplay-BbB-SR*, the *TGiven-Final* accuracies are almost identical to the runs with the full regularizations. But interestingly enough, in a task-agnostic setting, the stochastic regularization leads to better *TInfer-Final* accuracies in both methods. We hypothesize that the reason for this performance increase might be related to the reason why stochastic gradient descent performs in practice better than gradient descent. Specifically, this stochastic regularization may make it easier to escape local minima. Overall, this shows that a stochastic CL regularization of the hypernetwork outputs not only allows to considerably reduce computation, but can also lead to improved results.

When comparing the behavior of individual methods for different architectures, we generally observe improved uncertainty-based task inference with increasing main network complexity (i.e., the results obtained for MLP-100,100 are generally worse than for MLP-400,400, which in turn are worse than for Lenet). This is especially noticeable for *PosteriorReplay-Dirac*, *PosteriorReplay-SSGE*, *VCL-multihead* and *PriorFocused-SSGE-multihead*, whereas the performance of *EWC-multihead* in all three considered settings is similar. We speculate that improved performance in increasingly complex architectures is due to differences in the resulting inductive biases [93]. For example, compared to an MLP, a convolutional architecture such as Lenet is supposed to have a much better inductive bias towards data with local structure (e.g., SplitMNIST), and might therefore be better suited for detecting whether an image belongs to a certain task or not.

For the MLP-400,400 we provide *TInfer-Final* results using the *KU* criterion described in SM C.6. Results can be found in Table S7. Perhaps surprisingly, we observe that this uncertainty estimate leads to quite poor task-inference results, even lower than the confidence criterion (*Conf*), suggesting that epistemic uncertainty is not properly captured by this metric on OOD data. We also tested this criterion with our coreset method (*PR-BbB-CS*), which explicitly calibrates for high aleatoric uncertainty in the data that was originally OOD (i.e., other tasks) and therefore causes the OOD data to become in-distribution (cf. SM C.7). Thus, if on in-distribution data aleatoric uncertainty is properly discounted by the proposed uncertainty estimate, poor task-inference can be expected. We indeed observe this in our new results (the task-agnostic performance obtained with this estimate is very low, i.e. 42% vs. 90% for *Ent* or 60% for *Agree*).

D.4 PermutedMNIST-10

In this section, we consider the PermutedMNIST benchmark [20], another adaptation of MNIST to CL, where different tasks are obtained by applying, for each task, a different pixel permutation to the input digits. The results of learning ten different tasks with an MLP with two hidden layers of 100 neurons (MLP-100,100) are presented in Table S8, and with an MLP with two hidden layers of 1000 neurons (MLP-1000,1000) in Table S9. Note that, for compatibility with previous literature [87, 91], the experiments with the MLP-1000,1000 are done by padding the original MNIST images with zeros before applying the permutation, which results in inputs of size 32×32 instead of the original 28×28 dimensions.

In the MLP-100,100 experiments (Table S8), catastrophic forgetting is successfully prevented by all *PosteriorReplay* methods, as indicated by the similar performance in *TGiven-During* and *TGiven-Final* accuracies. Note, that if no explicit CL strategy is applied as in *Fine-Tuning*, severe catastrophic interference can be observed for this small network architecture. In a setting where task iden-

[9] The results reported here have been obtained by selecting one task embedding at random for regularization at each iteration.

Table S8: Accuracies of PermutedMNIST-10 experiments when using an MLP-100,100 (Mean $\pm$ SEM in %, $n = 10$). PR refers to *PosteriorReplay*.

	TGiven-During	TGiven-Final	TInfer-Final (Ent)	TInfer-Final (Conf)	TInfer-Final (Agree)
PR-Dirac	95.70 ± 0.03	95.05 ± 0.04	75.84 ± 0.51	75.14 ± 0.50	N/A
PR-BbB	95.44 ± 0.04	94.35 ± 0.06	89.90 ± 0.33	88.38 ± 0.33	70.52 ± 0.86
PR-Radial	94.31 ± 0.03	94.30 ± 0.03	81.78 ± 0.36	79.87 ± 0.33	76.73 ± 0.45
PR-SSGE	93.58 ± 0.10	92.88 ± 0.10	78.94 ± 0.73	77.43 ± 0.73	68.93 ± 0.88
Fine-Tuning	97.44 ± 0.01	47.89 ± 0.46	N/A	N/A	N/A

Table S9: Accuracies of PermutedMNIST-10 experiments when using an MLP-1000,1000 (Mean $\pm$ SEM in %, $n = 10$). Column *TInfer-Final* represents final accuracies when task identity is inferred with the *Ent* criterion, if applicable. Otherwise this column is used to report results of methods that learn a shared softmax across all tasks. Results denoted with * are taken from van de Ven and Tolias [87] and those denoted with ** are taken from von Oswald et al. [91]. SI stands for *synaptic intelligence* [96], and DGR for *deep generative replay* Shin et al. [80]. HNET+TIR and HNET+R are CL methods based on hypernetwork-protected replay proposed in von Oswald et al. [91]. PR refers to *PosteriorReplay*.

	TGiven-During	TGiven-Final	TInfer-Final	TInfer-Final (Conf)	TInfer-Final (Agree)
PR-Dirac	96.78 ± 0.03	96.73 ± 0.03	94.15 ± 0.18	93.41 ± 0.16	N/A
PR-BbB	96.33 ± 0.02	96.21 ± 0.03	96.14 ± 0.03	95.86 ± 0.05	85.92 ± 0.32
PR-Radial	97.19 ± 0.02	97.19 ± 0.02	92.92 ± 0.20	92.68 ± 0.19	92.26 ± 0.19
PR-SSGE	97.57 ± 0.02	97.39 ± 0.02	93.58 ± 0.13	93.39 ± 0.12	93.02 ± 0.10
EWC-multihead	96.87 ± 0.02	94.73 ± 0.11	81.12 ± 0.62	79.32 ± 0.59	79.46 ± 0.57
VCL-multihead	95.15 ± 0.02	89.72 ± 0.24	85.40 ± 0.49	81.66 ± 0.56	79.80 ± 0.86
Fine-Tuning	98.13 ± 0.01	90.08 ± 0.45	N/A	N/A	N/A
EWC-growing*	N/A	N/A	33.88 ± 0.49	N/A	N/A
SI-growing*	N/A	N/A	29.31 ± 0.62	N/A	N/A
DGR*	N/A	N/A	96.38 ± 0.03	N/A	N/A
PR-Dirac**	N/A	N/A	91.75 ± 0.21	N/A	N/A
HNET+TIR**	N/A	N/A	97.59 ± 0.01	N/A	N/A
HNET+R**	N/A	N/A	97.76 ± 0.76	N/A	N/A

tity is given (*TGiven*), all methods perform similarly, except for *PosteriorReplay-SSGE* which exhibits slightly lower performance. However, whenever task identity needs to be inferred, all three probabilistic methods outperform *PosteriorReplay-Dirac*, highlighting the advantages of using a Bayesian approach for inferring task identity via predictive uncertainty. In agreement with our SplitMNIST results, *PosteriorReplay-BbB* performs considerably better than *PosteriorReplay-Radial*. *PosteriorReplay-SSGE*, despite using more flexible *implicit* distributions, performs poorly compared to *PosteriorReplay-BbB*. Note that, here, individual tasks are more difficult than in SplitMNIST, and a method as complex as SSGE might be disproportionately affected by an increase in task difficulty. As opposed to our SplitMNIST results, when comparing different methods to quantify uncertainty for task inference one can observe that *Ent* systematically yields the best results, closely followed by *Conf*. However, when applicable, accuracies based on the *Agree* criterion lead to lower performance. A potential reason could be that all employed approximate inference methods lead to poor approximations that do not capture the space of admissible solutions well.

Similar trends can be observed for the MLP-1000,1000 (Table S9). Catastrophic forgetting only seems to be an issue for the prior-focused methods *EWC-multihead* and *VCL-multihead*. Interestingly, the *Fine-Tuning* baseline shows that, despite not adopting any strategy for CL, catastrophic interference is also not very severe due to the capacity of this large network. We could not find viable hyperparameter configurations for an *implicit* prior-focused method, i.e., *PriorFocused-SSGE*, and

therefore do not report results for this method. The deterministic solution *PosteriorReplay-Dirac* performs surprisingly well, specially in a task-agnostic setting (*TInfer-Final* in the Table), for which we significantly improve upon the previous baseline (*PosteriorReplay-Dirac***), and that is only outperformed by *PosteriorReplay-BbB* and methods based on replay. Interestingly, despite having similar performance when task identity is given (especially *EWC-multihead*), *PriorFocused* approaches perform considerably worse than *PosteriorReplay* approaches whenever task identity needs to be inferred. The performance we obtain for *EWC-multihead* in a task-agnostic setting is, however, vastly superior to that reported by prior work (*EWC-growing** and *SI-growing**), highlighting the benefits of using a multihead architecture in *prior-focused* CL. Again, when task identity needs to be inferred, *Ent* results in the best performance, but as opposed to the MLP-100,100 case, *Agree* often leads to comparable results. While results reported by prior work when using generative replay methods (DGR, HNET+TIR and HNET+R) perform best, the gap with *PosteriorReplay-BbB*, which does not use generative models, is small.

When comparing the results obtained with both architectures, as expected, performance is slightly higher for the larger MLP when task identity is given. This gap in performance is much more noticeable when task identity needs to be inferred. However, this could also be explained by the fact that for the larger MLP, the dimensionality of the input images is considerably larger due to padding, which might render task inference easier.

D.5 PermutedMNIST-100

To study whether our *posterior meta-replay* approach scales to longer task sequences, we also experimented with *PosteriorReplay-BbB* in PermutedMNIST with 100 tasks. Results for an MLP-1000,1000 are reported in Table S10. The results are obtained using the stochastic regularization *SR* in order to avoid a linear runtime increase with the number of tasks.

Table S10: Accuracies of PermutedMNIST-100 experiments when using an MLP-1000,1000 (Mean $\pm$ SEM in %, $n = 5$). PR refers to *PosteriorReplay*.

	TGiven-During	TGiven-Final	TInfer-Final (Ent)	TInfer-Final (Conf)	TInfer-Final (Agree)
PR-Dirac-SR	96.73 ± 0.02	95.90 ± 0.06	70.08 ± 0.52	69.82 ± 0.51	N/A
PR-BbB-SR	96.92 ± 0.05	96.84 ± 0.05	85.84 ± 0.31	84.35 ± 0.31	81.33 ± 0.52

We observe that, even though task inference becomes considerably more difficult (as shown by lower *TInfer-Final* compared to PermutedMNIST-10), accuracy when task identity is provided is high. For the considered methods almost no forgetting occurs despite the large number of tasks (similar *TGiven-During* and *TGiven-Final*). Notably, we see a substantially better task inference performance of *PosteriorReplay-BbB* compared to *PosteriorReplay-Dirac*, emphasizing the importance of using principled uncertainties. The same experiment was conducted in von Oswald et al. [91], also considering a task-agnostic inference setting (termed CL3, cf. Fig. A4b in von Oswald et al. [91]). They observe that common replay methods such as DGR [80] drop to chance level because the underlying generative model is retrained on its own data, causing a drift that accumulates over many tasks. Only the proposed method HNET+R performs well with *TInfer-Final* 96.00 ± 0.03. This method is based on task-conditioned replay models that are regularized via Eq. 4. While this performance may appear vastly superior to the performance of *PosteriorReplay*, it should be noted that the underlying MNIST data can be easily learned with simple generative models. In general, however, the generative task of learning $p(\mathbf{X})$ is more difficult than the discriminative one $p(\mathbf{Y} \mid \mathbf{X})$, which is why we hypothesize the performance gap will shrink or even reverse for more complicated input data (e.g., natural images). However, investigating this question by scaling generative models to natural images is beyond the scope of this study.

D.6 SplitCIFAR-10

Our results from the SplitCIFAR-10 experiment (cf. Sec. 4.4) conducted with a Resnet-32 as main network [23] are reported in Table S11. We use batch normalization in all convolutional layers. The batch normalization weights are part of the trainable weights captured by the WG system. The

Table S11: Accuracies of SplitCIFAR-10 experiments on a Resnet-32 (Mean $\pm$ SEM in %, $n = 10$). PR refers to *PosteriorReplay* and SP to *SeparatePosteriors*.

	TGiven-During	TGiven-Final	TInfer-Final	TInfer-Final (Conf)	TInfer-Final (Agree)
PR-Dirac	94.59 ± 0.10	93.77 ± 0.31	54.83 ± 0.79	54.83 ± 0.79	N/A
PR-BbB	95.59 ± 0.08	95.43 ± 0.11	61.90 ± 0.66	61.90 ± 0.64	61.36 ± 0.71
PR-Radial	94.82 ± 0.12	94.67 ± 0.15	52.89 ± 1.19	52.89 ± 1.19	50.92 ± 1.50
PR-SSGE	94.25 ± 0.07	92.83 ± 0.16	51.95 ± 0.53	51.93 ± 0.52	51.81 ± 0.48
PR-BbB-BW	95.59 ± 0.08	95.43 ± 0.11	92.94 ± 1.04	91.34 ± 1.45	93.57 ± 0.83
PR-BbB-CS	95.15 ± 0.11	92.48 ± 0.13	64.76 ± 0.34	64.76 ± 0.34	41.21 ± 0.85
SP-Dirac	N/A	95.42 ± 0.13	58.67 ± 0.94	58.62 ± 0.93	N/A
SP-BbB	N/A	96.06 ± 0.06	61.35 ± 0.91	61.36 ± 0.91	59.24 ± 1.05
EWC-growing	N/A	N/A	20.40 ± 0.95	N/A	N/A
VCL-growing	N/A	N/A	19.84 ± 0.53	N/A	N/A
VCL-multihead	95.78 ± 0.09	61.09 ± 0.54	15.97 ± 1.91	15.86 ± 1.90	15.86 ± 1.88
EWC-Dirac	82.50 ± 0.27	82.50 ± 0.26	25.46 ± 0.52	25.46 ± 0.52	–
Exp-Replay	N/A	N/A	41.38 ± 2.80	N/A	N/A
Fine-Tuning	96.59 ± 0.03	60.25 ± 0.77	N/A	N/A	N/A

batchnorm statistics are checkpointed and stored at the end of training for each task. Specifically, in the final model, each task embedding has an associated set of batchnorm statistics that will be loaded into the main network when the task embedding is selected.

In this experiment, *PosteriorReplay-BbB* performs best, followed by *PosteriorReplay-Dirac*. As for PermutedMNIST, *PosteriorReplay-SSGE* struggles, potentially due to the increased task difficulty. All three task inference criteria perform similarly, with *Ent* usually leading to the best results. The *Fine-Tuning* baseline reveals that *PosteriorReplay* methods slightly suffer from a stability-plasticity dilemma, and the use of a shared meta-model seems to affect *TGiven-During* accuracies. Also here we see that when using batches of samples for task inference as in *PosteriorReplay-BbB-BW*, one can almost match task-given (*TGiven*) and task-inferred (*TInfer*) scores. Note, that this is just a statistical accumulation effect based on the fact that we choose the correct task identity for individual sample points above chance level, and therefore the improvements due to batch-wise inference are not directly linked to the task-difficulty. We also observe improvements in *TInfer-Final (Ent)* when fine-tuning on coresets (*PosteriorReplay-BbB-CS*). However, these improvements are not as large as for SplitMNIST (cf. Table S5). In addition, the small coresets interfere with the *TGiven-Final* accuracy, suggesting that this coreset size is not sufficient to capture the richness and diversity of the data from a task.

VCL-multihead performs poorly in this benchmark. The correct task identity is chosen below chance level, which indicates that inducing task-specific uncertainty through the output head only is not sufficient for this challenging benchmark. We also experimented with *EWC-multihead* but observed instabilities similar to those reported in SM D.2. In particular, some weights had very low Fisher values, which led to high variance in the predictions made by the post-hoc constructed posterior, even in-distribution. We therefore consider a heuristic modification of *EWC-multihead*, where the proper post-hoc posterior construction is omitted (cf. Eq. 38), and a Dirac posterior based on the current MAP solution is used, called **EWC-Dirac**. In this case, there is still task-specific aleatoric uncertainty (similar to *PosteriorReplay-Dirac*), but no epistemic uncertainty and therewith no instability issues arising from the posterior construction using the EWC importance values. In the growing softmax baselines, *EWC-growing* and *VCL-growing*, only instances from the last task are correctly classified.

As consistently observed in all our experiments, *PosteriorReplay-Radial* underperforms *PosteriorReplay-BbB*. While this is in disagreement with the superior performance obtained with *radial* posteriors in [18], their results were obtained for a medical dataset, and are therefore not comparable to the experiments that we consider. We leave it open for future work to investigate under which scenarios *PosteriorReplay-Radial* might be a useful replacement for *PosteriorReplay-BbB*.

Table S12: Accuracies of SplitCIFAR-10 experiments on a WRN-28-10 (Mean $\pm$ SEM in %, $n = 5$). PR refers to *PosteriorReplay* and SR denotes *StochasticRegularization* on a subset of randomly selected past tasks.

	TGiven-During	TGiven-Final	TInfer-Final (Ent)	TInfer-Final (Conf)	TInfer-Final (Agree)
PR-Dirac-SR	96.23 ± 0.12	95.75 ± 0.20	57.50 ± 2.42	54.09 ± 2.43	N/A
PR-BbB-SR	93.77 ± 0.51	92.24 ± 0.93	50.23 ± 3.96	50.20 ± 3.96	49.95 ± 3.68

To study whether the *posterior meta-replay* approach can scale to even more complex architectures, we also performed SplitCIFAR-10 experiments with a Wide Resnet [95] (WRN-28-10) containing a total of 36.5 million weights. The results for *PosteriorReplay-Dirac* and *PosteriorReplay-BbB* are shown in Table S12. Here, the trend starts to reverse and even the mean-field BNN *PosteriorReplay-BbB* starts to encounter scalability issues. We hypothesize that these scalability issues can be mitigated by a more carefully chosen prior, e.g., a mean-field prior that adapts the variance of each weight by the layer's fan-in to counteract exploding or vanishing activations as they are particularly harmful in wide architectures. We again use stochastic regularization (*SR*) to showcase that even for these very complex models the full regularization as described by Eq. 1 is not necessary.

Results reported in related work. We are aware of several papers that considered SplitCIFAR-10 to benchmark CL algorithms under varying experimental conditions (such as the used architecture). The purpose of this paragraph is to give a brief overview over previously reported results, while appealing to the reader's experience for comparing numbers obtained under such varying conditions. For instance, Li et al. [50] consider a class-incremental scenario [87] and report results consistent with ours for a variety of well established regularization approaches such as *EWC-growing*. Best results in this study are achieved when using large random coresets (size 1000), which still perform below 45% *TInfer-Final*. Aljundi et al. [2] propose an approach for building coresets with which they obtain 49% accuracy for an overall coreset size of 1000. Also Mundt et al. [63] studies several approaches for coreset selection considering various coreset sizes, e.g., they report 53% *TInfer-Final* for a coreset of size 1500. De Lange and Tuytelaars [12] use nearest neighbor-based prediction on a set of continually evolving prototypes, obtaining up to 49% *Final* accuracy. In addition, some papers study this benchmark in a domain-incremental setting [87]. In this case, the overall problem is a binary classification, where objects with labels 0,2,4,6,8 belong to the negative class and objects with labels 1,3,5,7,9 belong to the positive class. Since in a class-incremental setting the inputs additionally need to be assigned to the correct task, the domain-incremental setting is simpler. Our framework can be readily adapted to the domain-incremental evaluation setting by changing the way the accuracy is computed. Specifically, our *TInfer-Final* accuracies necessarily become higher in the domain-incremental setting since, even if the incorrect output head has been chosen, there is still a 50% chance that the correct binary class is predicted. In this domain-incremental setting, Borsos et al. [7] provide a careful comparison of coreset methods, where all reported domain-incremental accuracies are below 40%. Chen et al. [10] propose Discriminative Representation Loss, a CL method based on decreasing gradient diversity, and report a *Final* accuracy of 40% when training in an online fashion (i.e., training the model with a single epoch on the training data). Finally, we would like to mention the work of Prabhu et al. [74], which proposes GDumb where models are trained from scratch on stored coresets. While this method is not trained on non-i.i.d. data, and thus not strictly comparable to a CL method, it provides a simple baseline whose performance questions the effectiveness of all modern CL methods. For instance, they achieve 61.3% *TInfer-Final* by training on only 1000 samples from CIFAR-10.

D.7 SplitCIFAR-100

We conducted additional experiments on the more challenging SplitCIFAR-100 benchmark, which considers the CIFAR-100 dataset split into 10 tasks of 10 classes each. The results of this experiment conducted with a Resnet-18 as main network [23] (where the first layer has only a kernel size of 3 with stride 1 and the max-pooling is dropped as in Verma et al. [90]) are reported in Table S13.

We again see a minor improvement in performance when using *PosteriorReplay-BbB* compared to *PosteriorReplay-Dirac*. Interestingly, the trend is reversed when considering the *SeparatePosteriors*

Table S13: Accuracies of SplitCIFAR-100 experiments on a Resnet-18 (Mean $\pm$ SEM in %, $n = 10$). PR refers to *PosteriorReplay* and SP to *SeparatePosteriors*.

	TGiven-During	TGiven-Final	TInfer-Final (Ent)	TInfer-Final (Conf)	TInfer-Final (Agree)
PR-DIRAC	85.25 ± 0.34	85.16 ± 0.34	40.35 ± 0.37	39.69 ± 0.35	N/A
PR-BBB	84.97 ± 0.17	84.78 ± 0.19	42.36 ± 0.26	42.00 ± 0.23	41.78 ± 0.25
PR-DIRAC-SR	84.56 ± 0.12	84.57 ± 0.12	40.68 ± 0.09	39.46 ± 0.08	N/A
PR-BBB-SR	86.68 ± 0.09	86.56 ± 0.10	45.22 ± 0.18	44.55 ± 0.21	44.77 ± 0.19
SP-DIRAC	N/A	89.52 ± 0.05	50.80 ± 0.16	47.79 ± 0.15	N/A
SP-BBB	N/A	82.73 ± 0.10	38.86 ± 0.19	38.52 ± 0.20	38.57 ± 0.20
EWC-DIRAC	66.86 ± 0.25	66.83 ± 0.24	16.96 ± 0.19	17.46 ± 0.18	N/A
FINE-TUNING	91.10 ± 0.05	24.97 ± 0.47	0.98 ± 0.01	0.99 ± 0.01	N/A

baseline. We hypothesize that this result is due to optimization difficulties. In *SeparatePosteriors-BbB*, one has to train ten approximate posterior distributions independently per hyperparameter configuration. For most hyperparameter configurations that were tested, some of these ten posterior approximations failed in solving the respective task. In contrast, for *PosteriorReplay-BbB* we observed that all tasks were successfully learned if the first task could be learned (due to transfer in the meta-model). To optimally boost the performance among considered prior-focused methods, we again considered *EWC-Dirac* (SM D.6), which performs far worse than *PosteriorReplay* methods.

An overview on how other continual learning methods perform on this benchmark can be found in concurrent studies [89, 90], where EFT exhibits very similar performance to our method. Note, the results in van de Ven et al. [89] are based on pretrained models and thus not directly comparable. Another recent study that considers this benchmark and evaluates the effect of coresets on common class-incremental methods is Masana et al. [60].

D.8 Task boundary detection during training

So far, we assumed that task identity is known during training. To overcome this constraint, methods for task boundary detection can be used, and the use of uncertainty for this purpose was already proposed by Farquhar and Gal [16].

Here we analyze, for PermutedMNIST, the feasibility of task boundary detection based on the uncertainty computed on a training batch, and compare it to using the loss as a boundary indicator. We consider the entropy of the predictive distribution as uncertainty measure (*Ent*). In both cases, the transitions to new tasks can be detected based on peaks in the evolution of the signals. The criterion for boundary detection can be implemented as a simple threshold crossing. As both loss and uncertainty will stay high in the initial phase of training on a new task, the detection algorithm is paused for a grace period after a detected transition. Furthermore, to improve detection stability, loss and uncertainty can be considered over a window of several training iterations.

To compare how useful loss and uncertainty values are for detecting task boundaries, we analyze the sensitivity of the two approaches to the choice of the detection threshold when using a grace period of 1000 iterations and a detection window of 10 iterations (Fig. S8). The threshold value that detects task boundaries without errors is bounded from above by the minimum of the values at actual task boundaries (such that all boundaries are detected), and from below by the maximum value outside of task boundary periods (such that false positives are avoided). While perfect boundary detection is possible with both signals, we found that the range of viable thresholds is much larger for the uncertainty signal (65.80% of the signal range) than for the loss signal (14.11% of the signal range).

These results suggest that task boundary detection based on an uncertainty measure might be a more robust way to detect task boundaries during training than a loss criterion. Interestingly, using uncertainty for task boundary detection does not require access to labelled data, as opposed to a loss-based criterion. However, an uncertainty criterion relies on the assumption that input distributions of subsequent tasks are sufficiently distinct, which might not always be case. Crucially, both of these simple threshold criteria assume some sort of continuity for the training of individual tasks.

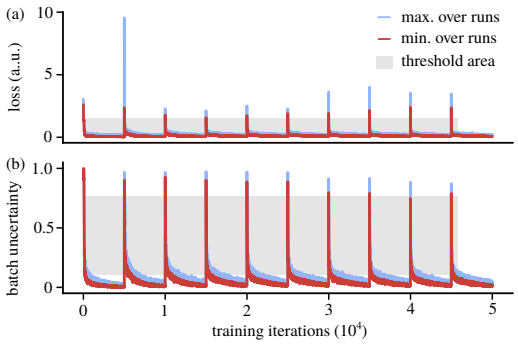

Figure S8: Task boundary detection in PermutedMNIST-10. Evolution of **(a)** the loss and **(b)** batch uncertainty when training tasks for 5000 iterations. The detection threshold of a potential task boundary detection system is bounded by the minimum (red) and maximum (black) values over 10 runs. The gray area indicates the range in which a threshold would successfully detect all task boundaries without causing false positives or false negatives.

E Experimental Details

In this section, we provide detailed descriptions of the two low-dimensional problems considered in this paper, and explain how hyperparameter configurations were chosen for all methods and experiments. The exact hyperparameter choice of all reported experiments can be found in the code repository accompanying the paper, which also contains the instructions to reproduce all results.

E.1 1D Polynomial Regression Dataset

The 1D polynomial regression dataset consists of three tasks, each defined by a different ground-truth function $g^{(t)}(x)$ that operates on a specific input domain $p^{(t)}(X)$:

$$\begin{aligned} g^{(1)}(x) &= (x+3)^3 & p^{(1)}(X) &= \mathcal{U}(-4,-2) \\ g^{(2)}(x) &= 2x^2 - 1 & p^{(2)}(X) &= \mathcal{U}(-1,1) \\ g^{(3)}(x) &= (x-3)^3 & p^{(3)}(X) &= \mathcal{U}(2,4) \end{aligned} \tag{49}$$

where $\mathcal{U}(a,b)$ denotes a continuous uniform distribution between the bounds a and b. Note that input domains are non-overlapping, and therefore task identity can be inferred by looking at the inputs alone.

Twenty noisy training samples are collected from each of these polynomials according to $\{(x,y) \mid y = g^{(t)}(x) + \epsilon \text{ with } \epsilon \sim \mathcal{N}(0,\sigma^2), x \sim p^{(t)}(X)\}$. We set $\sigma = 0.05$ in this experiment. We also scale the NLL properly using $\sigma_{\text{ll}} = 0.05$ (cf. Eq. 9) to circumvent model misspecification when testing Bayesian approaches.

E.2 2D Mode Classification Dataset

The 2D mode classification experiment is comprised of three binary classification tasks. The 2D inputs $\mathbf{x}$ are sampled from a Gaussian mixture model with six modes and uniform mixing coefficients:

$$p(\mathbf{X}) = \sum_{t=1}^{6} \frac{1}{6} \mathcal{N}(\mathbf{X}; \boldsymbol{\mu}^{(t)}, \boldsymbol{\Sigma}^{(t)}) \tag{50}$$

We set $\boldsymbol{\Sigma}^{(t)} = (0.2)^2 I$ for $t \in \{1,..,6\}$ and equidistantly locate the modes in a circle of radius five around the origin. Specifically, the angular position of each mode was determined by $\alpha^{(t)} = \frac{t-0.5}{6} 2\pi$, and the corresponding Cartesian coordinates by: $\boldsymbol{\mu}^{(t)} = [5\sin(\alpha^{(t)}), 5\cos(\alpha^{(t)})]^T$. The dataset contains 10 training samples per mode, i.e., 20 training samples per task.

Table S14: Hyperparameter values scanned across methods in our basic search. Note that these values were subsequently further tuned for each method and experiment. BNNs refer to all probabilistic methods (i.e. all considered methods except *PosteriorReplay-Dirac*). *PR* refers to all *PosteriorReplay* methods, which therefore require a TC network. *Implicit* refers to all methods using implicit posterior approximations, which therefore require a WG network.

Methods	Hyperparameter	Searched values
All	learning rate	1e-5, 1e-4, 1e-3, 1e-2
	batch size N_{mb}	32, 64, 128
	clip gradient norm	None, 100
	main network activation function	ReLU
	optimizer	Adam
	number of iterations (1D-Regression)	5000, 10000
	number of iterations (2D Mode Class.)	2000, 5000
	number of iterations (SplitMNIST)	2000, 5000
	number of iterations (PermutedMNIST)	5000, 10000
	number of epochs (SplitCIFAR-10)	20, 40, 60
BNNs	prior variance σ^2_{prior}	1
	prior-matching term scaling factor	1e-6, 1e-5, . . . 1e0 (1 for low-dim. experiments)
BNNs (except VCL and PR-BbB)	number of samples for *prior-matching term* estimation	1, 10, 20
	number of MC samples for NLL estimation K	1, 10, 20
PR-BbB and VCL	CL regularizer	MSE, fKL, rKL, W2
	local reparametrization trick	True (only for MLPs), False
EWC	regularization strength	1e-4, 1e-3, . . . , 1e3, 1e4
All PR	CL regularizer strength β	1e-3, 1e-2, . . . 1e2, 1e3
	TC hidden layers	None, 10-10, 50-50, 100-100
	TC activation function	ReLU, sigmoid
	size of task embeddings $\mathbf{e}^{(t)}$	16, 32, 64
	initial SD of task embeddings $\mathbf{e}^{(t)}$	0.1, 1
	size of TC chunk embeddings $\mathbf{c}^{(l)}$	16, 32, 64
	initial SD of TC chunk embeddings $\mathbf{c}^{(l)}$	0.1, 1
All *implicit*	variance σ_{noise} of WG output perturbation	None, 1e-2, 1e-1
	dimensionality of the latent vector $\mathbf{z}$	8, 16, 32
	initial SD of the latent vector $\mathbf{z}$	0.1, 1
	WG hidden layers	None, 10-10, 50-50, 100-100
	WG activation function	ReLU, sigmoid
	size of WG chunk embeddings $\mathbf{c}^{(l)}$	16, 32, 64
	initial SD of WG chunk embeddings $\mathbf{c}^{(l)}$	0.1, 1
AVB	batch size K for D training	1, 10
	number of D training steps	1, 5
	use batch statistics	False, True
	D hidden layers	10-10, 100-100
SSGE	kernel width	0.1, 1
	use heuristic kernel width	True, Ralse
	number of samples S for gradient estimation	10, 20, 50
	threshold τ for eigenvalue ratio of eigenvalues J	1, 5, All
PR-BbB-CS	number of iterations for fine-tuning stage	2000, 5000
	method for OOD uncertainty increase	random labels, high entropy targets
	prior-matching term scaling factor during fine-tuning	1e-6, . . . , 1e0
Exp-Replay	regularization strength	1e-1, 1e0, 1e1, 1e2
	coreset batch size	8, 16, 32, 128
	fixed mini-batch size for regularizing	True, False

E.3 Hyperparameter selection

To gather the results, we performed extensive hyperparameter searches for all the methods across all experiments. Unless noted otherwise, we selected the hyperparameter configurations according to the best final performance in a task-agnostic setting using the *Ent* criterion. In Table S14 we describe the basic grid of hyperparameter values used for all methods. Note that we only report the initial search grid from which a random subset of 100 calls was generated. The results of this initial search were thoroughly evaluated and the grid was fine-tuned individually for each method and experiment if parameter choices appeared inappropriate.

Notably, the network architectures differ considerably across methods and across experiments, and the lists below are not exhaustive. We use chunked hypernetworks (cf. Sec. C.2) with architectures where the total number of parameters of the TC system is smaller than $\dim(\mathbf{w})$, except for low-dimensional problems where we only experiment with non-compressive MLP hypernetworks. In addition, we experiment with principled hypernetwork initializations (e.g., cf. Chang et al. [8]), that we adapted for chunked hypernetworks. However, we do not find a noticeable influence of the initialization on the training outcome when using the Adam optimizer.

The hyperparameter searches were performed on the ETH Leonhard scientific compute cluster. For exact configurations of the reported results, please refer to our list of command line calls provided in the README files of the accompanying code base.

F Further Discussion and Remarks

F.1 On Posterior Meta-Replay as a Bayesian method

Proper Bayesian inference is intractable and approximations are needed in practice, and our approach is no exception to this. However, we believe *posterior meta-replay* can be considered a Bayesian method and outline in this section why.

First of all, just like *Online EWC*, our method can be derived through a series of approximations from a probabilistic graphical model, which additionally assumes the existence of discrete tasks and therefore has as additional variable the task identifier t (a design choice resulting in high performance gains). The joint can be written as $p(t)(\mathbf{x} \mid t)p(\mathbf{W} \mid t)p(\mathbf{y} \mid \mathbf{W}, \mathbf{x})$ with $p(\mathbf{x} \mid t)$ being the task-specific input distribution and $p(\mathbf{y} \mid \mathbf{W}, \mathbf{x})$ being the likelihood. $p(\mathbf{W} \mid t)$ is a Dirac distribution such that there is one ground-truth model $\mathbf{W}^{(t)}$ per task, allowing each task to be represented by a dataset $\mathcal{D}^{(t)}$ drawn i.i.d. from $p(\mathbf{x} \mid t)p(\mathbf{y} \mid \mathbf{W}^{(t)}, \mathbf{x})$. This setting naturally induces task-specific posteriors $p(\mathbf{W} \mid \mathcal{D}^{(t)})$ (cf. Fig. 1). To bring this graphical model to a practical CL method, we apply several approximations. First, the intractable posteriors $p(\mathbf{W} \mid \mathcal{D}^{(t)})$ are approximated by $q_{\boldsymbol{\theta}^{(t)}}(\mathbf{W})$ using variational inference (where we remain flexible regarding the choice of variational family). Second, as storing separate posteriors is undesirable from a CL perspective, we entangle all posteriors within a shared hypernetwork, which is trained continually. Third, in the case of task-agnostic inference (e.g., class-incremental learning), the task identity t has to be explicitly inferred from the current input $\tilde{\mathbf{x}}$, which requires access to the posterior $p(t \mid \tilde{\mathbf{x}}) = \frac{p(\tilde{\mathbf{x}}|t)p(t)}{\sum_{t'} p(\tilde{\mathbf{x}}|t')p(t')}$. Since explicit modelling of $p(\tilde{\mathbf{x}} \mid t)$ is difficult, we heuristically opt for uncertainty-based task inference.

Second, *posterior meta-replay* solutions can approximate the true posteriors. Indeed, although the parameters of the TC system influence both the ELBO and the regularization term, the approximate posterior of the task being currently learned only appears in the ELBO. Therefore our optimization objective still aims to learn an approximate posterior using a proper lower bound, and if forgetting of the learned posteriors is prevented, the final per-task solutions correspond to valid posterior approximations (indendently of which mechanism is used against forgetting). This is the case in the non-parametric limit (the TC system being a universal function approximator) if the objective is optimally minimized; in this case the introduction of the hypernetwork does not impose any constraints compared to the separate posterior view prescribed by the graphical model. Although in practice the capacity of the TC system is limited and optimization is not perfect, we empirically show

that the introduced errors only marginally affect performance.[10] This is also the reason why we did not consider more sophisticated forms of regularization (for instance, as outlined in SM F.3) for our empirical analysis.

Nevertheless, forgetting is happening in practice and our current approach does not allow such forgetting to be reflected in uncertainty estimates, which would be an interesting avenue for future research. Specifically, distributions outputted by the TC system are always assumed to be approximations to the task-specific posteriors and forgetting can currently only be detected by having access to a withheld test set for each past task.

F.2 Runtime and storage complexity

A BNN has an intrinsic runtime disadvantage during inference compared to a deterministic network due to the incorporation of parameter uncertainty. As in practical scenarios the posterior predictive distribution cannot be analytically evaluated, it has to be approximated via an MC estimate (cf. Eq. 39). Thus, if the MC estimate incorporates K samples from the approximate parameter posterior, then inference of every input is approximately K times as expensive as for a deterministic model.

Task inference via predictive uncertainty comes into play as an additional factor during inference, since the predictive distribution has to be estimated for every task in order to chose the prediction corresponding to lowest uncertainty. Hence, inference time is additionally increased by a factor T. Note, this is not the case for the considered multihead *PriorFocused* methods, where in every forward pass the output of all T heads is computed anyways. Certainly, proper parallelization on modern graphics hardware can ensure that these extra demands are not noticeably reflected in the actual runtime.

During training via variational inference, BNNs require an MC estimate of the NLL term (cf. Eq. 3), which also leads to a linear increase for the loss computation compared to the deterministic case. However, it should be noted that this hyperparameter K_{NLL} (the MC sample size) is often chosen to be rather small, e.g., $K_{\text{NLL}} = 1$.

Apart from these general remarks, we also would like to comment on method-specific resource demands.

BbB and Radial posteriors. Both methods are very similar in their implementation as well as their resource complexity. A notable difference is that an analytic expression for the *prior-matching term* is known for BbB when using certain priors, while the training of radial posteriors requires an MC estimate of the involved cross-entropy term (cf. SM C.3.2). Compared to the deterministic case, the number of trainable parameters is doubled (a mean and variance per weight) in both cases.

Implicit methods. Implicit methods, such as AVB and SSGE, require an additional neural network that in combination with the base distribution forms the approximate posterior. The architecture of this WG network is a hyperparameter. Note, that the choice of architecture has a considerable influence on runtime and storage complexity. Every sample drawn from such an approximate posterior requires a forward pass through the WG network.

AVB requires yet another network during training, the discriminator. Also here, the architecture of the discriminator is a hyperparameter. In every training iteration, the discriminator is optimized inside an inner-loop for a predefined number of steps. For loss computation, the *prior-matching term* has to be evaluated via an MC sample, where forward passes through the discriminator are required.

SSGE requires an eigendecomposition at every training iteration which has cubic runtime complexity in the number of samples S used for the construction of the kernel matrix (cf. SM 20). Most of our results were obtained for $S = 10$ or $S = 20$.

Posterior meta-replay. To evaluate whether the use of task-conditioned hypernetworks requires increased computational and memory resources, we evaluated the runtime and memory usage of several methods in SplitMNIST runs (Table S15). To enable a fair comparison, we used the same set

[10] We empirically show this through the SP and SP-TC baselines, e.g. Table S5, where all posteriors are trained separately (i.e., the objective is only the ELBO) such that the influence of the regularizer (SP-TC baseline) or both the regularizer and TC-system (SP baseline) can be understood.

of hyperparameters across all methods. Furthermore, in methods requiring an MC estimate of the NLL or *prior-matching term*, we run experiments using a single sample, but note that both runtime and memory resources will increase with this hyperparameter. For methods using SSGE, we use 10 weight samples to construct the kernel matrix.

Table S15: Resources needed by *PosteriorReplay* in terms of runtime and memory usage. Results are reported for SplitMNIST results using an MLP-400,400 and identical hyperparameters (if applicable) for all methods (Mean $\pm$ SD in %, $n = 5$). PR refers to *PosteriorReplay* and PF to *PriorFocused* methods.

	Runtime (s)	Memory usage (MiB)
Fine-Tuning	95.51 $\pm$ 1.32	389.0
HNET Fine-Tuning	185.7 $\pm$ 1.9	397.0
PR-Dirac	426.1 $\pm$ 1.9	439.0
PR-Dirac-SR	314.5 $\pm$ 2.1	407.1
PR-BbB	542.3 $\pm$ 6.6	473.0
PR-SSGE	1201.2 $\pm$ 9.6	537.6
PF-SSGE-multihead	834.2 $\pm$ 4.8	482.2
VCL-multihead	221.4 $\pm$ 4.9	452.6
EWC-multihead	289.0 $\pm$ 4.1	392.1

All results are obtained using the same compute hardware and the provided code base. Therefore, the computational complexity depends on the efficiency of this implementation and does not necessarily reflect theoretical time or space complexity. We especially want to stress that for the sake of flexibility and simplicity we use a naive hypernetwork implementation, where we first generate all main network weights before feeding them into the main network. A more efficient implementation or specialized hardware may improve the reported runtimes substantially [22].

Compared to *Fine-Tuning*, where a main network is updated without any CL protection, *PosteriorReplay-Dirac* leads to a four-fold increase in runtime, but only a slight increase in memory usage. To disentangle whether the considerable increase in runtime is linked to the addition of the hypernetwork or the computation of the CL regularizer, we also evaluated the runtime of a system consisting of a main network and a task-conditioned hypernetwork, but where no CL protection is applied (i.e., equivalent to fine-tuning the hypernetwork, denoted *HNET Fine-Tuning*). Memory usage is again in the same ballpark, but runtime only constitutes this time a two-fold increase with respect to the *Fine-Tuning* baseline that has no hypernetwork. Altogether these results show that, although memory usage is not noticeably affected by the use of our *posterior meta-replay* framework, the introduction of the hypernetwork and the CL regularization each lead to a two-fold increase in the runtime for this particular experiment.

We show that the runtime of *posterior meta-replay* experiments can be considerably shortened by doing a stochastic CL regularization and considering a subset of tasks for computing the regularizer (noted *SR* and reported here for a subset of size 1). Indeed, runtime for *PosteriorReplay-Dirac-SR* is larger than when no regularizer is computed (*HNET Fine-Tuning*), but only about 70% of the runtime when all tasks are regularized upon (*PosteriorReplay-Dirac*). Compared to the deterministic *PosteriorReplay* solution, *PosteriorReplay-BbB* requires about 20% more memory and 30% longer runtime, which can partly be explained by the fact that, when the same hyperparameters are used (including main network size), BbB has to generate twice as many parameters for the main network parametrization as *PosteriorReplay-Dirac* (since it generates means and variances, and not weight values directly). Finally, *PriorFocused* methods such as *VCL-multihead* or *EWC-multihead* again have similar memory usage, but considerably shorter runtimes than *PosteriorReplay-Dirac*. However, compared to the solution with stochastic regularization *PosteriorReplay-Dirac-SR*, the runtime of *EWC-multihead* is only about 8% faster; a negligible amount compared to the gains in performance that can be achieved. SSGE requires substantially more resources, especially in terms of runtime. This is to be expected as in every training iteration an estimate of the log-density has to be computed. It is important to keep in mind that these values will vary substantially for other hyperparameters and experiments, but we expect the trend across methods to hold.

F.3 Continual learning regularization in distribution space

The goal of the CL regularization in the *posterior meta-replay* framework is to ensure that found posterior approximations do not change when learning new tasks, as discussed in Sec. C.2. This desideratum can be directly enforced if, for the considered variational family, an analytic expression for a divergence measure is accessible (e.g., cf. Sec. C.3.1/ Eq. 1). Whenever such divergence measure is not available, we avoid sample-based regularization, and thus regularize at the level of the output of the TC system, resorting to an L2 regularization of the distributional parameters (cf. Eq. 2). In our experiments this L2 regularization is sufficient, as we do not observe that forgetting is a major problem. A potential reason for the success of this simple regularization could be the discovery of flat minima as speculated in Ehret et al. [15]. However, a sound application of the *posterior meta-replay* framework should regularize towards closeness in distribution space, as the chosen parameterization of the variational family is arbitrary, and it is unclear how perturbations in parameter space affect the encoded distributions. Therefore, this section provides guidance for future work on how a simple regularization acting on the outputs of the TC system can be interpreted as enforcing closeness in distribution space. Our discussion on this topic is inspired by the derivation of the natural gradient [72], that allows to cast parameter updates into distribution updates.

Recall that the goal of regularization is to ensure that (cf. Eq. 1):

$$\min_{\boldsymbol{\theta}^{(t)}} \mathrm{D}\big(q_{\boldsymbol{\theta}^{(t,*)}}(\mathbf{W}) || q_{\boldsymbol{\theta}^{(t)}}(\mathbf{W})\big) \tag{51}$$

where $q_{\boldsymbol{\theta}^{(t,*)}}(\mathbf{W})$ denotes the approximate posterior of task t obtained from a checkpoint of the TC network before learning the current task, and D denotes some divergence measure. In particular, we consider the KL as a choice for the divergence measure, which for small parameter perturbations behaves like a metric in distribution space.[11] Assuming the outputs $\boldsymbol{\theta}^{(t,*)}$ do not change much when learning task t (i.e. $\boldsymbol{\epsilon} = \boldsymbol{\theta}^{(t)} - \boldsymbol{\theta}^{(t,*)}$ is sufficiently small), we consider a Taylor approximation of Eq. 51 around $\boldsymbol{\theta}^{(t,*)}$. To compute this expression, we use the fact that the KL between identical distributions is zero, and we compute the first and second order terms of the approximation as follows. For the first order term we require the first derivative of the KL with respect to $\boldsymbol{\theta}^{(t)}$ at $\boldsymbol{\theta}^{(t)} = \boldsymbol{\theta}^{(t,*)}$:

$$\begin{aligned} &\big[\nabla_{\boldsymbol{\theta}^{(t)}} \mathrm{KL}\big(q_{\boldsymbol{\theta}^{(t,*)}}(\mathbf{W}) || q_{\boldsymbol{\theta}^{(t)}}(\mathbf{W})\big)\big]\Big|_{\boldsymbol{\theta}^{(t)}=\boldsymbol{\theta}^{(t,*)}} \\ &= -\int q_{\boldsymbol{\theta}^{(t,*)}}(\mathbf{W}) \big[\nabla_{\boldsymbol{\theta}^{(t)}} \log q_{\boldsymbol{\theta}^{(t)}}(\mathbf{W})\big]\Big|_{\boldsymbol{\theta}^{(t)}=\boldsymbol{\theta}^{(t,*)}} d\mathbf{W} \\ &= 0 \end{aligned} \tag{52}$$

For the second order term we need the respective second derivative:

$$\begin{aligned} &\big[\nabla_{\boldsymbol{\theta}^{(t)}} \nabla^T_{\boldsymbol{\theta}^{(t)}} \mathrm{KL}\big(q_{\boldsymbol{\theta}^{(t,*)}}(\mathbf{W}) || q_{\boldsymbol{\theta}^{(t)}}(\mathbf{W})\big)\big]\Big|_{\boldsymbol{\theta}^{(t)}=\boldsymbol{\theta}^{(t,*)}} \\ &= -\int q_{\boldsymbol{\theta}^{(t,*)}}(\mathbf{W}) \\ &\qquad \big[\nabla_{\boldsymbol{\theta}^{(t)}} \nabla^T_{\boldsymbol{\theta}^{(t)}} \log q_{\boldsymbol{\theta}^{(t)}}(\mathbf{W})\big]\Big|_{\boldsymbol{\theta}^{(t)}=\boldsymbol{\theta}^{(t,*)}} d\mathbf{W} \\ &= -\int q_{\boldsymbol{\theta}^{(t,*)}}(\mathbf{W}) \big[\mathcal{H}_{\log q_{\boldsymbol{\theta}^{(t)}}(\mathbf{W})}\big]\Big|_{\boldsymbol{\theta}^{(t)}=\boldsymbol{\theta}^{(t,*)}} d\mathbf{W} \\ &= -\mathbb{E}_{q_{\boldsymbol{\theta}^{(t,*)}}(\mathbf{W})} \big[\mathcal{H}_{\log q_{\boldsymbol{\theta}^{(t,*)}}(\mathbf{W})}\big] \end{aligned} \tag{53}$$

And we therefore obtain the following local approximation of the KL:

$$\begin{aligned} &\mathrm{KL}\big(q_{\boldsymbol{\theta}^{(t,*)}}(\mathbf{W}) || q_{\boldsymbol{\theta}^{(t)}}(\mathbf{W})\big) \\ &\qquad = \mathrm{KL}\big(q_{\boldsymbol{\theta}^{(t,*)}}(\mathbf{W}) || q_{\boldsymbol{\theta}^{(t,*)}+\boldsymbol{\epsilon}}(\mathbf{W})\big) \\ &\qquad \approx -\frac{1}{2}\boldsymbol{\epsilon}^T \mathbb{E}_{q_{\boldsymbol{\theta}^{(t,*)}}(\mathbf{W})} \big[\mathcal{H}_{\log q_{\boldsymbol{\theta}^{(t,*)}}(\mathbf{W})}\big] \boldsymbol{\epsilon} \end{aligned} \tag{54}$$

[11] As we will see below, the KL divergence is for infinitesimal parameter perturbations approximately equal to the Rao distance [66].

Thus, regularization in distribution space as demanded by Eq. 51 can be achieved for small $\boldsymbol{\epsilon}$ using the quadratic form in Eq. 54. We denote the regularization matrix by $R^{(t)} \equiv \mathbb{E}_{q_{\boldsymbol{\theta}^{(t,*)}}(\mathbf{W})}\big[\mathcal{H}_{\log q_{\boldsymbol{\theta}^{(t,*)}}(\mathbf{W})}\big]$ to highlight the elegance and computational simplicity of the final CL regularizer:

$$\min_{\boldsymbol{\theta}^{(t)}} \frac{1}{2}(\boldsymbol{\theta}^{(t)} - \boldsymbol{\theta}^{(t,*)})^T R^{(t)} (\boldsymbol{\theta}^{(t)} - \boldsymbol{\theta}^{(t,*)}) \tag{55}$$

Note that $R^{(t)}$ has to be computed once after task t has been trained on,[12] and for $R^{(t)} = I$ we recover the isotropic regularization of Eq. 2.

When interpreting $q_{\boldsymbol{\theta}^{(t,*)}}(\mathbf{W})$ as a likelihood function, it can be seen that $R^{(t)}$ is the corresponding Fisher information matrix (cf. Eq. 31) and can be computed via:

$$\begin{aligned} R^{(t)} = \mathbb{E}_{q_{\boldsymbol{\theta}^{(t,*)}}(\mathbf{W})}\big[&\big(\nabla_{\boldsymbol{\theta}^{(t,*)}} \log q_{\boldsymbol{\theta}^{(t,*)}}(\mathbf{W})\big) \\ &\big(\nabla_{\boldsymbol{\theta}^{(t,*)}} \log q_{\boldsymbol{\theta}^{(t,*)}}(\mathbf{W})\big)^T\big] \end{aligned} \tag{56}$$

Note, that the quantity estimated by algorithms such as SSGE (cf. Sec. C.4.2) is $\nabla_{\mathbf{W}} \log q_{\boldsymbol{\theta}^{(t)}}(\mathbf{W})$ and not the score function $\nabla_{\boldsymbol{\theta}^{(t)}} \log q_{\boldsymbol{\theta}^{(t)}}(\mathbf{W})$. It is therefore not straightforward to see how to approximate the Fisher information matrix and thus the regularization matrix $R^{(t)}$.

However, as deep learning often benefits from coarse approximations, we propose the following heuristic to estimate $R^{(t)}$ if the simple regularization of Eq. 2 is not sufficient. Assuming the training of each task is successful and the variational family contains the correct posterior, we have that $q_{\boldsymbol{\theta}^{(t,*)}}(\mathbf{W}) \approx \frac{1}{Z} p(\mathcal{D}^{(t)} \mid \mathbf{W}) p(\mathbf{W})$, where Z is some unknown normalization constant. We can therefore rewrite the Hessian as $\mathcal{H}_{\log q_{\boldsymbol{\theta}^{(t,*)}}(\mathbf{W})} \approx \mathcal{H}_{\log p(\mathcal{D}^{(t)}|\mathbf{W})} + \mathcal{H}_{\log p(\mathbf{W})}$. The term $\mathcal{H}_{\log p(\mathbf{W})}$ has a simple analytic expression for a Gaussian prior and $\mathcal{H}_{\log p(\mathcal{D}^{(t)}|\mathbf{W})}$ can be computed for a given variate $\mathbf{w}$ as long as the data $\mathcal{D}^{(t)}$ is available and the model is twice differentiable. If $R^{(t)}$ is computed right after a task has been learned, it can be safely assumed that $\mathcal{D}^{(t)}$ is still available (similar to the Fisher computation in EWC (cf. Sec. C.5.2)). Hence, $R^{(t)}$ can be approximated via an MC estimate since sampling from $q_{\boldsymbol{\theta}^{(t,*)}}(\mathbf{W})$ is always possible. Crucially, the actual CL regularization via Eq. 56 is efficient to compute and does not require sampling from $q_{\boldsymbol{\theta}^{(t,*)}}(\mathbf{W})$.

F.4 Optimization considerations in Posterior-Replay

We discuss here important aspects regarding the ease of optimization of our *posterior meta-replay* framework. Chang et al. [8] found that the initialization of the hypernetwork is important for training stability when optimizing via SGD. We therefore use the Adam optimizer throughout, with which the choice of initialization does not seem to be crucial. While we do not suffer noticeably from instabilities (note, that we apply gradient clipping), we do observe that certain hyperparameter choices are crucial for loss minimization (improper choices might cause the optimizer to plateau at chance level performance). For instance, as already noted in von Oswald et al. [91], the choice of hypernetwork architecture strongly influences how easy it is to find suitable hyperparameter configurations. To the best of our knowledge, there is currently no principled or agreed upon approach for choosing such architecture and the choice thus solely relies on the experimenter's expertise. Interestingly, von Oswald et al. [91] studied the sensitivity of PR-Dirac to changes in the regularization strength, and found that the accuracies are robust for a wide range of values (Fig. SM A2 in von Oswald et al. [91]).

F.5 Deep Ensembles

A successful approach for OOD detection are deep ensembles [82], which in the simplest case correspond to several deterministic networks trained independently, and whose predictions are aggregated during inference [42]. Due to the non-convexity of the loss landscape and the stochasticity

[12] In the strict sense, $R^{(t)}$ is specific to the used checkpoint $q_{\boldsymbol{\theta}^{(t,*)}}$, which can change whenever a new checkpoint of the TC system is made and thus whenever a new task arrives. We ignore this detail for computational simplicity and due to the approximate nature of the proposed regularization.

innate to maximum-likelihood training, distinct solutions are obtained despite training with the same dataset. Although, to the best of our knowledge, such an ensemble of models cannot be interpreted as a sample from the Bayesian posterior, having access to a set of diverse predictions makes it possible to infer task identity based on model disagreement, which is not possible in the plain deterministic case. In addition, deep ensembles are just as easy to train as single deterministic solutions, but do require more training resources. This is in contrast to the increased training difficulty of BNNs, where continuous weight distributions are sought. However, despite their attractiveness, ensembles lack some of the advantages that come with a Bayesian approach. These include the ability to drop i.i.d. assumptions within tasks or the ability to revisit and update existing knowledge.

Analogously to *PosteriorReplay-Dirac*, our framework can also be adapted to work with ensembles. In this case, the TC system maintains multiple embeddings per task; one per ensemble member. Although not in the context of CL, this idea has already been explored by Oswald et al. [68], who showed improved OOD detection compared to the single model baseline. To combine the advantages of BNNs and deep ensembles, Wilson and Izmailov [93] proposed to train an ensemble of BNNs. This is an intriguing future direction for our framework, as the beneficial CL properties of BNNs are preserved. For instance, a simple and scalable approach such as *PosteriorReplay-BbB* could be turned into an ensemble of Gaussian posterior approximations by allowing the use of more than one embedding vector per task, which may allow to capture multiple modes of the posterior and ultimately lead to better task inference.

F.6 Continual learning in function space

The focus of this paper is on Bayesian continual learning methods that operate primarily in weight space. However, especially from a prior-focused perspective (where a single shared solution is desired), methods like Titsias et al. [84] and Pan et al. [69], which operate in function space, offer a compelling alternative. This function space view might also be beneficial for *PosteriorReplay* methods for several reasons. First of all, Bayesian inference in function space might make it easier to encode (task-specific) prior information (e.g., via Gaussian processes). Furthermore, the function space view offers a better interpretability of OOD capabilities [11], which might ultimately be used for improving uncertainty-based task inference. For those reasons, it might be an interesting future direction to study *PosteriorReplay* methods while focusing on the function- rather than weight-space.

F.7 Graceful forgetting

Should a CL algorithm have the built-in ability to forget past knowledge in order to facilitate learning from new data? This is an intriguing question whose answer depends on the precise definition of "continual learning". As described in Sec. 1, we focus on supervised learning and under the term CL study algorithms capable of learning from a stationary unknown data distribution $p(\mathbf{X})p(\mathbf{Y} \mid \mathbf{X})$ using a non-i.i.d. sample. In our specific case (and in line with the vast majority of the CL literature), this non-i.i.d. sample is constrained to be a series of i.i.d. samples (called tasks), e.g., $p(\mathbf{X}, \mathbf{Y}) = \frac{1}{T} \sum_{t=1}^{T} p^{(t)}(\mathbf{X}) p^{(t)}(\mathbf{Y} \mid \mathbf{X})$.[13] Following this strict definition, there is no notion of *temporal valence* that we can assign to sample points. Or more specifically, there is no intrinsic reason why we should trade performance on old tasks (forgetting/stability) for learning new tasks (plasticity).

On the other hand, some studies consider a different, but related problem, namely learning from a non-stationary data distribution ([48, 41]). A good example of this scenario is learning from observations that are subject to sensor drift. The goal here is clearly different from typical CL (as defined above): the learner should adapt to current observations quickly while overwriting (possibly conflicting) previously acquired knowledge. The emphasis here is on *adapting quickly*, which requires transferring (or generalizing) acquired concepts to new observations. The contrast between these two types of online learning is clearly highlighted by the different ways in which performance is computed: in typical CL (as defined above) performance is measured across all data seen so far, whereas in settings subject to concept drift performance is measured only on the most recent data.

[13] Note, the overall (unknown) data distribution to be learned is stationary. However, the instantaneous data distribution that is sampled from may be considered non-stationary with discrete, non-continuous transitions (task boundaries).

Since CL algorithms should ideally also have built-in mechanisms for transfer learning, it is well justified to ask whether they can be modified to *gracefully forget* past data in order to facilitate new observations. *Prior-focused* methods incorporate past knowledge via the prior, which is the posterior of the previous task. As illustrated in Fig. 1, this prior progressively becomes more confident, which impedes learning. Therefore, Li et al. [48] suggest to broaden this prior by tempering the current prior $p(\mathbf{W})$ when task boundaries are detected: $p^\beta(\mathbf{W}) \equiv \frac{1}{Z_\beta} p(\mathbf{W})^\beta$, with inverse temperature β and normalization Z_β. Plugging this expression into the *prior-matching term* of Eq. 3 yields:

$$\begin{aligned} -\mathrm{KL}\big(q_{\boldsymbol{\theta}}(\mathbf{W}) \,||\, p^\beta(\mathbf{W})\big) = \\ - \mathbb{E}_{q_{\boldsymbol{\theta}}(\mathbf{W})}\big[\log q_{\boldsymbol{\theta}}(\mathbf{W}) - \beta \log p(\mathbf{W})\big] + \log Z_\beta \end{aligned} \tag{57}$$

Hence, whenever the *prior-matching term* is estimated via an MC sample, this type of tempering can be achieved by scaling the log-prior density. Note that this is different from the type of tempering that we apply (cf. Sec. D), which scales the *prior-matching term* as a whole.

Also Kurle et al. [41] proposes forgetting mechanisms for prior-focused learning, the first of which is similar in spirit to the one described above (cf. Eq. 11 in Kurle et al. [41]).

In this context, it is worth stressing that *PosteriorReplay* methods do not explicitly suffer the same plasticity (ability to learn new tasks) vs. stability (prevention of forgetting) trade-off. Instead, the prior of each task can be freely chosen without sacrificing previously acquired knowledge. For instance, the prior can be a weighted average of an arbitrary prior and previously learned posteriors, i.e., it can be broad to encourage exploration of solutions that fit upcoming data well while being biased towards solutions of previous tasks to exploit prior knowledge.

As a final remark, it is important to note that algorithms are always applied to systems with limited capacity. Therefore, it is natural to ask what happens to a CL algorithm if the system's capacity is exceeded but new data still arrives, i.e., what compromise will it find. The CL algorithms discussed in this paper have no active mechanisms to free up capacity, and therefore their behavior in the limiting regime can only be partially controlled via the regularization strength. For *PriorFocused* methods, the regularization strength can be tuned via tempering. Since *PosteriorReplay* methods explicitly regularize all previous tasks when learning on new data, forgetting can be concentrated on a subset of tasks by choosing task-specific regularization strengths. Therefore, also *PosteriorReplay* methods can employ *graceful forgetting* by discounting the regularization strength depending on the age of a task.